Thea Jahren Herud
Serine Ripman Haldorsen

Estimation of Aerodynamic Admittance Functions for a Twin-box Bridge

June 2020

NTNU
Norwegian University of
Science and Technology

Estimation of Aerodynamic Admittance Functions for a Twin-box Bridge

Thea Jahren Herud
Serine Ripman Haldorsen

Department of Structural Engineering
Faculty of Engineering
NTNU – **Norwegian University of Science and Technology**

MASTER THESIS 2020

TITLE:

Estimation of Aerodynamic Admittance Functions for a Twin-box Bridge

Estimering av aerodynamiske frekvensresponsfunksjoner for en dobbelt kassetverrsnitt bru

BY:

Serine Ripman Haldorsen
Thea Jahren Herud

SUMMARY:
This thesis place attention on the estimation of aerodynamic admittance functions and investigation of the pressure field around the twin-box model. Wind tunnel testing of a twin-box model was conducted at NTNU and the pressure and turbulent flow was measured using MSP4264 pressure scanners and Cobra probe.

The pressure field gave an unexpected amount of positive pressure, particularly at the downstream-box. The pressure was further converted to forces, by integrating it over the cross-section surface. A distinct peak was detected in the force spectra, mainly caused by the downstream deck, due to vortices shed from the upstream-box or in the wake of the downstream-box.

Aerodynamic admittance functions were estimated using three different methods, the general, the equivalent and cross-spectral method. The estimated functions were then compared to each other, Sears functions and with previous studies. All functions showed a distinct peak, the same peak as detected in the force spectra and the slopes were decreasing for increasing frequency. A deviation was seen between the functions corresponding to the horizontal and vertical turbulence components implying that the equivalent method gives inaccurate results. Comparison of the equivalent and cross-spectral method showed that the lift admittance matched previous studies, while drag and moment had some deviations. In addition, it was found that Sears function overestimated for all reduced frequencies, and not applicable for the twin-box bridge. The estimated admittance functions were considered as valid in terms of shape and can be used to understand the buffeting response of a twin-box bridge.

RESPONSIBLE TEACHER: Professor Ole Andre Øiseth

SUPERVISOR(S): Professor Ole Andre Øiseth

CARRIED OUT AT: Department of Structural Engineering

Abstract

Aerodynamic admittance functions is a tool to predict buffeting forces. Hence they are one of the most important factors in evaluating buffeting response. The objective of this thesis is to estimate the aerodynamic admittance functions and investigate the pressure field around the twin-box model. Wind tunnel testing of a twin-box model was conducted at the Department of Energy and Process Engineering at NTNU Gløshaugen. The surface pressure was measured using 256 plastic tubes distributed on 6 correlations lines connected to four MSP4264 pressure scanners. The turbulent flow was measured using a cobra probe. All data was processed and transferred to the frequency domain for the estimation of the admittance function.

An extra focus was put on the theory related to the admittance functions, as well as the wind tunnel test, and several previous studies have been evaluated to determine the methodology used in this thesis. The concept and geometry of the model are based on the shapes of previous masters thesis at NTNU. Several solutions were discussed due to challenges related to placement and attachment of the pressure scanners and tube system.

The pressure distributions were found for all tests. The results gave an unexpected amount of positive pressure, particularly at the downstream-box. The pressure was then converted to forces, by integrating it over the cross-section surface. The force spectra showed a distinct peak, mainly caused by the downstream deck, due to vortices shed from the upstream-box or in the wake of the downstream-box.

Admittance functions were estimated using three different methods, the general, the equivalent and the cross-spectral. The estimated functions were then compared to each other, then to the Sears functions and finally with previous studies. All functions showed a distinct peak, the same peak as detected in the force spectra. The slopes decreased for increasing frequency. Furthermore, the results showed that functions corresponding to the horizontal and vertical turbulence components deviates significantly, and implying that the equivalent method produces inaccurate results. The admittance functions for lift showed similarity with previous studies, while drag and moment had deviations. Besides, it was found that Sears function overestimated for all reduced frequencies and is not applicable for the twin-box bridge.

The estimated admittance functions were considered valid in terms of shape and can be used to understand the buffeting response of a twin-box bridge.

Sammendrag

Aerodynamiske frekvensresponsfunksjonene er et viktig verktøy for å predikere buffeting krefter. De er derfor en av de viktigste faktorene for å evaluere buffetingrespons. Hovedfokuset i denne oppgaven er å estimere frekvensresponsfunksjonene og undersøke trykkfordelingen rundt en dobbel kassetverrsnitt bru. Det er utført tester i vindtunnelen, ved Institutt for energi- og prosessteknikk ved NTNU Gløshaugen. Overflatetrykket til modellen ble målt ved å bruke 256 plastrør fordelt på 6 korrelasjonslinjer og koblet til 4 MSP4264 trykkskannere. Den turbulente vinden ble målt med en cobra probe. Alt av data er behandlet og transformert til frekvens domenet for å estimere frekvensrespons-funksjonene.

Det har blitt lagt fokus på teorien bak de aerodynamiske frekvensresponsfunksjonene samt vindtunneltestene. Flere tidligere studier er blitt evaluert, for å bestemme metodene som brukes i denne oppgaven. Konseptet og geometrien til modellen er basert på modeller fra tidligere masteroppgaver ved NTNU. Flere ulike løsninger ble diskutert, på grunn av utfordringer knyttet til hvordan trykkskanner og plastrørene skulle plasseres og festes til modellen.

Trykkfordelingen til tverrsnittet ble funnet for alle testene. Resultatene viste en uventet mengde med positivt trykk. Trykket ble deretter transformert til krefter, ved å integrere trykket over overflaten til tverrsnittet. Lastspekteret viste tydelige topper, hovedsakelig forårsaket av nedstrøms kassen, på grunn av virvler dannet av oppstrøms kassen, eller i bakkant av nedstrøms kasse. Videre ble lastspektrene brukt til estimeringen av frekvensre-sponsfunksjonene.

Frekvensresponsfunksjonene ble estimert ved bruk av tre forskjellige metoder, den generelle, ekvivalente og kryss spektrale. De estimerte funksjonene ble sammenlignet med hveran-dre, Sears-funksjonen og tidligere studier. Alle funksjonene viste en tydelig topp, den samme som ble observert i lastspektrene, og funksjonen synker for økende frekvenser. Videre viste resultatene at funksjonene som tilsvarer horisontale og vertikale turbulens komponenter avviker betydelig, og antyder at den ekvivalente metoden gir unøyaktige re-sultater. Frekvensresponsfunksjonen for løft viste samsvar med tidligere studier, mens drag og moment hadde avvik. Videre ble det oppdaget at Sears funksjonen overestimerte for alle reduserte frekvenser, og er derfor ikke anvendelig for dobbel kassetverrsnitt bru.

Frekvensresponsfunksjonene ble ansett som akseptable i henhold til form og kan bli brukt til å forstå buffetingresponsen til en dobbel kassetverrsnitt bru.

Preface

This report is the final product of our master thesis in Structural dynamics at the University of Science and Technology (NTNU), Department of Structural Engineering. We are very grateful and think it has been incredibly interesting to get a master's thesis with so many practical aspects. Having the opportunity to build the model ourselves and decide how it should look has been a great motivation to reach the finished product.

We have faced challenges we did not expect when we started on this thesis, due to COVID-19, the laboratories, and the campus at NTNU locked down. Over several weeks we did not know if we could return to the laboratory or not. Fortunately, we were able to return and complete our tests. Although it was difficult to wait for the laboratory to open, this allowed us to get a better understanding of the theory behind the aerodynamic admittance functions and to go deeper into previous studies done on this topic.

We want to show our gratitude to our supervisor Ole Andre Øiseth, who has helped us with challenging problems, Matlab scripts and his expertise. We would also like to thank PhD Candidate Øyvind Wiig Petersen for his great competence. An extra thank must be given to the days during the lock-down at NTNU when they spent a lot of time in the laboratories making us able to be ready for wind tunnel testing when the university opened. In addition, to the expertise under the testing in the wind tunnel.

Table of Contents

List of Tables

List of Figures

Chapter 1

Introduction

The investigation of long-span bridge structures is more important than ever. The limit of slenderness and span-length of bridges are constantly pushed, resulting in more sensitive structures when exposed to wind. The requirements of the aerodynamic stability are therefore increasing, and it is shown that closed-box bridges usually cannot satisfy these requirements. Twin-box bridges, on the other hand, are shown to improve the aerodynamic stability for long-span bridges. In addition, the use of twin-box bridges often results in lighter structures making them economically appealing. Consequently, applications of twin-box girder in bridge engineering design are becoming more common. Some of the words longest bridges, for instance, the Stone cutters bridge with a center span of 1018 m and the Xihoumen Bridge with a center span of 1650 m are twin-box bridges [4].

Twin-box bridges are effective in improving the flutter characteristics by altering the surface pressure distribution around the bridge deck. However, the flow characteristics around the deck are complicated due to the effects of the gap between the separated decks. The flow will induce vibrations in terms of vortex-induced vibration, often encountered by twin-box girders, and buffeting loads induced by fluctuating wind.

For the design and user comfort of a long-span bridge the prediction of buffeting forces are important. The estimation of the buffeting forces on a bridge deck depends on a transfer function, called the aerodynamic admittance function, transferring the turbulent wind to buffeting forces. Sears derived a theoretically aerodynamic admittance function of a thin airfoil in 1941. The same approach was extended to wind engineering by Davenport in 1962. For bluff bodies, such as a twin-box section, the theoretical exact expression for the admittance cannot be derived, due to complex forces caused by separation and reattachment of flow. Hence, the aerodynamic admittance of bridge decks has always been a challenging and difficult topic in the bridge aerodynamics and the admittance function are commonly found experimentally. A widely used method to estimate the aerodynamic admittance functions, is using wind tunnel tests, measuring the surface pressure and the turbulent flow. This is previous done by Larose (1992), who developed the theory by Davenport and included the the contribution from the cross-spectra between the buffeting forces and turbulence components. Zhu et al. (2018) identified six aerodynamic admit-

tance functions with a colligated residue least square method of auto and cross-spectra.

Most previous studies have focused on the aerodynamic admittance of closed-box bridges. Considering that the twin-box bridge will play an important role in the further development in the construction of long suspension bridges, its aerodynamic properties and the prediction of buffeting forces should be investigated further. For this reason, the main focus in this thesis is to estimate the aerodynamic admittance functions for a twin-box bridge. A model will be tested in the wind tunnel at NTNU for different wind velocities and the admittance functions will be estimated using three different methods. To investigate the pressure distribution, aerodynamic forces, and admittance functions, the pressure is measured using 256 tubes distributed along 6 correlation lines at the surface of the cross-section. Separating the tubes on 6 different lines allows investigating of the correlation between the buffeting forces. As mentioned, the flow around a twin-box section is complicated. By measuring the surface pressure it is possible to get a clear picture on the pressure distribution and the related flow. These are two important factors for understanding the aerodynamic characterises of a twin-box bridge.

This thesis describes the relevant theory related to the aerodynamic admittance function, wind tunnel testing and the experimental identification of the aerodynamic admittance.

1.1 Structure of the Report

Chapter 2: Theory
In this chapter, the relevant background theory is presented. It is assumed that the reader has an understanding of basic structural dynamics and wind engineering.

Chapter 3: Model
In this chapter, the concept and design of the sectional model is described.

Chapter 4: Wind Tunnel Tests
This chapter presents the experimental setup and experiments performed in the wind tunnel test.

Chapter 5: Results and Discussion
The results from the wind tunnel experiments is presented and discussed in this chapter

Chapter 6: Conclusion and Further Work
In the last chapter, the main conclusions are presented together with possible further work.

Chapter 2

Theory

This chapter gives a theoretical introduction of the theory relevant for the work done in this thesis.

2.1   Cross Section

The shape of the cross-section of a bridge has big importance on the aerodynamic properties of a bridge. Bridges are built more slender and longer than ever before, by this, higher requirements for optimal design is necessary. Today, the twin-box sections have received much attention due to their flutter stability properties and are widely used in many of the world's longest bridges, such as Stonecutters Bridge and Xihoumen Bridge. When the span lengths increase, the bridge will be more sensitive to wind-induced vibrations, which underline the importance of understanding the vibration caused by the interaction between the wind and the structure.

Twin-box bridges are effective in improving the flutter characteristics by altering the surface pressure distribution around the bridge deck. The pressure distribution is greatly affected by the width of the center gap and by the angle of wind incidence. In the study done by Kwok et al. [5] the pressure distribution of cross-sections with different gap-width was investigated. The pressure distribution was used to determine force and moment coefficients and to highlight regions of flow separation corresponding to large negative surface pressures. It is shown that, when the gap-width is increased, the downstream-box was immersed in the wake of the upstream-box which is associated with the vortices shed from the upstream-box. As a result large mean positive pressure occur at the upstream windward surface of the downstream-box and a the drag forces increases significantly. This underlines the importance of the gap-width and how it affects the aerodynamic properties of the cross-section. The effect of the lift force and pitching moment due to the gap-width is neglectable.

2.2 Equation of Motion

To understand the behaviour of a dynamic system it is necessary to introduce the equation of motion.

$$\boldsymbol{M}\ddot{\boldsymbol{x}}(t) + \boldsymbol{C}\dot{\boldsymbol{x}}(t) + \boldsymbol{K}\boldsymbol{x}(t) = \boldsymbol{p}(t) \tag{2.1}$$

The equation describes a systems motion as a function of time and consists of the mass matrix, $\boldsymbol{M}$, the stiffness matrix, $\boldsymbol{K}$ and the damping matrix, $\boldsymbol{C}$. $\boldsymbol{p}(t)$ is a vector consisting of external forces and $\boldsymbol{x}(t)$ is the displacement vector. The equation of motion can be solved in many different ways. However, in dynamic analysis it is normal to operate in the frequency domain and the equation is solved by the frequency response method. This is done by taking the Fourier transform of the input forces and the output displacement vectors giving the following expression.

$$\boldsymbol{M}\ddot{\boldsymbol{X}}(\omega) + \boldsymbol{C}\dot{\boldsymbol{X}}(\omega) + \boldsymbol{K}\boldsymbol{X}(\omega) = \boldsymbol{P}(\omega) \tag{2.2}$$

In order to solve the equation it is desirable to have the relation between the input $\mathbf{X}(\omega)$ and the output $\mathbf{P}(\omega)$ and the equation of motion can be expressed without the derivatives.

$$\left(-\omega^2\boldsymbol{M} + i\omega\boldsymbol{C} + \boldsymbol{K}\right)\boldsymbol{X}(\omega) = \boldsymbol{P}(\omega) \tag{2.3}$$

The Fourier Transform $\boldsymbol{X}(\omega)$ of the the solution $x(t)$ is then given as.

$$\boldsymbol{X}(\omega) = \boldsymbol{H}(\omega)\boldsymbol{P}(\omega) \tag{2.4}$$

Where

$$\boldsymbol{H}(\omega) = \left[-\omega^2\boldsymbol{M} + i\omega\boldsymbol{C} + \boldsymbol{K}\right]^{-1} \tag{2.5}$$

is the frequency response function (FRF) describing the transfer from load to response in a system.

2.3   Wind Induced Response

If the airflow is met by a line-like body, the interaction between the flow and the structure gives rise to forces which will start to fluctuate. The oncoming flow contains turbulence and on the surface of the body, additional turbulence and vortices are created due to friction. If the body has sharp edges the flow will separate by the edges. Further, the flow becomes unstable caused by a variable part alternating from side to side and resulting in vortices. Additionally, the fluctuating forces may cause the body to oscillate, and the flow and oscillating body may interact and generate further forces. To sum up, the wind forces stem from pressure fluctuations, vortices, and interaction between the flow and the oscillating body. The first of these effects is called buffeting, the second vortex shedding, and the last is usually called motion-induced forces. All of the mentioned effects occur at all wind velocities, but the degree of importance for each effect varies with wind speed. Vortex shedding is at its strongest at low wind velocities, buffeting dominates at strong wind velocities while motion-induced forces are significant at even stronger velocities. Therefore the corresponding response calculations are usually treated separately [1].

2.3.1   The Strip Theory

The strip theory assumption was originally used on aerofoils, but are now often used for bridges as well. For bridge structures extended in only one direction, the main concern is the behavior when the wind attack perpendicular to its longitudinal axis. The spatial loading can be modeled by the strip theory, considering a unit thickness in the span length direction. The idea is the same as in the plane strain analysis in the theory of elasticity. By this, it is only necessary to consider the lift force F_L, drag force, F_D, and pitching moment F_M acting on the bridge [6].

2.3.2   Quasi-Steady Theory

The quasi-steady theory approximation is a well-known theory used in bridge engineering. When applying quasi-steady aerodynamics the history of motion can be ignored. For this reason, forces at any time depend only on the position and velocity at that moment. The theory is an acceptable assumption when the wind speed is relatively high but unacceptable in the case of vortex shedding, where the wind speed is relatively low.

The Buffeting Theory

The buffeting theory is based on the quasi-steady theory. The buffeting response includes the part of the total load on the structure associated with the velocity fluctuations in the oncoming flow and motion induced contributions. It is assumed that wind consist of two parts, the stationary wind speed (V) and a fluctuating part (u,v,w). The fluctuating part is depending on time and place. However, the stationary wind is only depending on the position.
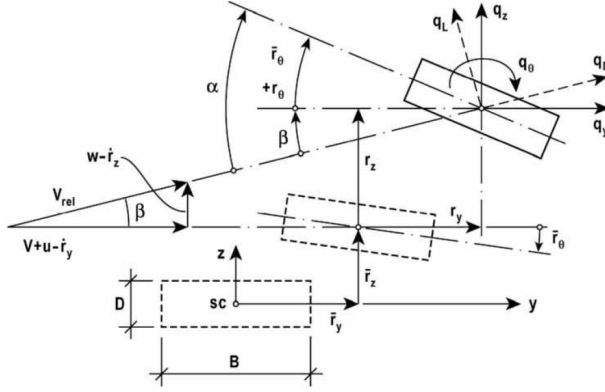
Figure 2.1: Bridge cross-section at an arbitrary position [1].

In figure 2.1 a bridge cross-section shown. At an arbitrary position the cross section is first given the displacements $\bar{r}_y$, $\bar{r}_z$ and $\bar{r}_\theta$. When the section starts to oscillates the cross section is given additional dynamic displacement r_y, r_z and r_θ. In this position the drag force, lift force and the pitching moment can be expressed as:

$$\begin{bmatrix} q_D(x,t) \\ q_L(x,t) \\ q_M(x,t) \end{bmatrix} = \frac{1}{2}\rho V_{rel}^2 \cdot \begin{bmatrix} D \cdot C_D(\alpha) \\ B \cdot C_L(\alpha) \\ B^2 \cdot C_M(\alpha) \end{bmatrix} \tag{2.6}$$

Where α is the corresponding angel of flow, ρ is the air density, C_D, C_L and C_M are the drag, lift and pitching moment coefficients and V_{rel} is the instantaneous relative wind velocity given by:

$$V_{rel}^2 = (V + u(t) - \dot{r}_y(t))^2 + (w(t) - \dot{r}_z(t))^2 \tag{2.7}$$

Further, the drag, lift and pitching moment can be transformed into a structural axis by a transformation matrix.

$$\boldsymbol{q_{tot}}(x,t) = \begin{bmatrix} q_y \\ q_z \\ q_\theta \end{bmatrix}_{tot} = \begin{bmatrix} cos\beta & -sin\beta & 0 \\ sin\beta & cos\beta & 0 \\ 0 & 0 & 1 \end{bmatrix} \cdot \begin{bmatrix} q_D \\ q_L \\ q_M \end{bmatrix} \tag{2.8}$$

β, the relative angel of attack, is given by:

$$\beta = arctan\left(\frac{w - \dot{r}_z}{V + u - \dot{r}_y}\right) \tag{2.9}$$

In the buffeting theory, a basic assumption is that linearization of any fluctuating parts will give sufficient results. The forces from equation 2.6 are in general nonlinear, but a common assumption is that the fluctuating flow components and structural displacements are small compared to the mean wind velocity: $V >> u(t), w(t), \dot{r}_y(t), \dot{r}_z(t)$. Further, assuming

that β is small, then $cos\beta \approx 1$ and $sin\beta \approx tan\beta \approx \beta \approx (w - \dot{r}_z)/(V + u - \dot{r}_y) \approx (w - \dot{r}_z)/V$. By this, V_{rel}^2 and α can be written as [1]:

$$V_{rel}^2 \approx V^2 + 2Vu - 2V\dot{r}_y \tag{2.10}$$

$$\alpha = \bar{r}_\theta + r_\theta + \beta \approx \bar{r}_\theta + r_\theta + \frac{w}{V} - \frac{\dot{r}_z}{V} \tag{2.11}$$

The load coefficients are nonlinear and vary with the relative angle of attack, and are replaced by the following linear approximation:

$$\begin{bmatrix} C_D(\alpha) \\ C_L(\alpha) \\ C_M(\alpha) \end{bmatrix} = \begin{bmatrix} C_D(\bar{\alpha}) \\ C_L(\bar{\alpha}) \\ C_M(\bar{\alpha}) \end{bmatrix} + \alpha_f \cdot \begin{bmatrix} C_D'(\bar{\alpha}) \\ C_L'(\bar{\alpha}) \\ C_M'(\bar{\alpha}) \end{bmatrix} \tag{2.12}$$

where $\bar{\alpha}$ and α_f are the mean value and the fluctuating part of attack and C_D', C_L' and C_M' are the slopes of the load coefficients curves at $\bar{\alpha}$ [1].

By using the linear approximations and rewriting equation 2.8, the loads can be written as:

$$\boldsymbol{q}_{tot}(x,t) = \begin{bmatrix} \bar{q}_y(x) \\ \bar{q}_z(x) \\ \bar{q}_\theta(x) \end{bmatrix} + \begin{bmatrix} q_y(x,t) \\ q_z(x,t) \\ q_\theta(x,t) \end{bmatrix} = \bar{\boldsymbol{q}} + \boldsymbol{B}_q \cdot \boldsymbol{v} + \boldsymbol{C}_{ae} \cdot \dot{\boldsymbol{r}} + \boldsymbol{K}_{ae} \cdot \boldsymbol{r} \tag{2.13}$$

where

$$\boldsymbol{v}(x,t) = [u \; w]^T \tag{2.14}$$

$$\boldsymbol{r}(x,t) = [r_y \; r_z \; r_\theta]^T \tag{2.15}$$

$$\bar{\boldsymbol{q}}(x) = \begin{bmatrix} \bar{q}_y(x) \\ \bar{q}_z(x) \\ \bar{q}_\theta(x) \end{bmatrix} = \frac{\rho V^2}{2} \begin{bmatrix} D\bar{C}_D \\ B\bar{C}_L \\ B^2\bar{C}_M \end{bmatrix} = \frac{\rho V^2 B}{2} \begin{bmatrix} D/B\bar{C}_D \\ \bar{C}_L \\ B\bar{C}_M \end{bmatrix} \tag{2.16}$$

$$\boldsymbol{B}_q(x) = \frac{\rho V B}{2} \begin{bmatrix} 2(D/B)\bar{C}_D & ((D/B)C_D' - \bar{C}_L) \\ 2\bar{C}_L & (C_L' + (D/B)\bar{C}_D) \\ 2B\bar{C}_M & BC_M' \end{bmatrix} \tag{2.17}$$

$$\boldsymbol{C}_{ae}(x) = -\frac{\rho V B}{2} \begin{bmatrix} 2(D/B)\bar{C}_D & ((D/B)C_D' - \bar{C}_L) & 0 \\ 2\bar{C}_L & (C_L' + (D/B)\bar{C}_D) & 0 \\ 2B\bar{C}_M & BC_M' & 0 \end{bmatrix} \tag{2.18}$$

$$\boldsymbol{K}_{ae}(x) = \frac{\rho V^2 B}{2} \begin{bmatrix} 0 & 0 & (D/B)C'_D \\ 0 & 0 & C'_L \\ 0 & 0 & BC'_M \end{bmatrix} \qquad (2.19)$$

$\bar{\boldsymbol{q}}(x)$ is the static part and $\boldsymbol{q}(x,t) = \boldsymbol{B}_q \boldsymbol{v} + \boldsymbol{C}_{ae}\dot{\boldsymbol{r}} + \boldsymbol{K}_{ae}\boldsymbol{r}$ the fluctuating/dynamic part. $\boldsymbol{B}_q \boldsymbol{v}$ is associated with the turbulence, while $\boldsymbol{C}_{ae}\dot{\boldsymbol{r}}$ and $\boldsymbol{K}_{ae}\boldsymbol{r}$ are motion induced loads associated with structural velocity and displacement [1]. $\boldsymbol{K}_{ae}$ and $\boldsymbol{C}_{ae}$ are respectively the aerodynamic stiffness and damping.

2.3.3 Identification of Static Coefficients

The static coefficients C_D, C_L and C_M are dependent on the angle of attack and can be found from the measured forces for different angles. The coefficients can be extracted from static tests in the wind tunnel. The following relationship is assumed between the measured forces and the static coefficients:

$$\begin{bmatrix} C_D(\alpha) \\ C_L(\alpha) \\ C_M(\alpha) \end{bmatrix} = \frac{1}{\frac{1}{2}\rho V^2 L} \begin{bmatrix} \frac{F_D(\alpha)}{D} \\ \frac{F_L(\alpha)}{B} \\ \frac{F_M(\alpha)}{B^2}) \end{bmatrix} \qquad (2.20)$$

Where F_D, F_L and F_M are the drag, lift and pitching moment forces measured in the static test, and D, B and L are the height, width and length of the bridge deck. The coefficients are defined as the measured forces normalised by the area normal to the force and the Bernoulli's pressure equation.

2.3.4 Vortex Shedding

As mentioned, when airflow is met by a line-like structure flow separation will occur on the surface and cause alternating vortices in the wake of the body. It takes place at a certain wind velocity depending on the geometry. The vortices have alternating rotations and vertical forces will arise. For each vortex, the forces change directions and cause vibrations of the deck [7].

The vortex shedding frequency, f_s, is proportional to the mean wind velocity, V, and the inverse proportional to the across wind width, D. The f_s are given by:

$$f_s = St \cdot \frac{V}{D} \qquad (2.21)$$

 where St is the Strouhal number depending on the geometry and flow conditions (Reynolds number) [8]. Resonance will first occur when f_s becomes equal to the lowest natural frequency of the structure. When resonance is occurring, the mean wind velocity is according to equation 2.21 given by:

$$V = \frac{f_s D}{St} \qquad (2.22)$$

Experiments have shown that f_s will deviate from equation 2.22, when resonance occurs due to interaction between the flow and oscillating structure. This will happen for a certain range of wind velocities, and stay close or equal to, the natural frequency, f_n. The effect is called lock-in. Such vortex-induced interaction is accompanied by two load effects: The fluctuating load becomes better correlated in the span-wise direction and a significant motion-induced part is added. The motion is self-destructive, the induced motions are disturbing the vortex shedding and will diminish when the fluctuating structural displacement becomes large [1]. A twin-box is more exposed to vortex shedding due to the gap between the two sections. Although vortex shedding is not the main concern in this thesis, the phenom is likely to occur during testing and cause problems if the critical velocity region is the same as for the wind tunnel test.

2.4 Scaling Laws

In order to compare tests done in a wind tunnel with a full-scale model, it is necessary to introduce some non-dimensional quantities and scaling laws. In this thesis the bridge and cross-section considered is not a replicate of a real structure and the results obtained can not be compared to full-scale model results. However, the scaling laws are important when results from the wind tunnel are used in the design of a full-scale bridge.

2.4.1 Reduced Frequency and Velocity

The structural non-dimensional frequency is often refereed to as the reduced frequency and is given by:

$$f^* = \frac{fB}{V} \tag{2.23}$$

where f is the frequency, B is the deck width and V is the mean wind velocity. The reduced mean velocity is defined as:

$$V^* = \frac{V}{f_n B} \tag{2.24}$$

Where f_n is the natural frequency and B and V as mentioned above. The reduced frequency indicates how unsteady the system is. If the reduced frequency approaches 0, it indicates that the corresponding mode is approaching a steady behaviour. As the reduced frequency increases the more unsteady the mode becomes.

The reduced frequency and velocity can be used for comparison between the wind tunnel model (WT) and the full-scale structure (FS) by the following relation:

$$\frac{V_{FS}}{\omega_{FS} B_{FS}} = \frac{V_{WT}}{\omega_{WT} B_{WT}} \tag{2.25}$$

2.4.2 Reynolds Number

Reynolds number is a dimensionless number and defined as the ratio between fluid inertia force and viscous force given by the following formula:

$$
\begin{aligned}
Re &= \frac{inertia\, forces}{viscous\, forces} \propto \frac{mass \times acceleration}{shear\, stress \times area} \\
&= \frac{\rho L^3 \frac{V_\infty}{T}}{\mu \frac{V_\infty}{T} L^2} = \frac{\rho L^2}{\mu T} = \frac{\rho L^2}{\mu \frac{L}{V_\infty}} = \frac{\rho V_\infty L}{\mu} = \frac{V_\infty L}{\nu}
\end{aligned}
\tag{2.26}
$$

Where L is the characteristic length of the gust, V_∞ is the characteristic velocity, $\mu = 15 \times 10^{-6} m/s^2$ the dynamic viscosity and ν is the kinematic viscosity equal μ/ρ.

Ideally, the Reynolds effects should be accounted for when performing a wind tunnel test of a real structure duplicate. In practice, it is almost impossible to obtain similar Reynolds number on the model and the full-scale bridge due to limitations of the wind tunnel. Since

the kinematic viscosity of air varies little between test and full-scale conditions, the only way to account for the scaled length is to increase the wind speed. The increase in wind speed is normally so high that it is out of reach for most boundary layer wind tunnels [9]. According to Tanaka [10], the flow over a sharp edge body is less sensitive to change in Reynolds's number. The separation point influencing the action of the aerodynamic forces will generally occur at the leading edge with the exception of very extreme angles. The test executed in this master thesis, only small angles of attack will be used and therefore Reynolds number will not be included in the calculations.

2.4.3 Strouhal Number

The Strouhal number, S_t, is a dimensionless number that characterize vortex-induced oscillation that occur at the Strouhal frequency f_s given in section 2.3.4.

$$S_t = \frac{f_s D}{V} \tag{2.27}$$

V is the the mean wind-speed and D the shape of the cross-section [11].The Strouhal number needs to be equal in full scale and wind tunnel in order to scale the frequency, time, length and wind appropriately [12].

$$St_{WT} = St_{FS} \quad or \quad \frac{T_{WT}}{T_{FS}} = \frac{L_{WT}}{L_{FS}} \frac{V_{WT}}{V_{FS}} \tag{2.28}$$

According to Matsuda et al.[13] the Strouhal number is influenced by the Reynold number and therefore the flow on the body. Another point to consider is that for a twin deck section like the one in this thesis, the strouhals number, hence the vortex-shedding frequency will gradually increase with an increasing gap due to changes in the flow regime [5].

2.4.4 Froude Number

The Froude number is the ratio of the gravity force to the inertia force.

$$F_r = \frac{gL}{V^2} \qquad \frac{V_{WT}}{V_{FS}} = \sqrt{L_{WT}/L_{FS}} \tag{2.29}$$

Where V is the mean wind velocity, g is the acceleration of gravity and L the characteristic length of the gust.

Since the acceleration of gravity will be equal for both wind tunnel and full scale, Froude number shows that the velocity scale are equal to the square-root of the geometrical scale. This leads to a problem in the wind tunnel test because it require low wind velocity and the instruments are sometimes less accurate at lower wind speeds. Froude number should be similar in the WT model and FS model for suspension bridges where the gravitational force are important [9].

2.4.5 Turbulence Intencity

In a wind tunnel test the turbulence characteristics are represented by the turbulence intensity, spectral density function and the correlation lengths in the flow. The turbulence intensity is a non-dimensional property defined as the ratio between the standard deviation of fluctuating velocity, σ_u, and mean wind speed, V.

$$I_u = \frac{\sigma_u}{V} \tag{2.30}$$

In general cases, low turbulence intensity will lead to higher loads and will be considered as a conservative case of wind loading. For this reason, the turbulence intensity in a scaled wind tunnel test needs to be smaller than or equal to the value in a full-scale test [14].

$$I_{u,WT} \leq I_{u,FS} \tag{2.31}$$

The correlation length is represented by the integral length scale which is a measure of eddy sizes in meters in the different directions, $L_{u,v,w}$. The conversion between the wind tunnel and full-size integral length scale is done by the geometrical scale. However, it is difficult to determine the integral length scale in a wind tunnel and usually, several predictions are necessary.

2.5   Wind Tunnel Effects

The wind is influenced by its surrounding environment. Differences in temperature create pressure variations which make air move and affect the wind speed. The local topography also affects the wind speed as well as changing the wind pattern. A wind tunnel will not be able to reproduce the temperature and topography outside. Therefore it is necessary to manipulate the wind to get the desired flow. In addition, the wind tunnel has some effects that differ from the natural flow as a result of the limiting cross-section area of the tunnel. In this section, the effects considered most important for wind tunnel tests are discussed.

2.5.1   Boundary Layer

As the wind moves past an object there will be friction between the fluid and the surface causing a reduction in the wind velocity. This effect is referred to as boundary layer flow and is a replicate of flow at a given sight. The local topography has a great impact on the flow and can create turbulence. In order to have a laminar airflow with constant velocity, the model must be placed higher than the boundary layer. For the wind tunnel at NTNU, this length is approximately 200mm from the surface of the wind tunnel [2].
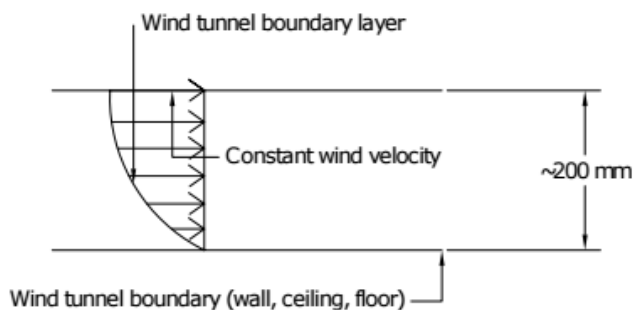
Figure 2.2: Boundary layer effects in the wind tunnel [2]

2.5.2   Blockage

When a model is tested in the wind tunnel the geometric scale of the model is critically limited by the blockage effect of the wind tunnel. While a real structure has infinite space around, the test model will have a limited space causing boundary layers. The blockage effect will vary for different models and is influenced by the shape of the body, aerodynamic effects, the wind field characteristics and the blockage ratio, $\frac{S}{C}$, where S is the area of the body normal to the wind flow, and C is the cross-sectional area of the wind tunnel. This distortion can be neglected if the blockage effect is no greater than 5%.

According to K.Takeda [15], both drag coefficient and wind-induced vibration can be affected by the wind tunnel blockage and found to be significantly even at 5% blocking ratio.

For the test model in this thesis, the blockage ratio is 0.044 and is therefore neglected and could be a source of error in the final results.

2.5.3 End Plates

In wind tunnel tests, end plates are used to produce a two-dimensional flow around the model. The purpose is to prevent the fluid outside the end plate from entering the wake of the test area. This is maintained by having the diameter of the end plates larger than 8.5d, where d is the body depth normal to the flow [16]. The bridge model used in this thesis spans the entire length of the wind tunnel and will not need end plates.

2.5.4 Grid Generated Turbulence

Generation of turbulence in a wind tunnel test can be achieved by installing a grid net. The grid is placed upstream of the model to make distortion of the passing wind. This type of simulation is called grid-generated turbulence and causes vortex shedding, separation, and reattachment's which are essential characteristics of the turbulence [17].

When using the turbulence is generated by a grid it is often described as isotropic and homogeneous. The placement and mesh of the grid play a significant role in the characteristics of the turbulence. An isotropic flow will occur when each of the three fluctuating velocity components is invariant due to an arbitrary rotation of the defining principal axis [18]. This condition happens at a specific distance behind the grid. Numerous studies have been done to predict this distance, such as Tresso [18] and Liu et al [17], and confirm the significance of a fixed position of the testing model in the wind tunnel.

2.6 Simulation of Turbulence

The objective of this section is to present the method used to simulate a 2D turbulence field with Monte Carlo simulation and the wind field characteristics defined by N400. The simulated wind field is later used in a Matlab example presented in section 2.8.

2.6.1 Turbulence Spectrum

A 2D turbulence field is simulated based on wind field characteristics defined in N400 based on the spectral properties of a Kaimal spectrum. In the following section, relevant definitions and constants from N400 are given [19].

The integral length scale given by N400 is defined as:

$$^x L_u = \begin{cases} L_1 (z/z_1)^{0.3}, & z > z_{min} \\ L_1 (z_{min}/z_1)^{0.3}, & z \leq z_{min} \end{cases} \tag{2.32}$$

Where L_1 is the reference length scale equal to 100m and z_1 is the reference height equal to 10m. Further, the turbulence intensity I_u can be calculated according to *NS-EN 1991-1-4:2005+NA:2009,table NA.4.1*. For a approximated homogeneous wind field, the other turbulence intensities and integral length scales for a 2D wind field are given by:

$$I_w = 1/4 \cdot I_u \quad \text{for} \quad \begin{bmatrix} ^y L_u \\ ^z L_u \\ ^y L_w \\ ^z L_w \\ ^x L_w \end{bmatrix} = \begin{bmatrix} 1/3 \\ 1/5 \\ 1/12 \\ 1/18 \\ 1/18 \end{bmatrix} {}^x L_u \tag{2.33}$$

The single point auto spectrum, $Si(f)$, for the turbulence components u and w are given by:

$$S_i(f) = \frac{\sigma_i^2 A_i \hat{n}_i}{(1 + 1.5 A_i \hat{n}_i)^{5/3}} \quad \text{for} \quad i = u, w \tag{2.34}$$

Where A_i is a constant, σ_i is the standard deviation of turbulence component i and $\hat{n}_i$ is given by equation 2.35. The single point auto spectrum for the turbulence components is shown in figure 2.3.

$$\hat{n}_i = \frac{f\ ^x L_i(z)}{v_m(z)} \tag{2.35}$$

$v_m(z)$ is the mean wind velocity at a given height. The cross-spectral density of the wind turbulence components normal to the main flow direction is given by:

$$Re[S_{i_1 i_2}(f, \Delta s_y)] = \sqrt{S_{i_1}(f) \cdot S_{i_2}(f)} \cdot e^{-C_{iy} \frac{f \Delta s_y}{v_m(z)}} \tag{2.36}$$

Where Δs_y is the horizontal distance between the considered points and $i_1, i_2 = u, w$, $C_{uy} = 10.0$, and $C_{wy} = 6.5$. The cross-spectral density of the wind field are further used as a basis for the Monte Carlo Simulation.
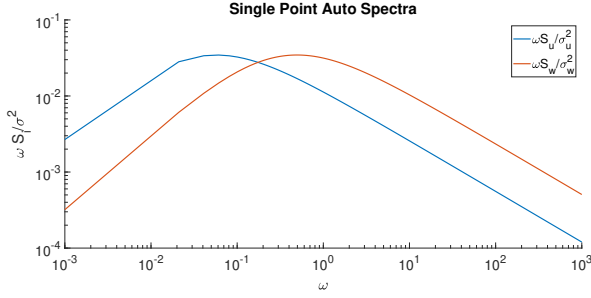
Figure 2.3: Normalized single point Kaimal auto spectrum for turbulence components u and w.

2.6.2 Monte Carlo Simulation

Monte Carlo simulation is a technique based on random number generation. The Monte Carlo method is a widely used algorithm when simulating physical systems like turbulence. The methods that will be presented here is based on the decomposition of stochastic processes where the spectral process has independent increments.

A spectral representation of a stochastic process presupposes that the process can be decomposed into harmonic components with stochastic amplitude and phase.

$$X(t) = \sum_{k=1}^{N} A_k cos(\omega_k t + \phi_k) \ , \qquad k = 1, 2, 3...., \tag{2.37}$$

Where ϕ_k is an independent stochastic variable in the range from 0 to 2π, $\omega_k = (k - \frac{1}{2})\Delta\omega$, where $\Delta\omega$ is a measure of frequency resolution, t is the time, and A_k the deterministic constants the are currently unknown. In numerical calculations ϕ is represented by the use of pseudo-random numbers.

The mean value and autocorrelation function of the process taken over the ensemble are given respectively:

$$E[X(T)] = \int_0^{2\pi} \sum_{k=1}^{N} cos(\omega_k t + \phi_k) \frac{1}{2\pi} d\phi_k \tag{2.38}$$

and

$$
\begin{aligned}
R_X(t+\tau, t) =& E[X(t+\tau)X(t)] \\
=& \int_0^{2\pi} \int_0^{2\pi} \sum_{k=1}^{N} \sum_{k=1}^{N} A_k A_l cos(\omega_k(t+\tau) + \phi_k) cos(\omega_l t + \phi_l) \frac{1}{(2\pi)^2} d\phi_k d\phi_l \\
=& \sum_{k=1}^{N} A_k^2 \frac{1}{2} cos(\omega_k t) = R_X(\tau)
\end{aligned}
$$

$$\tag{2.39}$$

From this, it is evident that the process is at least weakly stationary. Furthermore, by using the central limit theorem, it can be proved that the process converges towards a Gaussian process when $N \to \infty$, which again implies that the process converges towards a stationary process. The time average of the process is given by:

$$
\begin{aligned}
\langle X(t) \rangle &= \lim_{T \to \infty} \frac{1}{2T} \int_{-T}^{T} X(t) dt \\
&= \lim_{T \to \infty} \frac{1}{2T} \sum_{k=1}^{N} \int_{-T}^{T} A_k cos(\omega_k t + \phi_k) dt = 0
\end{aligned}
\tag{2.40}
$$

The autocorrelation function can be determined similarly by taking the time average as:

$$
\begin{aligned}
R_X(\tau) &= \langle X(t+\tau)X(t) \rangle \\
&= \lim_{T \to \infty} \frac{1}{2T} \int_{-T}^{T} X(t+\tau)X(t) dt \\
&= \lim_{T \to \infty} \frac{1}{2T} \sum_{k=1}^{N} \sum_{l=1}^{N} \int_{-T}^{T} cos(\omega_k(t+\tau) + \phi_k) cos(\omega_l t + \phi_l) dt \\
&= \sum_{k=1}^{N} A_k^2 \frac{1}{2} cos(\omega_k \tau)
\end{aligned}
\tag{2.41}
$$

By comparing equation 2.38 and 2.41 with 2.39 and using the central limit theorem, the process converges towards an ergodic process when $N \to \infty$.

It is possible to use equation 2.37 to simulate an ergodic Gaussian process with a prescribed spectral density $S_X^0(\omega)$ or an autocorrelation function $R_X^0(\omega)$ provided that N is sufficiently large. This is done by introducing the following expression:

$$
A_k^2 = 2S_X^0(\omega_k \delta \omega]
\tag{2.42}
$$

Inserted in equation 2.39 gives

$$
R_X(\tau) = \sum_{k=1}^{N} S_X^0(\omega_k) \Delta \omega cos(\omega_k \tau)
\tag{2.43}
$$

so that

$$
\begin{aligned}
R_X(\tau) &= \lim_{T \to \infty \,, \, \delta\omega \to d\omega} R_X(\tau) \\
&= \lim_{T \to \infty \,, \, \delta\omega \to d\omega} \sum_{k=1}^{N} S_X^0(\omega) \Delta \omega cos(\omega_k \tau) \\
&= \int_{-\infty}^{\infty} S_X^0(\omega) cos(\omega \tau) d\omega
\end{aligned}
\tag{2.44}
$$

That is, if A_k is defined by equation 2.42, $R_x(\tau)$ converges to the desired correlation function when $N \to \infty$.

A limitation with this simulation is that $X(t)$ will be periodic with the period:

$$T_0 = \frac{2\pi}{\Delta\omega} \qquad (2.45)$$

Which leads to that only half of the period being utilized. Similar requirements to $\Delta\omega$ are:

$$\Delta\omega = \frac{\pi}{T} \qquad (2.46)$$

Otherwise, $\Delta\omega$, should be chosen so that narrow peaks in the spectral density is represented in a reasonable way. This often require that $\Delta\omega$ is significantly smaller than the effective bandwidth of the narrowest peak and leads to a large number of harmonic component which is both expensive and time consuming.

The simulation method discussed requires a large number of cosine joints. These difficulties can be overcome by applying the Fast Fourier Transform (FFT) function to equation 2.37 and 2.42 when $\Delta\omega$ is constant. Equation 2.37 can be rewritten as follows:

$$X(t) = Re\left[\sum_{k=1}^{N}(A_k e^{i\phi}k)e^{i\omega}k^t\right] \qquad (2.47)$$

The expression inside () can be interpreted as the discrete fourier transform of the series $A_k e^{i\phi}k$, where $k = 1, 2..., N$. This transformation can easily be performed by using the FFT algorithm in matlab.

Using the Kaimal turbulence spectrum defined in subsection 2.6.1 and the method presented, a simulation of the turbulence, $u(t)$ and $w(t)$ can be shown in figure 2.4, where $T = 600$ s and $\Delta\omega = 0.0052 rad/s$. The spectrum of the turbulence component u is compared with the Kaimal spectrum from section 2.6.1 and shown in figure 2.5. The simulated turbulence field is used in an example presented in section 2.8.
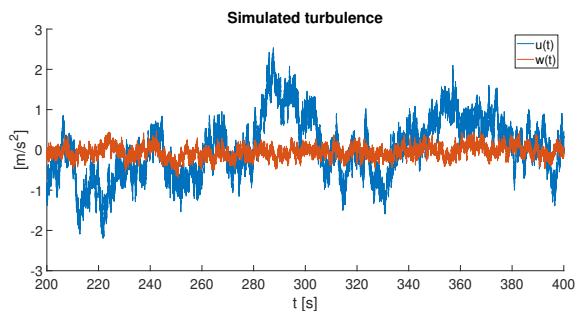
Figure 2.4: Simulated turbulence
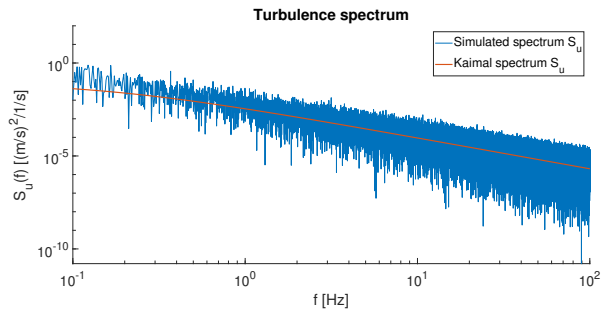
Figure 2.5: Turbulence spectrum of simulated turbulence compared to the Kaimal Spectrum.

2.7 Aerodynamic Admittance Functions

For the design and user comfort of a long-span bridge the prediction of buffeting forces is important. The estimation of the buffeting forces on a bridge deck depends on a transfer function, called the aerodynamic admittance function (AAF), transferring the turbulent wind to buffeting forces. It takes into account the unsteadiness of gust loading which leads to a reduction in the bridge response. A theoretical approach for the Aerodynamic admittance function was first proposed by Sears (1941) using thin airfoil theory and further developed by Davenport (1962) by including aerodynamic admittance in the quasi-steady assumption. This section will briefly describe the Admittance function and discuss how previous studies have estimated the function for different bridges.
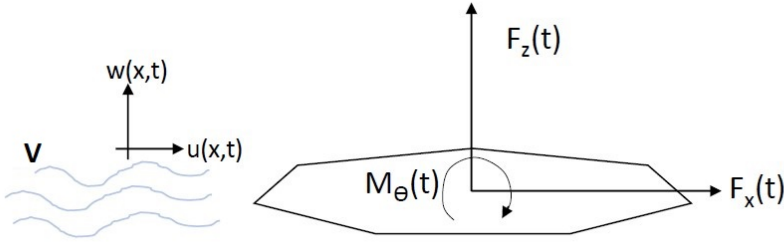
Figure 2.6: Wind acting on bridge cross section

The figure 2.7 presents a bridge section exposed to a turbulent 2D wind field. The wind field is characterized by the mean wind velocity, V, and the turbulent vector ,v, containing the longitudinal and vertical turbulence components $u(x,t)$ and $w(x,t)$. In addition the section is subjected to a set of generalized buffeting forces $F_x(t)$, $F_z(t)$ and $M_\theta(t)$, due to the wind acting on the cross-section. Assuming that the quasi-steady theory applies, the linearized buffeting load due to turbulence is given by

$$q_b(x,t) = B_q v(x,t) \qquad (2.48)$$

Where $B_q v$ is the dynamic load associated with the turbulence of incoming flow. Considering only the quasi-steady aerodynamic assumption the transfer matrix, B_q, will be as in equation 2.17.

The aerodynamic loads on a motionless rigid body in a turbulent flow are normally expressed in the frequency domain as a linear function. The frequency-domain amplitude of the buffeting load $Q_b(x,\omega)$ is obtained by taking the Fourier transform of equation 2.48.

$$Q_b(x,\omega) = B_q(\omega)v(x,\omega) \qquad (2.49)$$

Where

$$B_q(\omega) = \frac{\rho V B}{2} \begin{bmatrix} 2(D/B)\bar{C}_D A_{yu} & ((D/B)C'_D - \bar{C}_L)A_{yw} \\ 2\bar{C}_L A_{zu} & (C'_L + (D/B)\bar{C}_D)A_{zw} \\ 2B\bar{C}_M A_{\theta u} & BC'_M A_{\theta w} \end{bmatrix} \qquad (2.50)$$

The transfer matrix, $\boldsymbol{B_q}(\omega)$, contains frequency dependent flow induced dynamic loads including the admittance functions, $A_{mn}(\omega)$ where $m = y, z, \theta$ and $n = u, w$. Unsteady characteristics of the bridge deck are better described in the frequency domain making it the most preferred method.

A turbulent wind field is complex and hard to recreate. In order to simulate the turbulence physics, Taylor's frozen turbulence hypothesis is applied. This assumption states that the turbulence is transported by the mean wind and maintains its shape when passing through the observation point. Taylor himself described it as:

> If the velocity of the air stream which carries the eddies is very much greater than the turbulence velocity, one may assume that the sequence of changes in u at a fixed point are simply due to the passage of an unchanging pattern of turbulent motion over the point. [20]

He also stated that the correlation between two points with increasing distance will fall away more slowly for large eddies than for smaller eddies. This statement will be described with an example below:
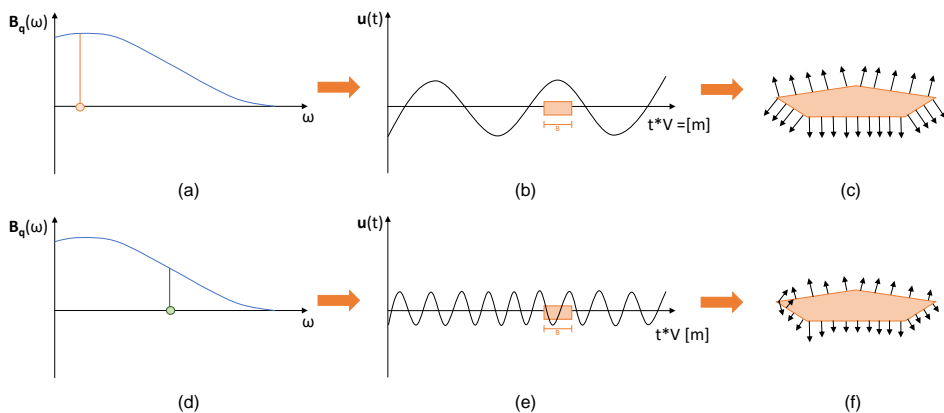
Figure 2.7: skriv tekst

The buffeting theory described in subsection 2.3.2 implies a perfect correlation of the wind forces over the cord of the deck. This is valid if the turbulence scale is significantly larger than the width of the bridge deck and is accurate for low frequencies. For low frequencies, the mean pressure represented by the vectors in figure 2.7 (c), are strongly correlated over the cross-section. This is related to how the cross-section lies inside the turbulence field, as seen in figure 2.7 (b). The x-axis is multiplied with the wind speed to see the sections position inside the turbulence field. In the low-frequency range, the quasi-steady theory is valid and the admittance function will approach 1. In contrast, for high frequencies, the

quasi-steady theory is not valid. The cross-section experience various fields of turbulence reducing the correlation in the pressure distribution. The aerodynamic admittance function takes in to account this lack of correlation between velocity fluctuation in the flow region adjacent to the body. The admittance will decrease towards zero as the frequency increases because high-frequency velocity fluctuations are less effective in producing changes in the aerodynamic forces. Briefly, the aerodynamic admittance function takes into account that low-frequency turbulence provides a high correlation in the distributed pressure, while the high-frequency turbulence results in a low degree of correlation causing a cancellation effect.

2.7.1 Analytical Aerodynamic Admittance

The aerodynamic admittance can either be measured, evaluated or approximated using analytical expressions as the Sears' function. Sears function is a complex theoretical expression for the aerodynamic admittance function for a thin airfoil. From the quasi-steady theory, it is assumed that the lift force at position, x, at time, t, on a bridge deck, is equal to the force occurring if instantaneous velocity $w(t, x)$ persisted for an infinitely long time everywhere on the deck. Further, from the strip theory, it is assumed that the lift force (per unit length) on a strip at position x along the bridge deck is equal to the lift force per unit length as if the wind fluctuations had been fully correlated along the deck. Sears analysis of the unsteady lift force, induced by a transversely fully coherent sinusoidal gust, is based on the strip assumption. He found from the linearized equations of fluid motion and the Kutta-Joukowski condition (no singularities at the rear end of the airfoil) that the lift force spectrum is given by [21]:

$$S_L(f^*) = 4\pi^2 |\phi(f^*)|^2 S_w(f^*) \tag{2.51}$$

Where S_w is the spectra of the turbulence component, $f^* = fB/V$ is the reduced frequency, B is the deck width, and $\phi(f^*)$ is the Sears' function:

$$|\phi(f^*)|^2 = \left| \frac{[J_0(f^*)K_1(if^*) + iJ_1(f^*)K_0(if^*)]}{K_1(if^*) + K_0(if^*)^2} \right|^2 \tag{2.52}$$

J_0, J_1 are the Bessel function of first kind and K_0, K_1 are modified Bessel functions of the second kind. An approximation of the Sears function, given by equation 2.53[9], is plotted together with Sears function in figure 2.8.

$$|\phi(f^*)|^2 = \frac{1}{1 + 2\pi^2 f^*} \tag{2.53}$$
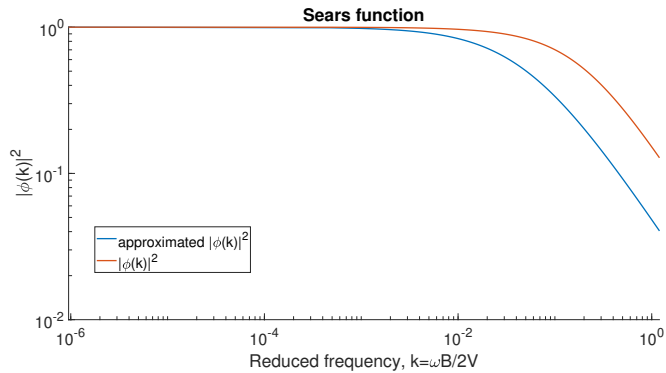
Figure 2.8: Sears' and approximated Sears' function.

Sears derived the lift formula for a two-dimensional wind in a sinusoidal vertical gust. In Sears' analysis, the velocity fluctuation is simplified by having a constant span-wise spatial distribution and is variable in the stream-wise direction only. Thin airfoil dynamic force theories depend on unique circulation functions, however, this cannot be realized for bluff bodies that experience flow separation. So the Sears function in the context of bridge deck buffeting is commonly used as an approximation for bluff bodies. Previous research, Jancauska et al. [22] and Han et al. [23], show that the Sears function underestimates the aerodynamic admittance functions for a bluff body. This will be discussed further in subsection 2.7.2.

Davenports Empirical Model

Davenport (1962) extended the theory of aerodynamic admittance developed by Sears (1938) to also apply for wind engineering. He introduced aerodynamic admittance functions relating to drag, lift and moment to longitudinal and vertical turbulence components. It is a statistical approach that uses the concept of the power spectrum to describe the stochastic loading of the stationary random type and the statistical properties of the turbulent flow. Considering that the quasi-steady aerodynamic approach is only valid for low reduced frequencies, Davenport improved this theory by suggesting the aerodynamic admittance to represent [21]:

- The loss of lift for the higher frequency components of the turbulence, also known as small gusts.

- And, the spatial variation in the flow since the force are nor necessarily due to wind fluctuations at one point but on a region surrounding a chord-wise strip.

In addition to the improvements of the aerodynamic admittance, he suggested using unsteady aerodynamic coefficients determined from the in-phase and out-of-phase components of the aerodynamic forces to evaluate the aerodynamic damping. This point goes beyond the scope of this thesis and will not be discussed further.

The following theory is based on the equations from the buffeting theory described in subsection 2.3.2. For simplicity only lift components will be considered. The wind load due to buffeting actions of the wind is expressed by:

$$F_{z,b} = \frac{\rho \bar{V} B}{2} [2C_z u + C_z' w] \tag{2.54}$$

Where C_z is the lift coefficient and C_z' is the slopes of the load coefficients curve. Given the assumption that the buffeting load is expressed as a stationary process, the load can be transformed into the frequency domain by the Fourier transform, while neglecting the effect of the cross-spectrum S_{uw}.

$$S_L(f^*) = \left(\frac{\rho \bar{V} B}{2}\right)^2 \left(4C_z^2 S_u(f^*)|A_{u,z}(f^*)|^2 + C_z'^2 S_w(f^*)|A_{w,z}(f^*)|^2\right) \tag{2.55}$$

where $S_L(f^*)$ is the spectrum of the lift force per unit length on a cross-sectional strip of the bridge deck. $S_{u,w}(f^*)$ is the spectral densities of the u and w components of the wind and $|A_{u,w,z}(f^*)|^2$ are the lift aerodynamic admittance due to the turbulence components u and w. In practice, it is challenging to differentiate the effects of u and w therefor the admittance is generally lumped and equation 2.55 becomes:

$$S_L(f^*) = \left(\frac{\rho \bar{V} B}{2}\right)^2 |A_z(f^*)|^2 \left(4C_z^2 S_u(f^*) + C_z'^2 S_w(f^*)\right) \tag{2.56}$$

The spectrum represent a point-like load and by introducing the joint acceptance function, $J_z(f^*)$, the spectrum can by transitioned into a load on a span with length l.

$$S_{F_z}(f_j^*) = S_L(f^*)|J_z(f_j^*)|^2 \tag{2.57}$$

where the joint acceptance function is given by:

$$|J_z(f^*)|^2 = \int_0^l \int_0^l \frac{S_{L_1 L_2}(\Delta y, f^*)}{S_L(f^*)} \mu_j(y_1)\mu_j(y_2)d(y_1)d(y_2) \tag{2.58}$$

μ_j is the jth mode shape and $S_{L_1 L_2}$ is the cross-spectrum of the lift force between line 1 and 2 separated by Δy. The joint acceptance function takes into account that the buffeting force is not fully correlated across the span, and that the gust will affect the structure in a different way for each mode of vibration. Therefore, there is one joint acceptance function for each mode of vibration measuring the correlation between the distributed forces across the span. By using the basis of the strip assumption, the cross-spectrum is given by:

$$\frac{S_{L_1 L_2}(\Delta y, f^*)}{S_L(f^*)} = \frac{S_{w_1 w_2}(\Delta y, f^*)}{S_w(f^*)} = coh_w^{\frac{1}{2}}(\Delta y, f^*) \tag{2.59}$$

Further, the spectrum of the response for a given mode, j, induced by the buffeting force can be calculated using:

$$S_{r_z}(f_j^*) = S_{F_z}(f_j^*)|H(f_j^*)|^2 \tag{2.60}$$

$H(f_j^*)$ is the single degree-of-freedom mechanical admittance function of mode j, and is a function of reduced frequency and damping influenced by the aerodynamic forcing.

$$|H(f_j^*)|^2 = \frac{1}{\left(1 - \frac{f^{*2}}{f_j^*}\right)^2 + \left(2(\zeta_{s,j} + \zeta_{a,j})\frac{f^*}{f_j^*}\right)^2} \tag{2.61}$$

The solution of the equation of motion, also known as the peak response, is composed by the following:

$$\hat{r} = \bar{r} + g\sqrt{\sigma_B^2 + \sum \sigma_{R_j}^2} \tag{2.62}$$

Where $\bar{r}$ is the mean response, g is the statistical peak factor, $\sigma_{R_j}^2$ is the mean square background response and σ_B^2 is the mean square modal response at or near the jth resonant frequency. The contribution of the w component of the turbulence to the mean square background and modal response can be given as:

$$\sigma_{B_z}^2 = \left(\frac{\rho \bar{V}^2 B C'}{2}\right)^2 \left(\frac{\sigma_w}{\bar{V}}\right)^2 \int_0^\infty \frac{f^* S_w(f^*)}{\sigma_w^2} |A_z(f^*)|^2 |J_z(f^*)|^2 d\, ln\, f^* \tag{2.63}$$

$$\sigma_{R_{z_j}}^2 \approx \left(\frac{\rho \bar{V}^2 B C'}{2}\right)^2 \left(\frac{\sigma_w}{\bar{V}}\right)^2 \frac{f^* S_w(f_j^*)}{\sigma_w^2} |A_z(f_j^*)|^2 |J_z(f_j^*)|^2 \frac{(\pi/4)}{(\zeta_{s,j} + \zeta_a(f_j^*))} \tag{2.64}$$

The background response covers a broad band of frequencies below the natural frequency and is the part of the dynamic response that acts quasi-statically due to the slow variation of wind speed. The resonant response is concentrated in a peak at the natural frequency which is controlled by the damping. Similar expressions can be written for torsional and lateral direction and can be found in [21].

Davenport expressed the aerodynamic admittance function using equation 2.64 and is given as:

$$|A_z(f^*)|^2 = \frac{S_F(f^*)}{\frac{1}{4}\rho^2 \bar{V}^2 B^2 C_z'^2 S_w(f)} \tag{2.65}$$

Further research of the aerodynamic admittance functions for bridge deck sections in wind tunnel tests has shown to be different from Davenports formula. Tanaka [10] found that Davenport's approximation function seamed to overestimate the aerodynamic admittance in the high-frequency domain. In contrast, Davenport was found to overestimate corresponding aerodynamic admittance in the low-frequency region.

2.7.2 Experimental Identification of Aerodynamic Admittance Functions

This subsection gives an overview of previous research on the estimation of the aerodynamic admittance functions.

Equivalent AAF

A well-known approach to identify the AAF is the Equivalent AAF method and is based on two assumptions: The first assumption is the auto-spectral method assuming that the cross-spectrum between the horizontal and vertical wind component is neglected, $S_{uw} = S_{wu} = 0$. The second assumption assumes that the same effect is reached in each component of the turbulence, giving one admittance function for each buffeting force.

$$A_{Fu} = A_{Fw} = A_F \qquad (F = L, D, M) \qquad (2.66)$$

The assumption is based on the fact that the derivative of the static wind coefficient, C'_F, is significantly larger than C_F. Conforming that the vertical component, w, plays a major role in the buffeting force and the horizontal turbulent wind velocity, u, can be neglected. The three admittance function found is a weighted average of A_{Fu} and A_{Fw} and is in most cases close to A_{Du}, A_{Lw} and A_{Mw}. For this reason, the vertical fluctuation, w, is the main contribution for the lift and moment, while the horizontal fluctuation contributes to the drag. Both assumptions in the equivalent AAF method are done in order to simplify the identification of admittance and might be inaccurate estimates.

Previous research, Davenport [9], used the assumption of equivalent AAF only considering the contribution of the vertical component of the turbulence. More recent studies have questioned this assumption by identifying six-component AAF's including the contribution of both horizontal and vertical components of the fluctuating wind velocity. These methods include measures of both u and w in addition to the cross-spectra, $S_{uw,wu}$. Zhu et al. [24] and Han et al. [23] found that the admittance function corresponding to the longitudinal and vertical components deviates from each other, indicating that it is necessary to estimate all six admittance functions.

The Response of a Suspension Bridge Deck to Turbulent Wind: the Taut Strip Model Approach

Larose's study of pressure investigation was to corroborate the use of taut strip models in the prediction of the response of long-span bridges to turbulent wind. His study was carried out in three major phases where the second one, concerns the topic of this thesis. This phase contained measurements of aerodynamic properties such as the aerodynamic admittance, the span-wise cross-correlation of the aerodynamic forces in a smooth flow, grid-generated turbulence and turbulent boundary layer flow.

Larose developed the work done by Davenport, given in subsection 2.7.1, using a more complete definition of the AAF. The definition includes the vertical and longitudinal com-

ponents of the turbulence as well as the cross-spectra between the turbulence and buffeting forces. The expression for the horizontal and vertical lift admittance is given by:

$$|A_{Lu}(f^*)|^2 = \frac{U}{C_z(0)\frac{1}{2}\rho U^2 B} \frac{S_{Lu}(f^*)S_w(f^*) - S_{Lw}(f^*)S_{wu}(f^*)}{S_u(f^*)S_w(f^*) - S_{uw}(f^*)S_{wu}(f^*)} \tag{2.67}$$

$$|A_{Lw}(f^*)|^2 = \frac{U}{\frac{dC_z}{d\alpha}\frac{1}{2}\rho U^2 B} \frac{S_{Lw}(f^*)S_u(f^*) - S_{Lu}(f^*)S_{wu}(f^*)}{S_u(f^*)S_w(f^*) - S_{uw}(f^*)S_{wu}(f^*)} \tag{2.68}$$

and moment:

$$|A_{Mu}(f^*)|^2 = \frac{U}{C_t(0)\frac{1}{2}\rho U^2 B} \frac{S_{Mu}(f^*)S_w(f^*) - S_{Mw}(f^*)S_{wu}(f^*)}{S_u(f^*)S_w(f^*) - S_{uw}(f^*)S_{wu}(f^*)} \tag{2.69}$$

$$|A_{Mw}(f^*)|^2 = \frac{U}{\frac{dC_t}{d\alpha}\frac{1}{2}\rho U^2 B} \frac{S_{Mw}(f^*)S_u(f^*) - S_{Mu}(f^*)S_{wu}(f^*)}{S_u(f^*)S_w(f^*) - S_{uw}(f^*)S_{wu}(f^*)} \tag{2.70}$$

The experimental technique provides direct measurements of the aerodynamic admittance as a function of the reduced frequency. For simplicity, the joint acceptance function is put equal to one, in order to isolate the admittance from any span-wise correlation effects.

For the execution of the test in the wind tunnel, the vertical and longitudinal turbulence was measured using a hot-wire anemometer placed at the leading edge of the model. Next, the surface pressure around the section was measured by two solid-state pressure scanners. Each scanner simultaneously measured the surface pressure from 32 equally spaced pressure taps. The aerodynamic forces were determined by integrating the measured surface pressure around the deck. The power spectra are found by a transformation from time to frequency domain using fast Fourier transform. The spectra of the forces and turbulence components constitute the basis for the evaluation of the aerodynamic admittance.

Larose found that Sears function seemed to be overestimating the admittance at low reduced frequencies, while underestimating at higher frequencies, compared to results from the measurements from the boundary layer flow. Another discovery was that the vertical component of the turbulence dominates the forces, which could be explained by the dominance of the lift slope and the low mean lift and moment coefficients at zero angle of attack. Furthermore, he found that the grid generated turbulence providing a high level of small-scale turbulence favoring the re-attachment of the flow and reducing the admittance to Sears function for a higher reduced frequency range.

Colligated Residue Least Square Method of Auto and Cross Spectra (CRLSMACS)

Zhu et al. [24] wanted to overcome the shortcomings of previous estimations methods of AAF. They introduced a new method called colligated residue least square method of auto and cross spectra (CRLSMACS). The method identifies six-component AAFs based on the well-known force and pressure measurement tests in a passive grid-generated turbulent flow.

The buffeting forces corresponding to measured data from a wind tunnel can be seen as a set of six equations. These six expressions are functions of the auto- and cross-spectra of the fluctuating wind, S_u, S_w and S_{uw}, and the six aerodynamic admittance function between the distributed buffeting force and the fluctuating wind velocity, A_{Lu}, A_{Lw}, A_{Du}, A_{Dw}, A_{Mu} and A_{Mw}. The colligated spectral residue function of the buffeting lift force, drag force and torsional moment can then be defined and the equation for the residual function for the lift is reproduced below.

$$R_L(A_{Lu}^{Re}, A_{Lu}^{Im}, A_{Lw}^{Re}, A_{Lw}^{Im}) = w_1 \varepsilon_{LL}^2 + w_2 \left[\left(\varepsilon_{Lu}^{Re} \right)^2 + \left(\varepsilon_{Lu}^{Im} \right)^2 \right] + w_3 \left[\left(\varepsilon_{Lw}^{Re} \right)^2 + \left(\varepsilon_{Lw}^{Im} \right)^2 \right] \tag{2.71}$$

$$\varepsilon_{LL} = 0.25(\rho U B)^2 \{ 4C_L^2 |A_{Lu}|^2 \hat{S}_{uu} + (C_D + C_L')^2 |A_{Lw}|^2 \hat{S}_{ww} + 4C_L(C_D + C_L') $$
$$\times \left[\left(A_{Lu}^{Re} A_{Lw}^{Re} + A_{Lu}^{Im} A_{Lw}^{Im} \right) \hat{S}_{uw}^{Re} - \left(A_{Lw}^{Re} A_{Lu}^{Im} - A_{Lw}^{Im} A_{Lu}^{Re} \right) \hat{S}_{uw}^{Im} \right] \} - \hat{S}_L \tag{2.72}$$

$$\varepsilon_{Lu}^{Re} = 0.5\rho U B \left[2C_L A_{Lu}^{Re} \hat{S}_{uu} + (C_D + C_L') \left(A_{Lw}^{Re} S_{wu}^{Re} + A_{Lw}^{Im} S_{wu}^{Im} \right) \right] - \hat{S}_{Lu}^{Re} \tag{2.73}$$

$$\varepsilon_{Lu}^{Im} = 0.5\rho U B \left[-2C_L A_{Lu}^{Im} \hat{S}_{uu} + (C_D + C_L') \left(A_{Lw}^{Re} \hat{S}_{wu}^{Im} - A_{Lw}^{Im} \hat{S}_{wu}^{Re} \right) \right] - \hat{S}_{Lu}^{Im} \tag{2.74}$$

$$\varepsilon_{Lw}^{Re} = 0.5\rho U B \left[2C_L \left(A_{Lu}^{Re} \hat{S}_{uw}^{Re} + A_{Lu}^{Im} \hat{S}_{uw}^{Im} \right) + (C_D + C_L') A_{Lw}^{Re} \hat{S}_{ww} \right] - \hat{S}_{Lw}^{Re} \tag{2.75}$$

$$\varepsilon_{Lw}^{Im} = 0.5\rho U B \left[2C_L \left(A_{Lu}^{Re} \hat{S}_{uw}^{Im} - A_{Lu}^{Im} \hat{S}_{uw}^{Re} \right) - (C_D + C_L') A_{Lw}^{Im} \hat{S}_{ww} \right] - \hat{S}_{Lw}^{Im} \tag{2.76}$$

where, w_i ($i = 1, 2, 3$) are weighted factors. "Re" and "Im" represent the real and imaginary part of the corresponding cross spectra or the aerodynamic admittance. The variables marked with " ˆ " corresponds to measured values. By applying the least square method, the real and imaginary parts of the six-component complex AAF's can be solved by seeking the minimal values of the residues defined above.

A widely used simplification is to assume full correlation along the longitudinal axes of the cross-section when identifying the AAF. CRLSMACS account for the fact that the buffeting force on a sectional model in turbulent flow is partially correlated and will affect the buffeting load. The span-wise correction function is obtained from pressure measurements of the model arranged with pressure tubes and measurements of the wind fluctuation with a cobra probe. Based on these measurements, the auto-spectra of distributed buffeting forces can be obtained from the measured buffeting forces.

The six AFFs of a flat closed-box deck of a single tower cable-stayed bridge is identified with the method described above and fitted by a target function. Three different cases of AAFs were considered for the calculation of the buffeting response: Sears function, 1.0, and the identified values using CRLSMACS. Results show that the identified aerodynamic admittance functions A_{Lw} and A_{Mw} are close to the theoretical Sears function. More importantly, the other four components of the admittance deviate significantly from the Sears function which is somewhat expected since the Sears function is only appropriate for lift and moment in the vertical direction. In addition, the vertical and horizontal AAF obtained with the CRLMACS deviates from each other, contradicting the equivalent AAF method. Last, the calculated displacements root-mean-square are compared to the displacement obtained from the wind tunnel test of a full bridge aeroelastic model. The results show that the six-component AFFs identified by CRLSMACS agree well with the results from the full-bridge model test, which demonstrates the reliability of CRLSMACS.

Six Complex Aerodynamic Admittance Functions

Han et al. [23] presented a separated frequency-by-frequency method for estimating six complex aerodynamic admittance functions using an active turbulence generator. The method considering the contribution of vertical and horizontal components of the turbulence. Similar, as for the equivalent AAF method, the cross-spectra between the two turbulence components is neglected. Considering that Sears function is complex, Han et al. [23] argued that the AAF for a bridge deck should also be complex. For this reason, the direct estimation method will cause problems, considering that the module square of AAF is estimated by the ratio of the power spectral density functions of fluctuating forces and the wind velocity fluctuations. In the study by Han et al. [23], six complex functions were identified by using the developed methodology and further compared with Sears function and Davenport's formula.

The six complex aerodynamic functions are derived theoretically using the aerodynamic lift force, drag force and pitching moment exposed to time-varying harmonic turbulent wind components, $u(t)$ and $w(t)$. Further, the FFT is applied to the aerodynamic forces and the harmonic turbulent wind components and the six complex aerodynamic functions are derived. The complex aerodynamic admittance functions χ_{Lu}, χ_{Du} and χ_{Mu} corresponding to the longitudinal turbulent component are given by:

$$\chi_{Lu}(\omega_1) = \frac{L_b(\omega_1)}{\frac{1}{2}\rho U^2 BDC_L\frac{2}{U} \cdot \frac{A_u T}{2}e^{i\theta_1}} \tag{2.77a}$$

$$\chi_{Du}(\omega_1) = \frac{D_b(\omega_1)}{\frac{1}{2}\rho U^2 BDC_D\frac{2}{U} \cdot \frac{A_u T}{2}e^{i\theta_1}} \tag{2.77b}$$

$$\kappa_{Mu}(\omega_1) = \frac{M_b(\omega_1)}{\frac{1}{2}\rho U^2 BDC_M\frac{2}{U} \cdot \frac{A_u T}{2}e^{i\theta_1}} \tag{2.77c}$$

χ_{Lw}, χ_{Dw} and χ_{Mw} corresponding to vertical turbulent component are given by:

$$\chi_{Lw}(\omega_2) = \frac{L_b(\omega_2)}{\frac{1}{2}\rho U^2 B D \frac{(C_L' + C_D)}{U} \cdot \frac{B_w T}{2} e^{i\theta_2}} \tag{2.78a}$$

$$\chi_{Dw}(\omega_2) = \frac{D_b(\omega_2)}{\frac{1}{2}\rho U^2 B D \frac{(C_D' - C_L)}{U} \cdot \frac{B_w T}{2} e^{i\theta_2}} \tag{2.78b}$$

$$\chi_{Mw}(\omega_2) = \frac{M_b(\omega_2)}{\frac{1}{2}\rho U^2 B D \frac{C_M'}{U} \cdot \frac{B_w T}{2} e^{i\theta_2}} \tag{2.78c}$$

where L_b, D_b and M_b is the FFT of the lift force, drag force and moment of the bridge deck. A_u and B_w are the amplitude of the harmonic functions $u(t)$ and $w(t)$. ω_1 and ω_2 are vibration circular frequency of $u(t)$ and $w(t)$, $\omega_1 \neq \omega_2$. ρ is the air density; B is the deck width; U is the mean longitudinal wind velocity; D is the length of the bridge deck and T is the total duration.

Wind tunnel tests of a thin plate model and a streamlines bridge section were conducted in a turbulent flow. An active turbulence generator was used for generating simultaneously harmonic oscillating longitudinal and vertical wind velocity components with different frequencies. The flow was measured by cobra probes and considered as perfect 2D flow. Before identifying the aerodynamic functions, the static aerodynamic coefficients of the section were determined. Further, the aerodynamic forces and the turbulence components were measured. Then, the six complex aerodynamic admittance functions, relating the three buffeting forces to the two turbulent wind components were identified using equation 2.77 and 2.78.

Based on the results, it was concluded that: (1) Drag-force admittance functions and admittance functions corresponding to the longitudinal component deviate significantly from the Sears function. (2) It is necessary to estimate all the six admittance function, since the admittance function corresponding to the longitudinal component are different from those corresponding to the vertical component. (3) The phases of estimated admittance functions increase with increasing reduced frequency, similar to Sears function [23]. The fact that the AAF corresponding to the vertical and the AAF corresponding to the horizontal turbulence deviates from each other, implies that the equivalent AAF method is a bit too simplified and may give inaccurate results.

2.8 Simulation Example

This section gives a description of how to use aerodynamic admittance function in the time and frequency domain. An example in Matlab is used to show a simplified method of finding the functions. The Discrete Fourier Transform is used repeatedly and will be explained.

Discrete Fourier Transform

In the time domain, the quasi-steady approximation for the buffeting load is given by equation 2.48. However, solving the equation in the time domain is time consuming and as mentioned in section 2.7, the buffeting loads can be expressed in the frequency domain by taking the Fourier transform. The fast Fourier Transform (FFT) are applied in Matlab, which is a discrete Fourier transform (DFT). However, the continuous and discrete Fourier transform and their inverse are related but not identical. For a discrete pair, discrete time and frequency scale is used. This requires that both the time and frequency scales must be finite. The discrete approximation, $F_a(i\omega)$, of the continuous Fourier transform $F(i\omega) = \int_{-\infty}^{\infty} f(t)e^{i\omega t}dt$ sampled over a finite interval including N samples is:

$$F_a(i\omega_k) = \sum_{n=1}^{N} f(t_n)e^{(-i\omega_k t_n)\Delta t} \tag{2.79}$$

where $t_n = n\Delta t$ and $\omega_k = k\Delta\omega = k2\pi/N\Delta t$, further, the DFT can be written as:

$$F_a(i\omega_k) = \Delta t \sum_{n=0}^{N-1} f(t_n)e^{-i2\pi kn/N} \tag{2.80}$$

Next, the standard definition of the discrete Fourier transform can be written as following:

$$X(k) = \sum_{n=0}^{N-1} x(n)e^{-i2\pi kn/N} \tag{2.81}$$

and the discrete inverse Fourier transform as:

$$x(n) = \frac{1}{N} \sum_{k=0}^{N-1} X(k)e^{i2\pi kn/N} \tag{2.82}$$

The $X(k)$ coefficients are complex numbers and the evaluation requires N^2 operations. To reduce the number of operations, the Fast Fourier transform algorithm were developed, which determines the DFT of an input significantly faster than computing it directly. Provided that the number of data points equals a power of 2, the number of operations is reduced to $Nlog_2 N$. This will save a great deal of time when N becomes large enough [25]. The FFT algorithm breaks the problem into smaller sub problems, where the computational cost is halved each time [26].

Time Domain Analysis

A simulation of how the admittance function affects the buffeting forces is done in Matlab in the time domain. The load coefficients are approximated to a flat plate and the turbulence components are simulated with the Monte Carlo simulations. To get an estimate on the output forces in the time domain, an assumed admittance function given by equation 2.83 is used [27]. The output is estimated by first taking the FFT of the simulated turbulence and multiplying it with the assumed admittance function. Next, the IFFT is used to obtain the output turbulence in the time domain. Then the buffeting loads in the time domain corrected by the admittance function are obtained.

$$A(f^*) = \frac{2}{(7f^*)^2}\left(7f^* - 1 + e^{-7f^*}\right) \qquad (2.83)$$

Both the buffeting quasi-steady load associated with the simulated turbulence and the buffeting load depending on the aerodynamic admittance function, are calculated according to equation 2.48, the plots for the moment and lift force can be shown in figure 2.9 and 2.10. From the plots, it can be seen that the forces deviate from each other due to the admittance function. Moreover, it is found that the standard deviation from the buffeting load without admittance is a bit higher than the standard deviation from the buffeting load with admittance functions.
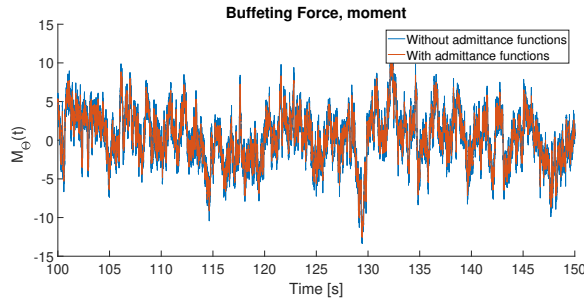
Figure 2.9: Buffeting Moment Force
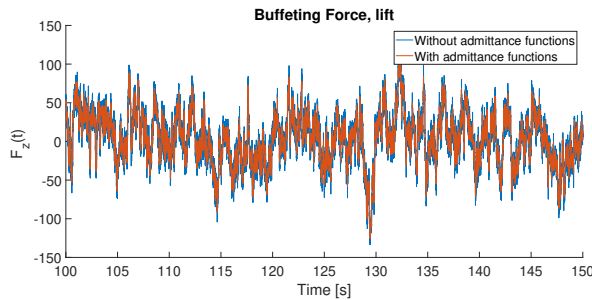
Figure 2.10: Buffeting Lift Force.

Frequency Domain Analysis

The power spectrum can be used to describe the stochastic loading as well as the statistical properties of the turbulence. Assuming that the buffeting loading is a stationary random process, the buffeting load can be transformed to the frequency domain and the buffeting load spectrum is given by:

$$S_q(x, \omega) = B_q(x, \omega) S_v(x, \omega) B_q(x, \omega)^T \tag{2.84}$$

Where S_v is the turbulence spectrum. Further, the procedure for estimating the admittance functions is presented by a Matlab example in the frequency domain. The load coefficients in, B_q, are approximated to a flat plate. The turbulence used for input is obtained by the Monte Carlo simulation. As explained in section 2.8, the turbulence corrected by the admittance functions is used as output and further referred to as filtered turbulence.

In figure 2.11, the spectra for vertical and longitudinal turbulence components are shown. The simulated turbulence is added white noise to account for measurement noise and other systematic errors that occur in recordings. The turbulence spectrum obtained in figure 2.11 is the mean spectrum of the 100 different simulated turbulence. This gives a smoother spectrum in contrast to a spectrum obtained by only one turbulence simulation.
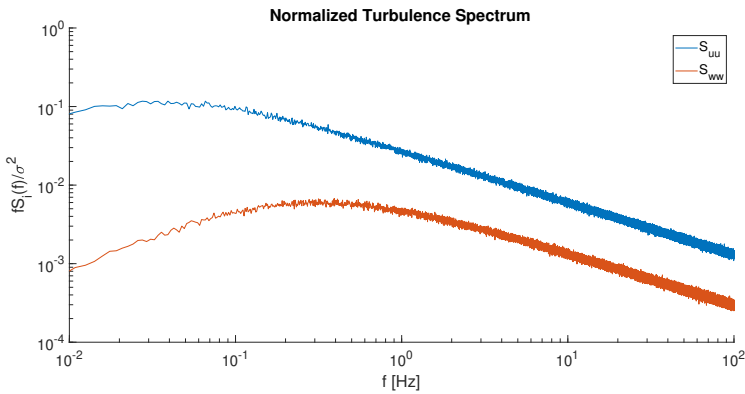
Figure 2.11: Normalized Turbulence spectrum of simulated turbulence

The buffeting load spectra are calculated by equation 2.84. Both the spectrum for the filtered turbulence and the simulated turbulence are calculated and shown in figure 2.12. As expected, the two spectra are similar for low reduced frequencies while the load spectrum with the filtered turbulence decreases faster for higher reduced frequencies.
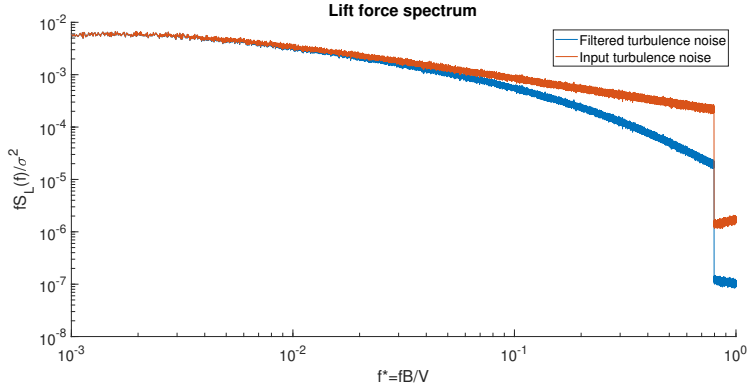
Figure 2.12: Normalized lift force spectrum for the simulated and filtered turbulence.

Furthermore, the admittance function for lift is estimated by finding the transfer function that transfer the turbulent wind into buffeting lift force. The cross-spectra between the u and w component of the turbulence is neglected. It is looked at a flat plate, for this reason it is only the vertical turbulence component, w, that contributes to the lift force. The admittance function for lift can be expressed as following:

$$A_L(f) = \frac{S_L(f)}{S_w(f)} \tag{2.85}$$

Where S_L is the lift force spectrum, based on the filtered turbulence and S_w is the vertical turbulence spectra. In order to compare the admittance function to the target admittance function, given by equation 2.83, the admittance function is normalized and expressed as:

$$A_L(f) = \frac{S_L(f)}{(\frac{\rho V B}{2})^2 C_L'^2 S_w(f)} \tag{2.86}$$

The aerodynamic admittance function estimate is compared to the target admittance function from equation 2.83, and shown in figure 2.13. It can bee seen that the estimated and the target function deviates from each other for higher reduced frequencies.

This example shows the procedure intended to find the admittance functions later in the thesis. The load coefficients are approximated to a thin plate and the buffeting loads obtained by using the filtered turbulence do not correspond to the output that will be obtained on the model under the testing. In the wind tunnel experiment, the output is loads obtained from the pressure scanner. However, the example shows a simplified method where the admittance functions are estimated.
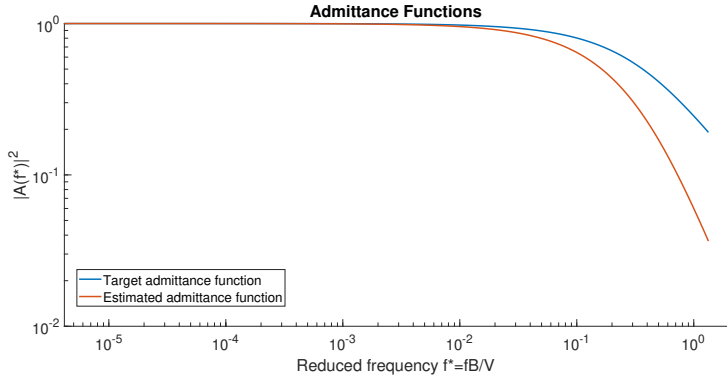
Figure 2.13: Estimated Admittance Function and the Target Admittance Function

2.8.1   Aerodynamic Admittance of a Twin-box Bridge Girder

All methods described so far in this thesis are implemented for closed-box bridges. In this section the effects of using a twin-box instead of a closed-box bridge will be discussed based on the newly developed studies by Wang et al. [28].

Wang et al.[28] investigated the characteristics of aerodynamic admittance of a twin-box bridge deck, by studying the pressure distribution, the buffeting coherence as well as comparing it to a closed-box girder bridge. The coherence function is introduced in order to describe the spatial distribution characteristics of aerodynamic forces and can be found by the following equation:

$$Coh_F = \frac{|S_F(y_1, y_2)|^2}{S_F(y_1)S_F(y_2)}, \qquad F = L, D, M \tag{2.87}$$

Where $S_F(y_1, y_2)$ are the cross-spectra between forces on two different correlation strips with distance, Δy. $S_F(y_1)$ and $S_F(y_2)$ are the corresponding auto spectrum for each correlation strip.

Buffeting forces on a twin-box girder were found to mainly be provided by the upstream-box, as the one-point force spectra of the lift and moment at this section is significantly larger than that of the downstream-box. The formation of buffeting forces acting on the bridge can be related to both the incoming turbulence and the flow separation. An explanation of why the lift on the downstream-box acts different can be due to the vortex shed from the trailing edge of the upstream-box.

The coherence of the lift and moment on the twin-box is found to be larger than those of the incident turbulent wind velocity. This indicates that the three-dimensional effects of the incident turbulent wind should be accounted for to avoid underestimation of the buffeting forces. On the other hand, the span-wise coherence of the twin-box was found to be smaller than those of the closed-box. Further, it was detected that the span-wise coherence

on the upstream-box was roughly consistent with the coherence from the closed-box, but much higher than the downstream box. The overall coherence of lift and moment on the twin-box was found to be significantly less than that of the closed-box which suggests that the downstream-box is the main factor in the overall coherence of the twin-box.

Another important mechanism of buffeting force coherence is not only the incident wind, but also the structure of the vortices. The pressure distribution of the twin-box and the closed-box is found to be similar at windward edge, while the difference at the trailing edge of the closed-box and downstream-box is more significant. The high fluctuating pressure observed at the downstream-box, is probably a result of the vortex shed from the windward box. When-Li et al. [29] studied the unsteady vortices and turbulent flow for twin-box girders with different gap widths. He found, that as the gap ratio increased the vortices shed from the windward-box, impinging on the leading edge of the downstream-box, resulted in a dramatic increase of the pressure fluctuation on the downstream-box. For this reason, the gap width should be large enough to keep the vortex shedding from the trailing edge of the windward-box and make the vortex exist in the gap region. These behaviors show the gap of twin-box girder produces a completely different flow pattern compared to the closed-box, which can explain why the coherence of a twin-box is much smaller than that for a closed-box.

The estimation of the admittance is based on experimentally determine the buffeting force spectrum, and the averaged aerodynamic force coefficients together with the wind velocity spectrum. The AAF of the twin-box, at low frequencies, was found to be higher than the AAF for a closed box. This fact indicates that the buffeting response of the twin-box can be underestimated when applying research obtained from a closed-box girder directly to a buffeting analysis of the twin-box deck.

Further investigation of the AAF of twin-box girders with different ratios of integral scale to the width of the cross-section, L_w/B, revealed that the admittance increases as the ratio increases. These results suggest that the AAF of a twin-box bridge is strongly dependent on the ratio and wind field characterises at low reduced frequencies. Comparing the AFF and the related pressure distribution, it was detected that the AAF not only depends on the incoming turbulence characteristics, but also the flow separation pattern. For this reason, the three-dimensional effects of turbulence should include both the effect of integral length scale and the effect of flow separation. It should be mentioned that as the gap ratio increases the more significant the vortex shedding becomes leading to vortex-induced peaks in the AAF.

2.9 Tube System

For the measurements of the fluctuating pressure on the twin-box section investigated in this thesis, Scanivalve pressure scanners are used. The pressure scanner is placed inside the model and connected to the measurement point through a plastic tube. As the pressure passes through the tube system, distortions can occur. To get accurate measurements it is important to take this into account.

According to He at al. [30] the distortion effect is a case of two aspects: (a) the amplitude of the signal may be attenuated or amplified due to inner friction or chamber resonance. (b) The phase of the recorded signal deviates from the original. Due to these drawbacks, the collected signal should be calibrated to reduce the distortions effects. Mechanical measures, such as adding dampers or restrictors to the system can be used to eliminate the chamber resonance. In practice, it is more convenient to correct the pressure signals numerically.

The distortion effects can be described by the frequency response function (FRF) of the tube system. The magnitude and phase of the FRF can reflect the effects of the tube system on fluctuating pressure. The FRF of a tube scanner system can be written as:

$$H(\omega) = Y(\omega)/X(\omega) = FFT(S_{out})/FFT(S_{in}) \tag{2.88}$$

Where S_{out} is the output pressure measured by the pressure scanner and S_{in} the pressure measured at the surface of the section. When the magnitude, $|H(\omega)|$, and the phase, $\phi(\omega)$, are close to 1 and 0 rad, the effects of the tube system are neglectable [31].

Wang et al. [31] analyzed the tube system parameters including the tube length, inside diameter, curvature, deflection angle, thickness, material, restrictor length, restrictor inside diameter, and restrictor place. All the tube system parameters, except the tube curvature, have non-negligible effects on the FRF of the tube system for fluctuating pressure measurement. Following, a short summary of the results by Wang et al. [31] is described.

Effects of tube length:
The length of the tubes has a great influence on the magnitude and phase of the FRF. It can be seen when the length increases the value of peak frequencies decreases, while the phase of the FRF increases. The frequency for a certain length of the tube is given by, f_0, if $f > f_0$, the signal magnitude is amplified, else the signal magnitude is minimized.

Effect of tube inside diameter:
When increasing the inside diameter of the tubes, the peak frequency raises while the phase decreases. A reason for this behavior may be caused by the tube damping, which for larger diameter results in smaller damping, and thus a greater peak value and peak frequency.

Effect of tube curvature:
Several different curvature radii were testes, few effects on the magnitude and phase of the FRF was observed.

Effects of tube deflection angle:
The deflection angle of the tubes has few effects on the accuracy, it is only necessary to avoid twisting of the tubes.

Effects of tube thickness and material:
The transmission of fluctuating pressure in the tube is a fluid-solid-interaction phenomenon, which is influenced by material strength, surface smoothness, and so on. Therefore, the tube thickness and material will influence the transmission of the pressure.

Another study by He at al. [30], the effects of the inner diameter (D) of the pressure tubes and the inner volume (V) of the pressure scanners were investigated. These are considered to be two key parameters for quantifying the distortion effects and for correcting the recorded pressure signal. Compared to the parameters discussed by Wang et al. [31], these parameters can be hard to measure directly. The FRF model for an air-tube-scanner system can be expressed theoretical, given in equation 2.89.

$$H(\omega) = \left[cosh(\phi L) + \frac{V}{V_t}(\sigma + \frac{1}{k})n\phi L \cdot sinh(\phi L) \right] \tag{2.89}$$

with:

$$\phi = \frac{\omega}{c}\sqrt{\frac{J_0(\alpha)\gamma}{J_2(\alpha)n}} \tag{2.90}$$

$$\alpha = i^{3/2}R\sqrt{\frac{\rho_s\omega}{\mu}} \tag{2.91}$$

$$n = \left[1 + \frac{\gamma - 1}{\gamma} \cdot \frac{J_2(\alpha\sqrt{p_r})}{J_0(\alpha\sqrt{p_r})} \right] \tag{2.92}$$

where $V_t = \pi R^2 L$ is the volume contained in the tube; L, R is the length and inner radius; V is the volume of the pressure scanner; σ is a dimensionless increase in scanner volume; k is a polytropic factor for air in the scanner volume; γ is the specific heat ratio of air; P_r is the Prandtl number; ρ_s is air density under room conditions; J_0 and J_2 are the 0th and 2nd order Bessel functions of the first kind.

Once the FRF of the system has been determined, the distorted pressure signals can be corrected through an inverse FFT (IFFT). Equation 2.88 gives:

$$FFT(S_{in}) = X(\omega) = Y(\omega)/H(\omega) = FFT(S_{out})/H(\omega) \tag{2.93a}$$
$$S_{in} = IFFT(X(\omega)) = IFFT(FFT(S_{out}))/H(\omega) \tag{2.93b}$$

To compute $H(\omega)$ via equation 2.89, the parameters D (inner diameter) and V (inner volume) of the pressure scanner should be predetermined. He et al. [30] proposed a method with indirect measurements. The tube inner diameter was measured with a water-weighting method, and V was determined by fitting measured FRF with theoretical predictions via equation 2.89. The study compared the measured FRF from experiments with

the theoretical FRF, for two different scanners, Scanivalve and a Honeywell scanners. It was concluded that the inner volume of the Scanivalve scanners was ignorable.

Furthermore, the theoretical FRF, given by equation 2.89 of the tube-scanner system is simulated for three different lengths, $L = 0.1m$, $L = 0.5m$ and $L = 1.0m$ with $V = 0$. The magnitude and phase of the FRF can be shown in figure 2.14. From the figure, it can be seen that phase and magnitude are close to 1 and 0 rad, for the tubes with length $0.5m$ at low frequencies. All tubes used in the experiments of this thesis are less than $0.5m$. The distortion effects are therefore neglected.
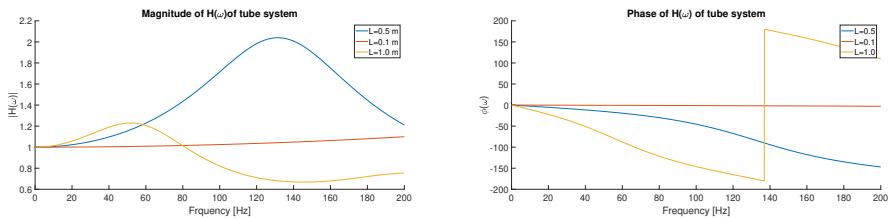
Figure 2.14: Magnitude and phase of theoretical FRF of tube-transduces sytem.

2.10 Estimation Methods for Aerodynamic Admittance Functions

The admittance functions is a transfer function between the turbulence and the buffeting forces on the structure. For bluff bodies, like a twin-box bridge, the exact expression of the admittance cannot be theoretically derived, due to complex aerodynamic forces caused by separation and reattachment of flow. In sections 2.7, several methods for estimation of the aerodynamic functions are described. In this thesis, an experimental method is conducted, where surface pressure and turbulence are measured. The admittance functions are estimated by using three different methods; the general, the equivalent and the cross-spectral method.

The general estimation method is based on the equivalent assumption, described in subsection 2.7.2. The method connects one force spectrum to one turbulent spectrum and the cross-spectra between the horizontal and vertical turbulence components are neglected. By finding the transfer function between the force spectrum and the turbulence spectrum the admittance function can be expressed as:

$$|A_F|^2 = \frac{S_j}{S_i} \tag{2.94}$$

Where S_j represents the power spectra for the drag force (D), lift force (L) or moment (M), and $S_i(f)$ is the turbulent component for the wind in horizontal (u) or vertical (w) direction. The result will be three aerodynamic admittance functions where lift and moment are connected to the vertical turbulence component, w, while drag is connected to the horizontal turbulence component,u.

The equivalent method is based on the auto-spectra of the forces and turbulence. The buffeting force spectra can be expressed as [32]:

$$S_D = (\frac{\rho V B}{2})^2 (4C_D^2 S_u |A_{Du}| + (C'_D - C_L)^2 S_w |A_{Dw}|) \tag{2.95a}$$

$$S_L = (\frac{\rho V B}{2})^2 (4C_L^2 S_u |A_{Lu}| + (C'_L + C_D)^2 S_w |A_{Lw}|) \tag{2.95b}$$

$$S_M = (\frac{\rho V B}{2})^2 (4C_M^2 S_u |A_{Mu}| + C_M'^2 S_w |A_{Mw}|) \tag{2.95c}$$

Where $A_{ij}(i = D, L, M)$ and $(j = u, w)$ is the aerodynamic admittance functions, V is the mean wind, B is the width of the section, C_D, C_L, C_M are the drag, lift and moment coefficients and $C'_D, C'_L C'_M$ are the derivatives of the drag, lift and moment coefficients. By using the assumption from the equivalent AAF method where $A_{iu} = A_{iw} = A_i, i =$

D, L, M, the equivalent aerodynamic admittance can be expressed as following:

$$|A_D|^2 = \frac{S_D}{(\frac{\rho V B}{2})^2(4C_D^2 S_u + (C_D' - C_L)^2 S_w)} \tag{2.96a}$$

$$|A_L|^2 = \frac{S_L}{(\frac{\rho V B}{2})^2(4C_L^2 S_u + (C_L' + C_D)^2 S_w)} \tag{2.96b}$$

$$|A_M|^2 = \frac{S_M}{(\frac{\rho V B^2}{2})^2(4C_M^2 S_u + C_M'^2 S_w)} \tag{2.96c}$$

Finally, the estimation of six aerodynamic admittance's will be found by the cross-spectral method in order to distinguishing between A_{Fu} and A_{Fw}. The method is based on the measured cross-spectra between the fluctuating force and each component of the turbulence. The cross-spectral equation for solving the AFFs are given as follows [33]:

$$S_{Fu} = \frac{\rho V B}{2}(a_F A_{Fu} S_u + b_F A_{Fu} S_{uw}) \qquad F = L, D \tag{2.97a}$$

$$S_{Fw} = \frac{\rho V B}{2}(a_F A_{Fu} S_{uw} + b_F A_{Fw} S_w)$$

$$S_{Fu} = \frac{\rho V B^2}{2}(a_F A_{Fu} S_u + b_F A_{Fu} S_{uw}) \qquad F = M \tag{2.97b}$$

$$S_{Fw} = \frac{\rho V B^2}{2}(a_F A_{Fu} S_{uw} + b_F A_{Fw} S_w)$$

where

$$a_F = 2C_F \qquad b_F = \begin{cases} [C_D' - C_L], & F = D \\ [C_L' - C_D], & F = L \\ [C_M'] & F = m \end{cases} \tag{2.98}$$

where $C_F, F = L, D, M$ is obtained with equation 2.20. The two AAF components for each force can then be calculated by the following expression:

$$A_{Fu} = \frac{S_w S_{Fu} - S_{wu} S_{Fw}}{a_F \frac{\rho V B}{2}(S_u S_w - S_{wu} S_{uw})} \qquad F = L, D \tag{2.99a}$$

$$A_{Fw} = \frac{S_u S_{Fw} - S_{uw} S_{Fu}}{b_F \frac{\rho V B}{2}(S_u S_w - S_{wu} S_{uw})}$$

$$A_{Fu} = \frac{S_w S_{Fu} - S_{wu} S_{Fw}}{a_F \frac{\rho V B^2}{2}(S_u S_w - S_{wu} S_{uw})} \qquad F = M \tag{2.99b}$$

$$A_{Fw} = \frac{S_u S_{Fw} - S_{uw} S_{Fu}}{b_F \frac{\rho V B^2}{2}(S_u S_w - S_{wu} S_{uw})}$$

Chapter 3

Design and Building Process of the Model

In this chapter, the design and building process of the bridge model is presented. The model was built in the Structural engineering laboratory at NTNU, Department for Structural engineering. The concept and choice of the cross-section are based on wind tunnel models from previous master thesis at NTNU. Figure 3.1 shows the completed model consisting of an inner core, aluminum pipe, molding material, Divinycell, and the mid-section made by Lexan plates and plastic tubes.

Figure 3.1: Complete wind tunnel model.

3.1 Choice of Cross Section

The bridge model in this thesis is a twin-deck bridge consisting of two identical sections. The shape and dimensions of the cross section are based on two previous master's thesis, one model showing a linear behavior [34], while the other showed a non-linear behaviour [35]. The intention with the model chosen for this thesis was to build a model in which the behaviour would be a mix of the two previous models, a weakly non-linear behaviour. Several designs of the cross-section were discussed before deciding the final shape. The
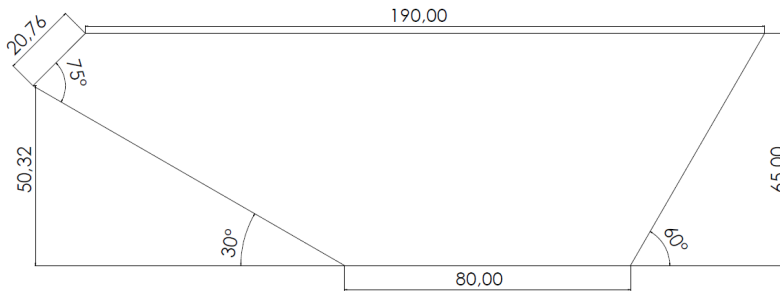
Figure 3.2: First cross section proposal

first cross-section discussed is shown in figure 3.2. Due to multiple angles, causing problems in the cutting process of the Lexan plates, it was decided that this was not a good fit.

Further, a new cross-section, shown in figure 3.3 was discussed. In this model, the right wall of the section is perpendicular to the top and bottom parts. Considering that the model needs space inside for both the aluminium pipe and pressure tube system, it was decided to increase the height of the cross-section with $15mm$. The final cross-section of the twin box model is shown in figure 3.4.
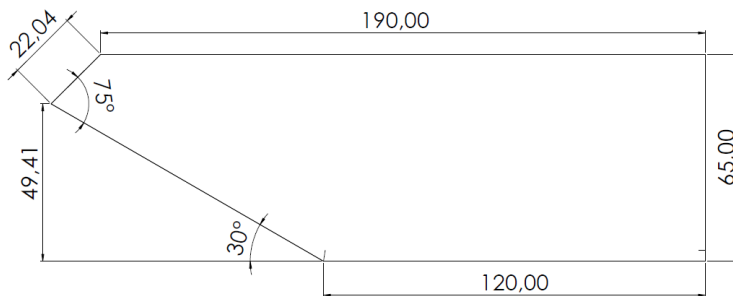
Figure 3.3: Second cross section proposal
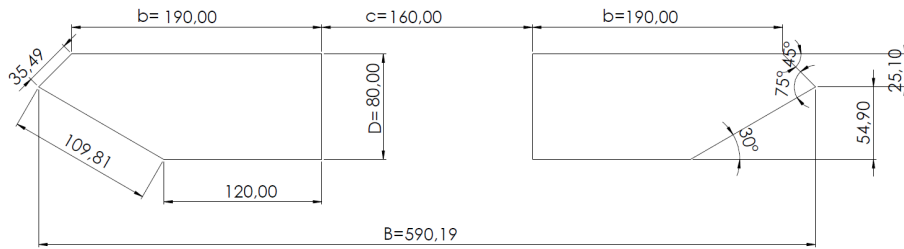
Figure 3.4: Final cross section

3.2 Material Properties

The model is made up of two identical sections consisting of three main parts; aluminium pipe, two Divinycell elements and in the middle, a section made of Lexan glass plates. The aluminium pipe is the core of the model and is the main contribution to the stiffness. In order to get the shape of the model Divinicell is used due to its low weight and formability. The mid-section is made by Lexan plates in order to have room for the plastic tubes measuring the pressure at the bridge surface. Table 3.1 shows a list of the materials used in the different parts on the sections.

Main part	Purpose	Material
Aluminium pipe	stiffness of model	50x1.5 mm Aluminium pipe
Foam model	Cross section shape Adherent Surface treatment	Divinycell 3M^{TM} Spraylim 74 Spray paint, glossy
Lexan plates	Cross section shape Pressure tubes Adherent	Lexan plates 1.02 mm Urethane tubes Glue

Table 3.1: Materials used for the twin-box model

3.3 Distrubution of Pressure Tubes

For the measurement of the fluctuating pressure at the chosen bridge deck, pressure tubes are placed at the mid-section consisting of Lexan plates. In previous studies, the distributions of the pressure tubes have been uniformly distributed over the cross-section. According to [36] the taps should be closely spaced where a strong pressure gradient is expected. By looking at the pressure distribution obtained from the wind tunnel test done by Larose [9], it is clear that the pressure gradient is significantly larger at the windward edge and then gradually decreases over the surface. The density of taps is therefore larger at the surface of attack and decreasing as the gradient decreases, giving a non-uniform distribution.

A total of 256 pressure taps was available and distributed along 6 lines aligned with the deck axis on both box sections. The first strip has a ring of 48 tubes distributed around the cross-section. In addition, the five remaining strips, acting as correlation lines, have a ring of 16 tubes, see figure 3.5. To keep track of which tube is attached to which channel on the pressure scanner, a numbering system is made to separate the tubes from each other. The numbering system consists of four numbers identifying each tube; the first number identifies which box section the tube belongs to, the second number identifies which correlation line the tube belongs to and the last two numbers identifies the tubes position in the given correlation line. For example, the tubes on the downstream box section are denoted by the numbers 1101-1148 on the first ring, 1201-1216 for the second ring up to 1601-1616 for the sixth ring. Figure 3.6 shows the numbering and placement of the first and second correlation line on the windward box.

(a)

(b)
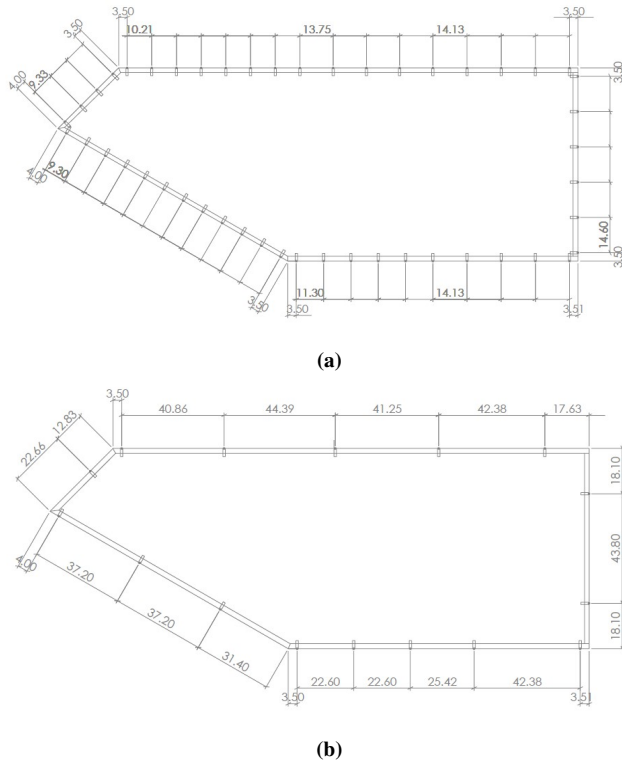
Figure 3.5: Distribution of tubes distance in millimeters, (a) first strip with and (b) second to sixth strip

The correlation lines, intended for the calculation of the span wise correlation of aerodynamic pressure, are partitioned in the span wise direction of the model. The span length is put equal to the width of the top surface of one section model, 190 mm. In order to detect correlation at different spacing's the arrangement of the lines are chosen as shown

in figure 3.7.

(a)

(b)
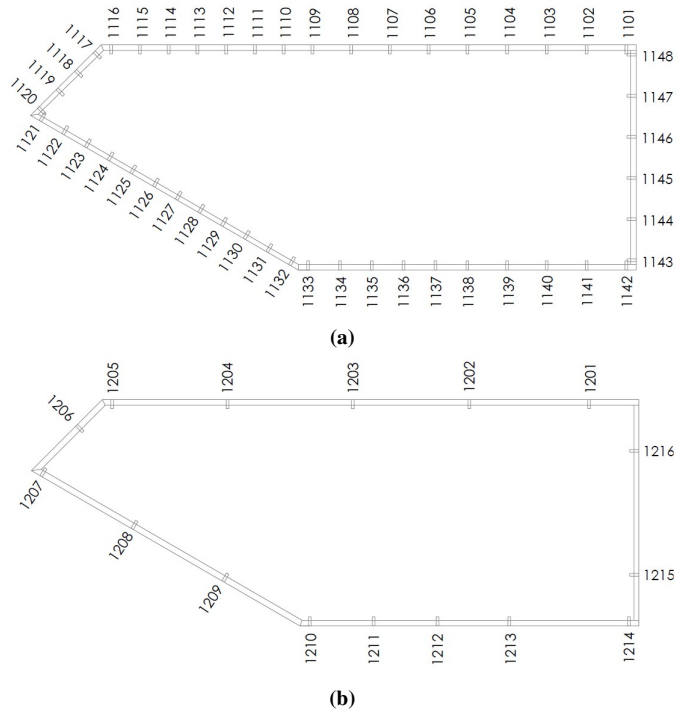
Figure 3.6: Numbering system for the first line on the windward box for (a) first strip and (b) second strip
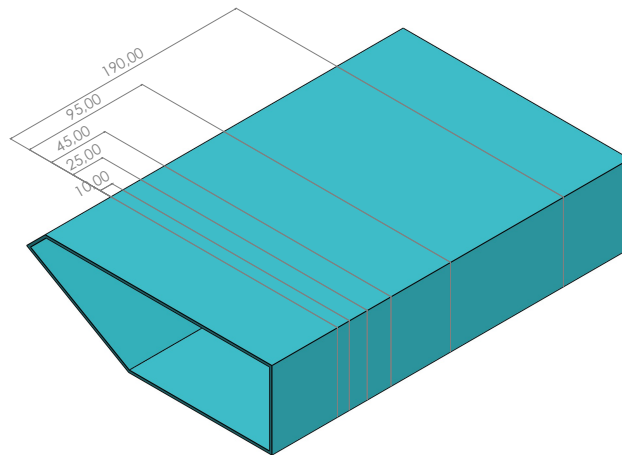
Figure 3.7: Spacing of correlation lines in millimeters

3.4 Building Process

In this section is the concept of the model and the building procedure presented. It was discussed several solutions, but the final solution fell on milling out the Divinycell and lowering the mid-section with 2mm. In this part, the Lexan plates were glued and most of the Divinycell were cut away to make room for the tube measurement system.

3.4.1 Choice of Concept

The first concept that was discussed is shown in figure 3.8. A suggestion of placing the Lexan plates over the entire length of the model, to improve stiffness, was first proposed. In addition, to have enough room in the mid-section for the tube system, the aluminium pipes were suggested to only penetrate the ends of the model. This concept would not give the desired stiffness of the model and therefore a new solution was suggested.

(a)

(b)
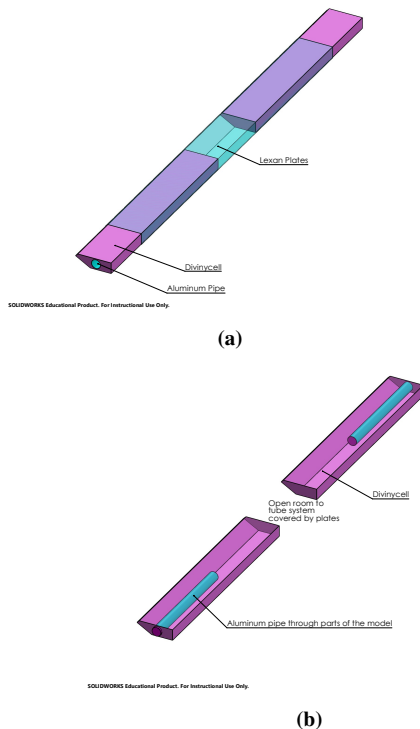
Figure 3.8: Sketch of the first concept of the model

The new solution proposed was to put the aluminium pipe throughout the model and only have Lexan plates in the mid-section of the model. This gave the required stiffness and was easier to implement, and therefor concluded to be the final solution.
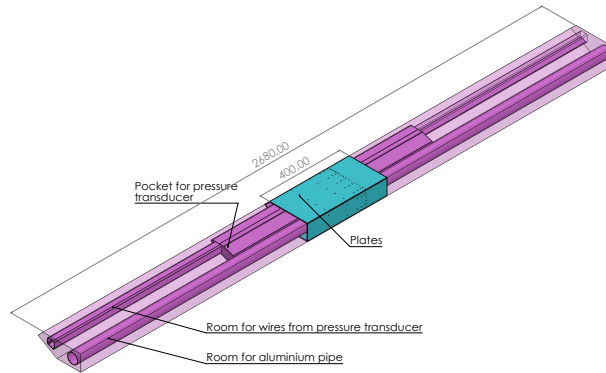
Figure 3.9: Sketch of Model

The first step in the building process was to sketch the final concept in SolidWorks. The sketches were used by the milling machine to mill out the model. First, the inside geometry, the room for pipes, wires and pressure scanners, was milled out on four Divinycell parts. Next, the aluminium pipes and the top and bottom parts of the model were glued together forming the base of the two sections of the twin-bridge. Last, the outside geometry of the model was milled out.

Figure 3.10: Milling of the inside geometry of the model.
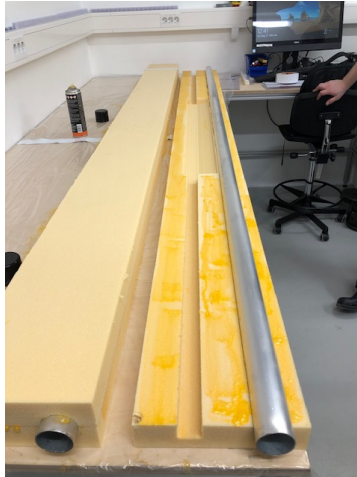
Figure 3.11: Gluing of aluminium pipe.

It is necessary to have easy access to the pressure scanner, placed inside the model, due to the possibility that the tubes detach from the pressure scanner or other complications can occur. Several solutions were discussed. The first suggestion was to cut a part of the Divinycell in two, making it possible to take the upper part on and off. The parts would be mounted together with small screws to be secure. A sketch on the solution is shown in figure 3.12, where the green part is the suggested cut in the model.
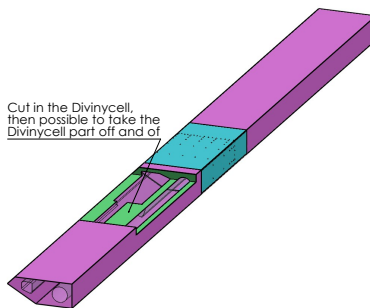
Figure 3.12: Discussed solution of opening to the pressure scanner.

It was concluded that this solution would not be optimal in the wind tunnel test and a new proposal was further discussed. The new proposal was based on making cuts in the top part of the model, over the scanners, and closed with Lexan plates. This was the chosen concept and a sketch can be shown in figure 3.13.

(a)

(b)
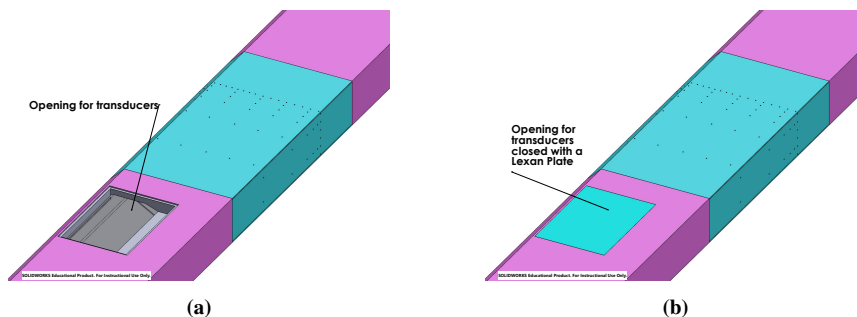
Figure 3.13: Solution of openings to the scanners.

The mid-section of the model was trimmed and milled out to make room for the tube system. Last, to prevent dust from the Divinycell, the model was surface treated with a glossy spray painting. The finished sections can be shown in figure 3.14

(a) Outside Geometry.

(b) Details of middle section.

Figure 3.14: Geometry of the model.

3.4.2 Application of Lexan Plates and Pressure Tubes

The Lexan plates are placed in the mid-section of the model, as shown in figure 3.9. Each plate was first sketched in SolidWorks and further milled out in the laboratory. Then, the 256 holes for the pressure tubes, with the arrangement as described in section 3.3, were drilled out. Next, the pressure tubes are pulled through the holes and glued to the Lexan plate as shown in figure 3.15 (a).
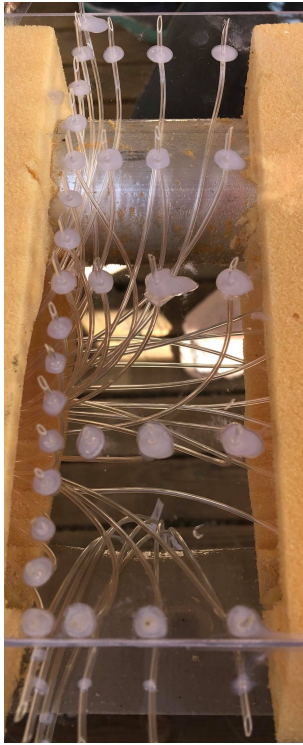
(a) Details of tubes glued to the Lexan plate

(b) Arrangement of tubes, and application of tubes on scanner

(c) Finished section model with tubes, Lexan plates and pressure scanners

Figure 3.15: Application of Lexan plates and tubes

The tubes are cut perfectly down to make the surface as smooth as possible. Before attaching the plates to the model it was found that a couple of the plates were longer than intended. For this reason the plates had to be cut and polished down by hand leading to some rough edges where the plates meet. An attempt of fixing the edges were made by applying glue to make a smoother transition between the plates, and to prevent the wind from entering through the gaps. These defects may lead to some errors in the measurements of the pressure.

Before gluing the plates together the tubes were threaded through the model and into the opening for pressure scanners as gentle as possible to prevent curving of the tubes. The tubes are then cut as short as possible which together with the curvature are factors that can affect the accuracy of the measurements as mentioned in section 2.9. At last the tubes are attached to the pressure scanners and placed inside the model, see figure 3.15 (c).

When both sections of the twin-box bridge was completed the sections were mounted on a plate with a gap width of 160 mm, giving a 241 mm center spacing between the aluminium pipes. It should be mentioned that the gap width has significant impact on the aerodynamic admittance, and should be chosen such that the gap width is large enough to keep the vortex shedding from the trailing edge of the windward-box and make the vortex exist in the gap region as described in section 2.8.1. Due to limited time in the laboratory it was decided to use and existing plate and the recommended gap width was therefore not considered. The attachment point where the aluminium pipes are connected to the plate is a load cell, and the plate are then again attached to the mounting system in the wind tunnel, figure 3.17.
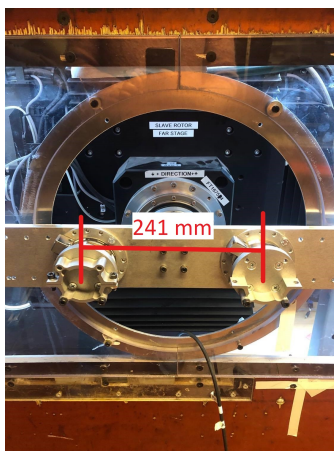
(a) Center spacing between aluminium pipes   (b) Gap with
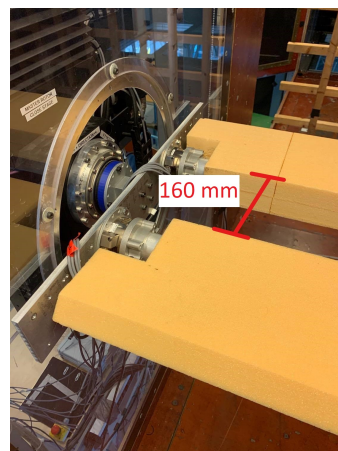
Figure 3.16: Details of the mounting system

Figure 3.17: Model mounted in wind tunnel

Chapter 4

Wind Tunnel Testing

The wind tunnel tests of the twin box model were done at the Fluid Mechanics Laboratory at Department of Energy and Process Engineering, NTNU. In this chapter, the experimental setup, the monitoring system and the tests in the wind tunnel are described. The main purpose of the wind tunnel testing is to investigate the pressure distribution caused by the incoming flow and to estimate the aerodynamic admittance functions.

4.1 Experimental Setup

This section describes the instruments needed for the wind tunnel test and how all the components are assembled. The three instruments required to achieve pressure and wind data are the Pitot probe, TFI Cobra probe and the MSP4264 Miniature Pressure Scanner.

The objective of the experimental setup was to synchronize the cobra probe and MSP with each other in order to register identical time histories, while the Pitot probe was used to measure the wind velocity. Due to lockdown at NTNU and the Fluid Mechanics Laboratory the authors of this thesis were not able to conduct the work of synchronizing the components and test them before the final wind tunnel test. Fortunately, this was done by the supervisor, Ole Andre Øiseth, and PhD candidate, Øyvind Wiig Petersen, to be ready when the lockdown was terminated. However, the components and the experimental setup was documented and described in the following sections. A flow chart illustrating the experimental setup from sampling to processed data are shown in figure 4.1.
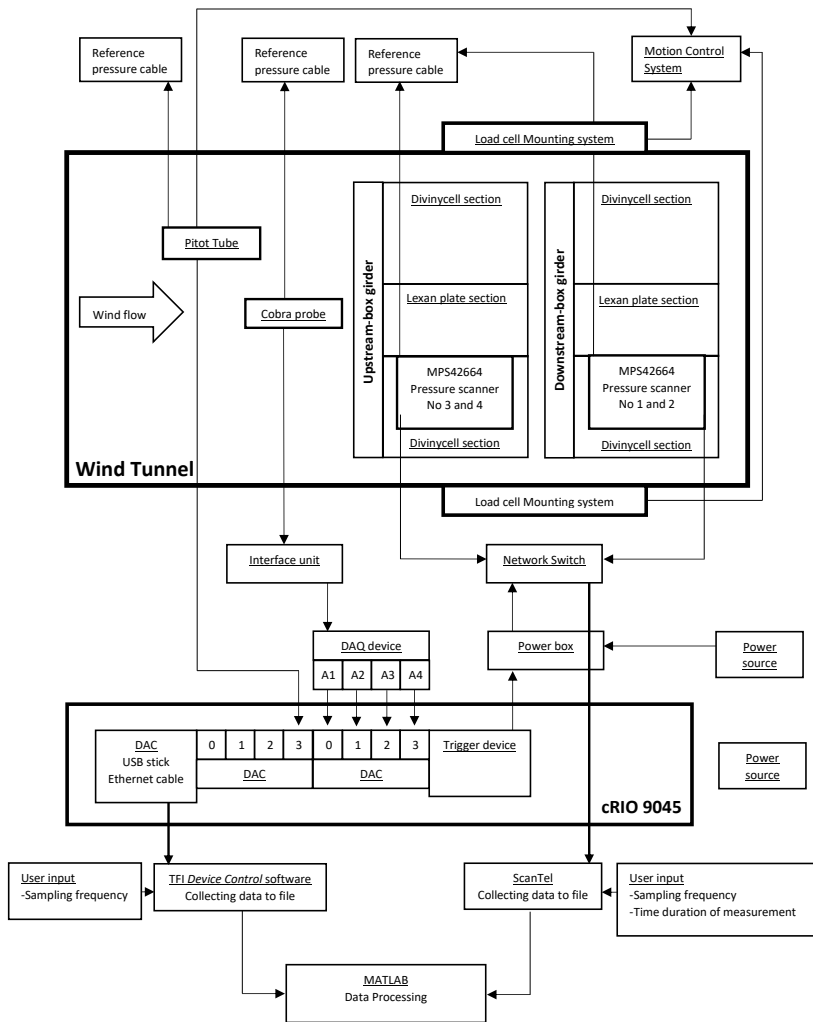
Figure 4.1: Flow chart of experimental setup

4.1.1 General Experimental Setup

Figure 4.2 shows the experimental setup in the wind tunnel.
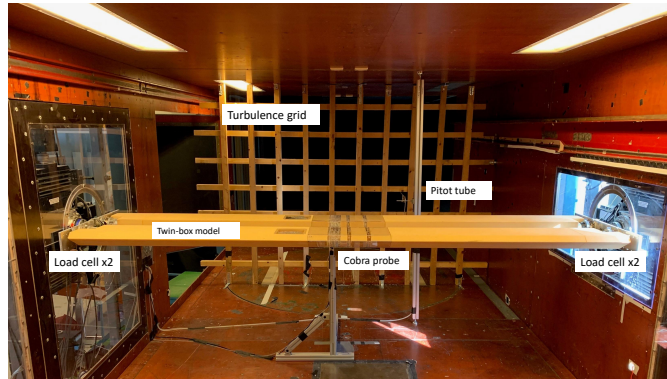
Figure 4.2: Setup inside the wind tunnel.

A uniform grid, generating turbulent flow, was placed 2 m upstream of the twin box model. Due to limited time in the wind tunnel laboratory, other positions of the grid were not tested, nor was an optimal wind field created. The grid setup can be shown in figure 4.2. The Cobra Probe, used to measure the turbulence, was placed 6 cm from the windward edge of the upstream-box, as shown in figure 4.3.

(a) Cobra Probe setup

(b) Distance from Cobra Probe to windward edge of upstream box.

Figure 4.3: Cobra Probe setup.

A clamping mechanism was used to connect the model to the load cells. The load cells are used to measure the wind induced forces on the section model, and each load cell measures three forces and three moments. Further, the load cells are connected to an actuator, which

can move the section into any desired 3 degrees of freedom. In figure 4.4, the load cells connected to the twin-box section model are shown.
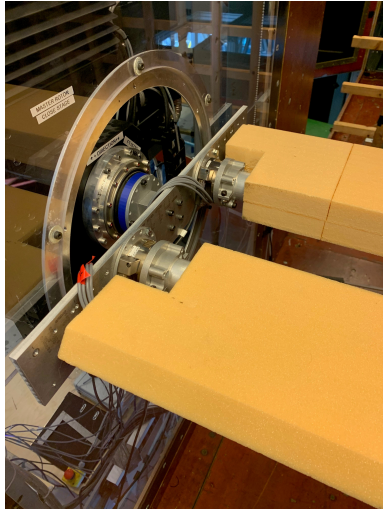
Figure 4.4: Load cells connected to the twin-box.

The pitot probe was placed upstream of the twin-box model, close to the turbulence grid to avoid turbulence effects when measuring the mean wind speed.

During the testing, it was observed vibrations, due to vortex shedding and it was decided to increase the stiffness of the twin-box model. A stiffening system with two timber beams supporting the model, shown in figure 4.5, was used. The tests were conducted with and without stiffening system.
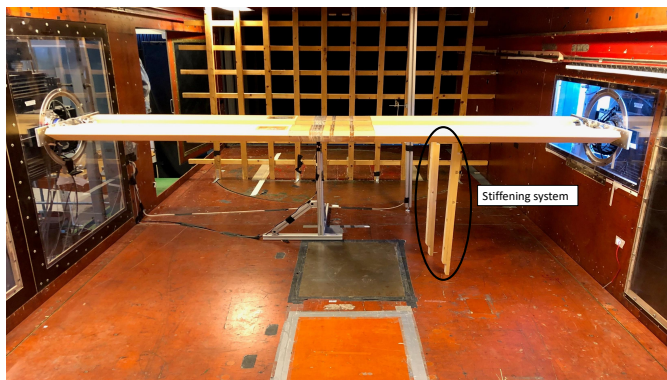
Figure 4.5: Stiffening system of the twin-box model.

4.1.2 MPS4264 – Miniature Pressure Scanner

Measurements of the fluctuating pressure on the cross-section of the bridge when exposed to wind are done by four MPS4264 Miniature pressure scanners. The pressure scanners are described by Scanivale in the *Hardware & Software manual* [37] as:

> The MPS4264 is a 64 channel, intelligent, miniature pressure scanner. Each MPS4264 series scanner incorporates 64 individual piezoresistive pressure sensors. In addition to the pressure sensors, the MPS4264 integrates all of the electronics for the analog-to-digital (A/D) conversion process and a processor running a digital signal processor (DSP) operating system supporting the engineering unit conversion process and all communications overhead.

The MSP is specifically designed for experiments conducted in wind tunnels where operational conditions are very space-constrained and pressures do not exceed 50 psi. For this reason and its small size, the MSP is user friendly and is a perfect fit for wind engineering applications.

For the wind tunnel tests conducted in this thesis a total of four MSP pressure scanners was used, two in the upstream-box and two in the downstream-box. The MSP's are configured to scan with an external trigger signal which synchronizes the data collection between the MSP and the Cobra probe. The trigger signal is received through the power box from the trigger device. Communication with the MPS's is through Ethernet cables connected to the computer via a network switch. This communication is established by the communication utility *ScanTel*, which is a text based, command line program that allows the user to modify the configuration variables and collect data in both TCP/IP and UDP format. All connections and components can be seen in the flow chart in figure 4.1.

The pressure tubes from the Lexan plate section are attached at the 64 input ports at the top of each MPS. In appendix A an overview of which pressure channel belongs to which pressure hole on the surface of each section is presented. An additional plastic tube is connected to the reference port (REF) while the other end is put outside the wind tunnel. The purpose of the tube is to serve as a reference pressure and to ensures that when a zero offset calibration is performed no unwanted offsets are introduced. All connectors and ports on the MPS4264 Pressure scanner are shown in figure 4.6.
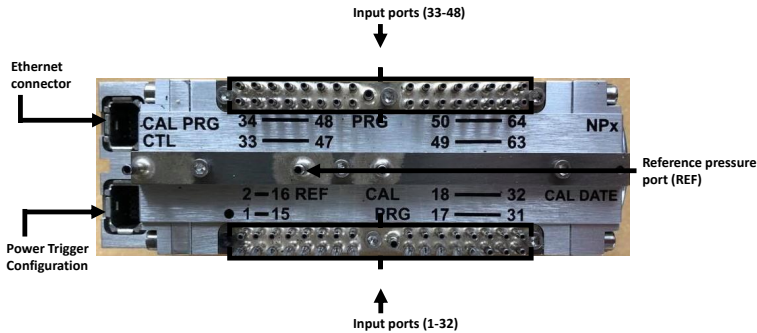
Figure 4.6: MPS4264 Miniature Pressure Scanner

4.1.3 Cobra Probe

Measurements of the wind data in the wind tunnel test is done by a Cobra Probe instrument. The Cobra probe is described by TFI [3] as:

> The Cobra Probe is a multi-hole pressure probe that provides dynamic, 3-component velocity and local static pressure measurements in real-time. The Probe is capable of a linear frequency-response from 0 Hz to more than 2 kHz and is available in various ranges for use between 2 m/s and 100 m/s. It can measure flow angles in a $\pm 45°$ cone, all six Reynolds stresses and allows calculation of other higher order terms.

The figure below show the Cobra Probes main features
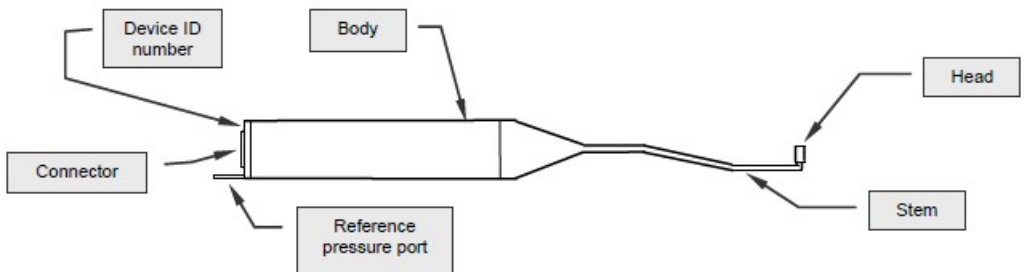
Figure 4.7: Series 100 Cobra Probe main features by TFI [3]

The components needed for recordings with the Cobra probe are explained and shown in figure 4.8.

- Series 100 Cobra probe

- – The cobra probe is connected through the interface unit via the 7-pin connector connected to a a group of four channels on the DAQ system labeled A1-A4.

- The DAQ device

  - – Transfers analogue signal to digital signal.

  - – Copies data in order to view the plots of time or frequency spectra in TFI Device Control System on the computer.

- DAC card placed in the cRIO

  - – The data recorded from the cobra probe goes directly to the DAC card in the cRIO.

  - – It is important that the cables from the DAQ device labeled A1-A4 is inserted in the right order from 0 to 3 in the DAC card in the cRIO.

  - – Data from the cRIO is stored on the USB stick.

- Ethernet cable gives connection between the cRIO and the computer.

- Reference pressure cable

  - – Connected to the Cobra probe on one side while the other end it put outside the wind tunnel.
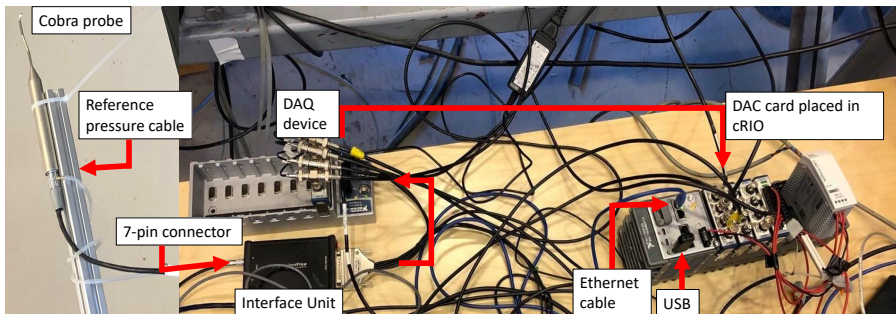
Figure 4.8: Overview of setup for Cobra probe

4.1.4 Pitot Probe

A Pitot probe is used to measure the wind-velocity inside the wind tunnel during tests. It consists of two tubes measuring the static and stagnation pressure at the same point. The difference between these pressures is contributed to the velocity pressure and used to calculate the wind speed. Before starting the test the pitot probe needs to be calibrated for different wind speeds with a manometer. A reference pressure cable connected to the pitot probe is put outside the wind tunnel with the other reference pressure cables from the Cobra probe and MSP pressure scanners.
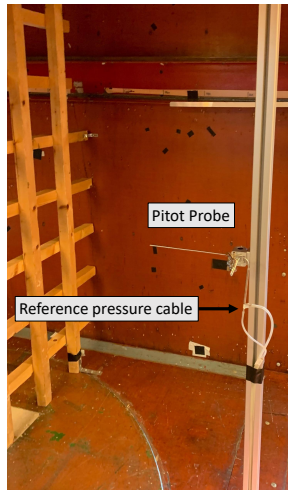
Figure 4.9: Setup of the Pitot probe

4.2 Wind Tunnel Tests

During the tests, the experimental setup described in section 4.1 was used. Tests were performed in both laminar and turbulent wind conditions and with and without the stiffening system. An overview of the tests is presented in table 4.1.

Filename	Direction	Flow	RPM	Notice
Master2020TD_20_00_001	Torsional	None	0	
Master2020TD_20_00_003	Torsional	Turbulent	320	
Master2020TD_10_00_002	None	Turbulent	320	
Master2020TD_10_00_003	None	Turbulent	320	
Master2020TD_10_00_004	None	Turbulent	490	
Master2020TD_10_00_005	None	Turbulent	180	
Master2020TD_10_00_901	None	Turbulent	220	Stiffening system
Master2020TD_10_00_902	None	Turbulent	300	Stiffening system
Master2020TD_10_00_903	None	Turbulent	450	Stiffening system
Master2020TD_10_00_904	None	Laminar	220	Stiffening system
Master2020TD_10_00_905	None	Laminar	271	Stiffening system
Master2020TD_10_00_906	None	Laminar	397	Stiffening system

Table 4.1: File history.

Without the stiffening system, vortex shedding was observed in a region between 200-300 RPM in the turbulent flow. The vibrations disturb the test results and should be excluded from the test regime. The vortex-induced vibrations happen when the frequency from the harmonic vortex shedding load coincides with the natural frequency of the section model, the measured forces will increase and vortex-induced vibrations occur. Besides, lock-in causes vibrations to built up close to the critical speed. Due to this, the range of velocities close to the critical vortex-induced vibration is excluded from the test regime.

The turbulence intensity for each test was calculated using equation 2.30. Optimally the Pitot probe should be used when measuring the mean wind velocity. Compared to the cobra probe, the pitot probe gives more accurate results. However, for the test with the stiffening system the wind tunnel motion control system was turned off and measures from the Pitot probe were therefore not collected. For this reason, the mean velocity for tests with stiffening is found by meaning the u-component from the Cobra probe. Examination of tests containing measurements from both pitot probe and cobra probe revealed that the cobra probe measured lower values for the mean wind velocity. This trend amplifies when the wind speed increases, indicating that the mean wind velocity for the test performed with stiffening will not be entirely accurate. Values of the turbulence intensity of each test are given in table 4.2 to 4.4.

Filename	I_u	I_w	V[m/s]	RPM
Master2020TD_10_00_002	11.3%	9.2%	6.7	320
Master2020TD_10_00_003	11.3%	9.2%	6.7	320
Master2020TD_10_00_004	10.9%	8.6%	10.1	490
Master2020TD_10_00_005	12.5%	10.4%	3.5	180

Table 4.2: Turbulence intensity in tubulent flow

Filename	I_u	I_w	V [m/s]	RPM
Master2020TD_10_00_901	13.1%	10.7%	3.9	220
Master2020TD_10_00_902	12.5%	10.4%	5.4	300
Master2020TD_10_00_903	12.2%	9.8%	8.3	450

Table 4.3: Turbulence intensity in turbulent flow with stiffening system

Filename	I_u	I_w	V[m/s]	RPM
Master2020TD_10_00_904	1.3%	1.5%	4.6	220
Master2020TD_10_00_905	1.3%	1.4%	5.7	271
Master2020TD_10_00_906	1.4%	1.3%	8.4	397

Table 4.4: Turbulence intensity in laminar flow with stiffening system

4.2.1 Static Tests

The static tests were performed to get estimates on the static force coefficients (lift, drag and moment). The wind speed was kept constant, with a mean wind velocity equal 6.5m/s, while the angle of attack of the twin box model was changed. The angle of attack was continuously changed, with a max amplitude of 8 degrees. The pressure scanners were not used in this test and force measurements were done by the load cells at the ends of the bridge. A still air test was done as a reference and control check.

4.2.2 Admittance Tests

The admittance tests were performed for different wind velocities for both uniform and turbulent flow, the angle of attack was equal to zero. From these tests, the aerodynamic admittance functions can be estimated. The first tests were run without the stiffening system in a turbulent flow. For the next tests, due to vibrations, the stiffening system was installed. Different velocities were tested for both uniform and turbulent flow. Due to the reduction of the velocity caused by the turbulence, the RPM had to be increased in the test with the uniform flow to achieve the same velocity. During a test, turbulence components, mean wind and surface pressure are measured. In addition, the load cells measured the forces acting at the end of each section when the the stiffening system was not installed.

4.3   Accuracy and Error Sources in the Experimental Setup

Inaccuracies and errors in the experimental setup may lead to inaccurate results. These may arise from both errors in the measurements and inaccurate assumptions concerning the test setup. For instance, when the twin box model was mounted inside the wind tunnel, a level meter was used to place the two sections correctly. Since this is done manually, some errors can be related to the placement of the girders. Further, the Lexan plates with the tube system were not completely sealed. The wind can therefore penetrate the section affecting the flow pattern and the pressure distribution. This uncertainty will be discussed further in the results.

Measured signals can be exposed to unwanted noise and vibration. Sources to noise in the wind tunnel tests can be due to electrical noise, or loose components. Electrical noise was detected in the measurements of the forces in the load cells during the test and for some of the measurements, it was decided to unplug the wiring from the load cells.

Other sources of disturbance in the signal are dynamic amplification and signature turbulence. The dynamic amplification is due to vibrations around the eigenfrequency of the test model and can be seen as peaks around the eigenfrequency in the power spectral density plots. Signature turbulence may be formed by the mix of unsteady vortexes in the gap and in the wake of the model that produces dynamic forces onto the section.

In addition, pressure changes in the reference pressure tube from the Pivot probe and the Cobra Probe can occur. For instance, if a door closes it can lead to small changes in the pressure inside the laboratory and affect the measured reference pressure. Last, it was detected that three of the pressure tubes, nr 1307, 1407 and 1507, had detached from the Lexan plates before the tests were executed. There are uncertainties about how this will affect the measurements and will also be discussed further in the results.

4.4 Post Processing

For each test executed in the wind tunnel, separate files were saved for the Cobra probe, pitot probe, MPS pressure scanners and load cells. The measurements and data acquisition systems were measured at a sampling rate of 200Hz per second. Data processing from raw to processed data with desired units was done by the supervisor. All time series were controlled and cut to avoid disturbance and noise at the start and end. Further processing of the data necessary to achieve the desired results is done in Matlab.

4.4.1 Pressure Data

The purpose of measuring the pressure with the pressure tubes is to estimate the aerodynamic forces around the twin box section for different wind velocities and flow conditions. The scanners measured the pressure perpendicular around the surface of the twin-box. Further, the surface pressure was integrated over the cross-section to obtain the aerodynamic forces on the twin-box model. Two different methods to estimate the aerodynamic forces were investigated, the piece-wise point load method and the interpolated method. The Matlab scripts can be seen in B. For the piece-wise point load method, the forces are considered as point loads located at the pressure tubes holes. For the interpolated method the forces are considered as a distributed load around the cross-section. The mean value of the pressure from the time series was used to obtain a static pressure and load representation, and the time series of the forces were used to obtain force spectra.

The surfaces and angles on the upstream and downstream deck are defined as in figure 4.10, and used when calculating the forces and moments in Matlab.
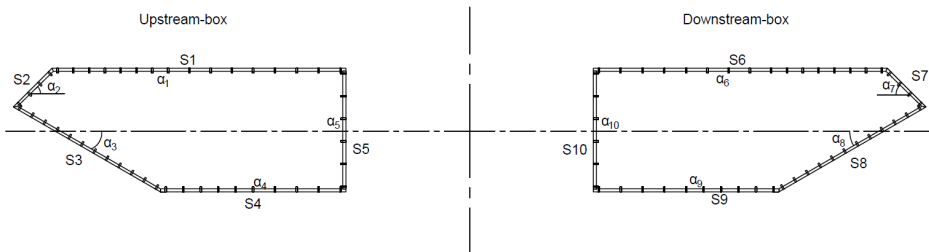
Figure 4.10: Definitions of the surfaces and angles on the twin-box model.

Further, when calculating the the moments, the definitions of positive and negative forces are shown in figure 4.11.
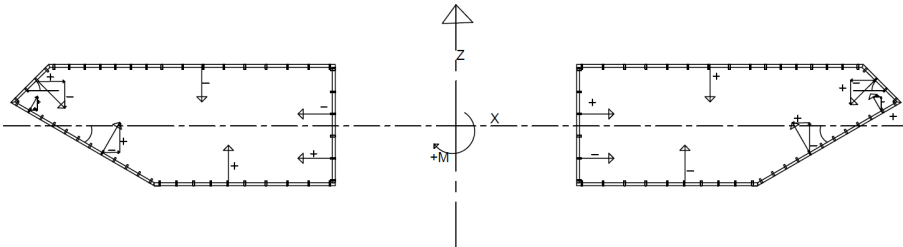
Figure 4.11: Moment calculations

The piece-wise point load method considers the pressure and load as point pressures and loads located at the pressure tubes holes. The loads are obtained by multiplying the pressure with a surface area. This surface area has a with equal 1 meter and the width is considered as the sum of two half surfaces between two pressure tubes. For the pressure tubes at the end, the width is assumed to be the sum of the half distance between the neighbor pressure tube and the length to the end of the surface. An illustration of the widths on the top surface is shown in figure 4.12, where a1-a16 denotes the width of the associated pressure tube.
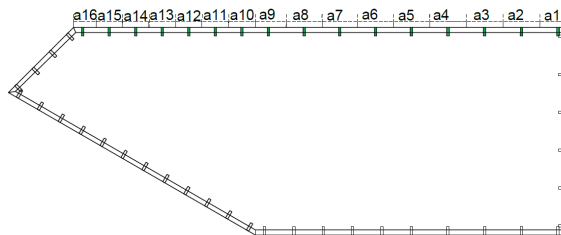
Figure 4.12: Illustration of the widths of the top surface, a1-a16 denotes the width to the associated pressure tubes.

Figure 4.13 and 4.14, shows an example of the pressure and load distribution. Pressure pointing inward is defined as pushing pressure and pressure pointing outward is defined as suction.
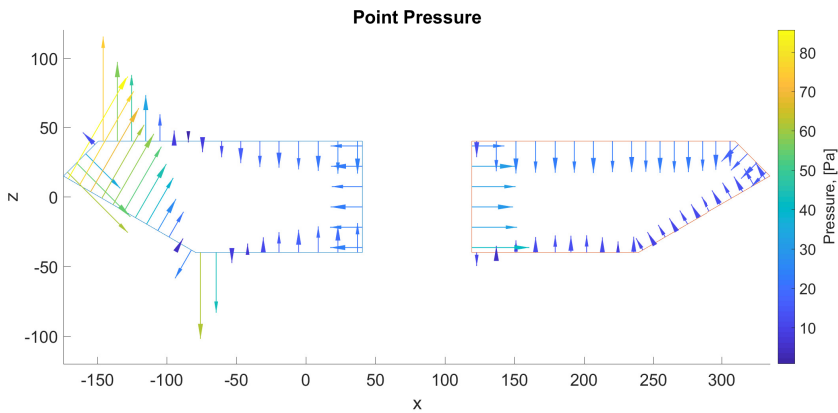
Figure 4.13: Example of point pressure Distribution.
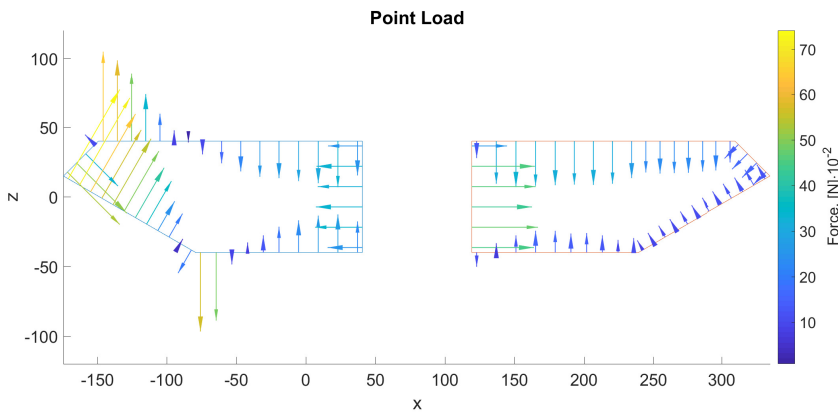
Figure 4.14: Example of point load distribution

The interpolated method calculates the aerodynamic forces and moments, as a distributed load over the surfaces of the cross-section. The distributed pressure and loads are calculated by a spline function in Matlab, where distributed pressure is piece-wise defined by the pressure data from each pressure tube around the twin-box cross-section. To obtain the distributed pressure with the spline function, query points with a spacing of 0.001 m were arranged around the section. Further, the distributed pressure is determined by cubic spline interpolation of each pressure signal and the associated location of the tube. The distributed load was obtained by multiplying the pressure with an area equal to $0.001 \cdot 1 m^2$, except for the ends of all surfaces which were multiplied with $0.001 \cdot 1/2 m^2$. Figure 4.15 and 4.16 shows the pressure and load distribution for a random time series obtained with the interpolated method.
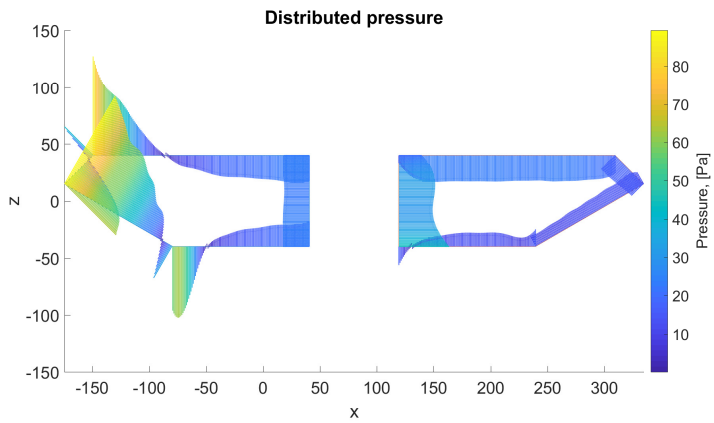
Figure 4.15: Example of interpolated pressure distribution.
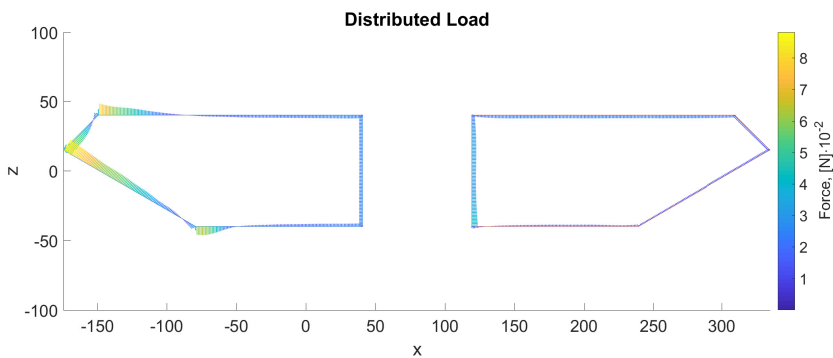
Figure 4.16: Example of interpolated load distribution.

4.4.2 Force Spectra

The time series of the forces, obtained from the pressure measurement and transformed into loads by the methods described above, are transformed into the frequency domain by the Welch method using 10 Hanning windows. The spectral densities of the forces are plotted with logarithmic axes and the different correlation lines are compared. The forces are further used to find the coherence between the six correlations lines with equation 2.87.

4.4.3 Wind Data

The raw data files obtained from Cobra probe during tests are collected in Voltage. The processing of the raw voltage data to velocity data was done by the PhD candidate Øyvind Wiig Petersen and given to the authors of this thesis for further use.

In order to use the wind data to estimate the aerodynamic admittance of the twin-box girders the processed velocity data is transferred to the frequency domain. The time series of the turbulence used for the spectral density function consists of zero mean signal, only giving the fluctuating part of the wind. The estimation of the power spectral density function is done using the Welch method which has the advantage of reducing noise in the estimated spectra. The data was transformed using 10 Hanning Windows.

4.4.4 Admittance Estimates

The aerodynamic admittance functions for the twin-box bridge were all estimated in the frequency domain. All the data obtained from the MSP pressure scanner and the cobra probe are zeroed by subtracting the mean of the signal. The spectral densities of the turbulence and the forces are then found by the Welch method as described in subsection 4.4.2 and 4.4.3.

Three different approaches were used for estimation of the Admittance functions, general, equivalent and cross-spectral approach. All methods are described in section 2.11 with their respective equations. The estimated admittance functions are plotted with logarithmic axes together with the Sears function for comparison. The script used for the estimation of the aerodynamic admittance functions is attached in Appendix C.

Chapter 5

Results and Discussion

5.1 Turbulence Spectra

The wind spectrum for each test was analysed to detect possible errors, that could cause inaccuracies in the final estimation of the admittance functions. Figure 5.1 shows the vertical and horizontal spectra for both turbulent and uniform flows. The spectra are a good representation of the wind flow and all other tested velocities are similar to those presented below.
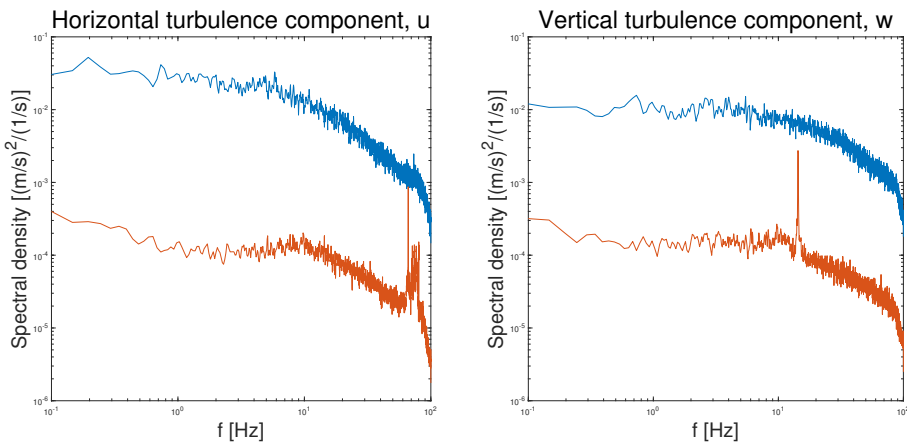
Figure 5.1: Spectra of turbulent, $V = 3.5m/s$, and uniform, $V = 4.6m/s$, flow in horizontal, u, and vertical, w, direction

As seen in figure 5.1 the turbulent wind spectrum has significantly higher spectral densities than the laminar flow, as expected. Another observation was that high peaks were detected in the laminar wind spectrum. These peaks are possibly caused by vibrations of the cobra probe at one of the Probe mount's natural frequencies. Since there is almost no turbulence

in these data, the natural frequencies of the probes mounting system will be significantly higher than rest of the signals.
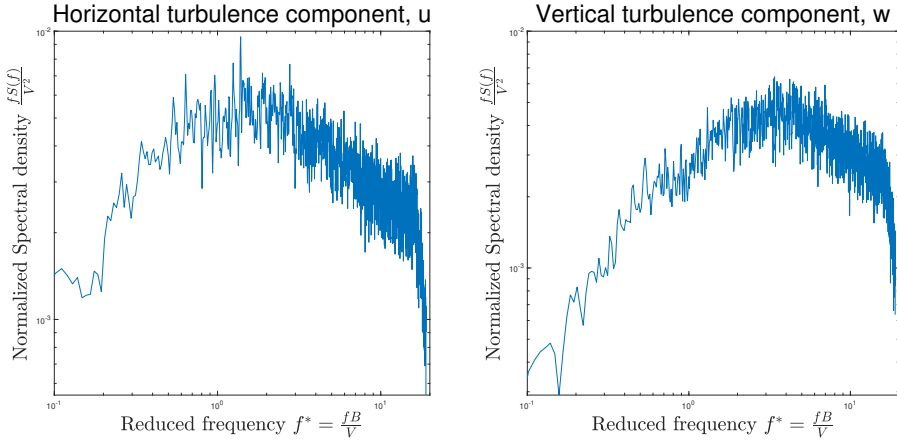
Figure 5.2: Normalized wind spectra for turbulent flow, $V = 3.5m/s$.
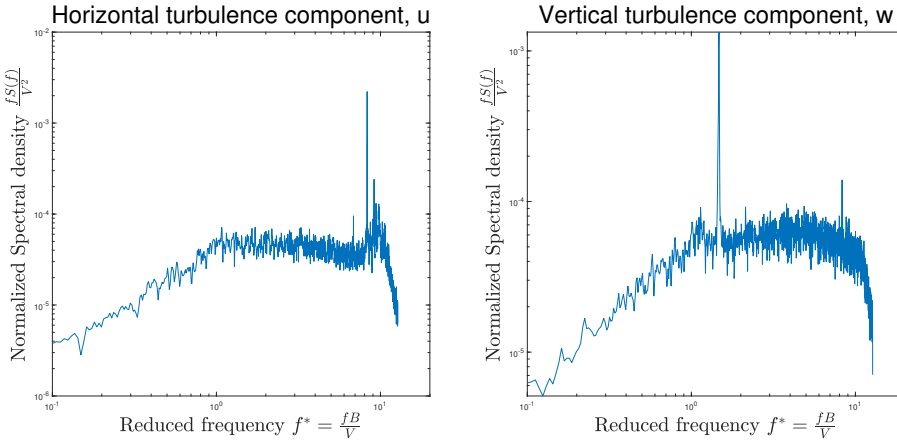
Figure 5.3: Normalized wind spectra for laminar flow, $V = 4.6m/s$.

Figure 5.2 and 5.3 shows the normalized spectra in vertical and horizontal direction for the two different flows. The measured data are normalized by multiplying with the frequency and divide by the squared mean wind and plotted against the reduced frequency. All plots have a maximum value around the reduced frequency 1, except from the distinct peaks caused by the probe mount's natural frequency. This is in accordance with turbulence spectra found by Larose [9], which implement that the spectra are a valid representation of the turbulent wind field.

For further validation, the turbulent wind spectra are plotted together with the Kaimal spectra, given by equation 2.34. The turbulence intensity is given in table 4.2 to 4.4, and the integral length scale is fitted to the measured data. It should be mentioned that the integral length scale is difficult to determine in a wind tunnel experiment. In the Kaimal spectrum the value of the integral length scale determines the peaks horizontal position in the spectra. To fit the Kaimal spectra to the given turbulence the integral length scale is put equal to $xLu = 0.07m$ and $xLw = 0.0233m$. As seen in figure 5.4 the measured data fits well with the Kaimal spectrum as it shows similar distribution of energy with the frequency. For this reason, the measured spectra are a good representation of the turbulent wind and should be adequate to use in the admittance estimation.
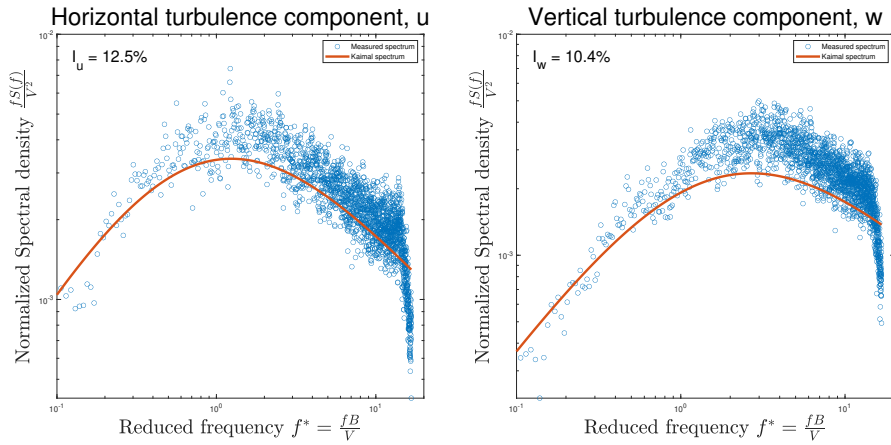
Figure 5.4: Normalized wind spectra for turbulent flow together with Kaimal spectrum, $V = 3.5m/s$.

5.2 Comparison of Forces

The forces from the interpolated- and the piece-wise defined load method, described in section 4.4.1, are presented in table 5.1. The forces are compared with the forces obtained from the load cells, given in table 5.2.

Table 5.1 and 5.2, presents the total static forces on the upstream- and downstream-box measured by the load cells and the pressure scanner. The static forces from the pressure scanner are generally lower than the static forces obtained from the load cells. When the wind speed increases, the deviation between the pressure measurement forces and the load cell forces increase. Moreover, the errors are greater on the upstream-box than the downstream-box. To sum up, when the forces increase the deviation between the pressure measurement and the load cell increases.

A small difference between the forces obtained from the interpolated load method and the piece-wise point load method was observed. In general, the interpolated load method gives higher force magnitude, expect the moment on the downstream-box. Both methods underestimate the forces on the bridge deck, compared to the load cells, but are considered sufficient for further work in this thesis.

V [m/s]	Interpolated load method		Piece-wise load method	
	Upstream	Downstream	Upstream	Downstream
Fx [N]				
6.7	0.56	0.56	0.57	0.56
3.5	1.81	1.82	1.82	1.81
10.1	3.91	3.99	3.92	3.97
Fz [N]				
6.7	0.95	-0.72	0.95	-0.71
3.5	4.07	-2.93	4.03	-2.92
10.1	9.83	-6.48	9.73	-6.47
My [Nm]				
6.7	0.28	0.08	0.23	0.10
3.5	1.09	0.35	0.94	0.38
10.1	2.5	0.80	2.25	0.86

Table 5.1: Static forces on upstream- and downstream-box obtained from the interpolated load method and the piece-wise load method.

V [m/s]	Load Cells	
	Upstream	Downstream
	Fz [N]	
6.7	0.99	1.02
3.5	2.85	2.74
10.1	6.31	5.80
	Fx [N]	
6.7	1.26	-1.07
3.5	5.06	-3.30
10.1	11.31	-6.94
	M [Nm]	
6.7	0.39	0.18
3.5	1.46	0.56
10.1	3.27	1.17

Table 5.2: Static forces on upstream- and downstream-box obtained from load cells.

5.3 Static Coefficients

For the estimation of the static coefficients, of the twin-box bridge, different tests were considered and compared to each other. First, the static coefficients are estimated by forces measured by the load cells, for the static test described in subsection 4.2.1. This gives the static coefficient as a function of angle of attack. In addition, the static coefficients of four tests in different wind velocities were considered. Every time series from the load cells and pressure scanner are filtered by a lowpass filter with a pass-band frequency of 0.5 Hz and a stop-band frequency of 1.0 Hz. Then the static coefficients are normalized as described in equation 2.20.

Static Test

Figure 5.5 to 5.7 shows the normalized static coefficients obtained from the static test for the total model as well as for the upstream- and downstream-box. The forces and moments used for the calculation on the upstream- and downstream-box are in global coordinates, and the whole width of the bridge, B, defined in figure 3.4 is used in the normalization. The unfiltered raw data of the measured forces are presented by the gray area of the plot while the blue lines are the filtered forces. Since the test is cycled more than once, the data were fitted by a third-degree polynomial function in order to extract values at different angles.
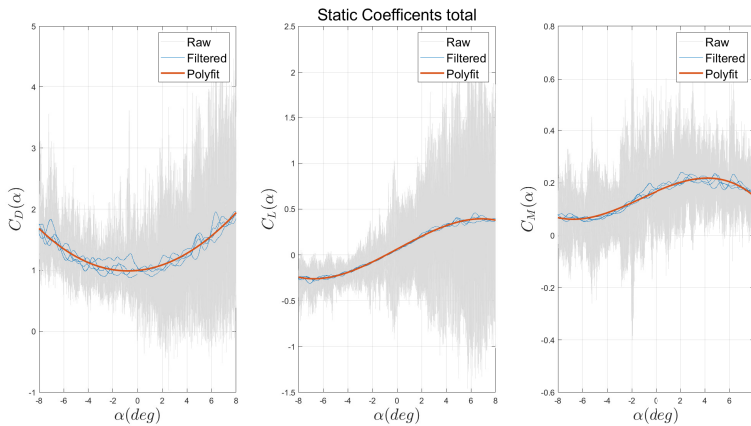
Figure 5.5: Static coefficients bridge model
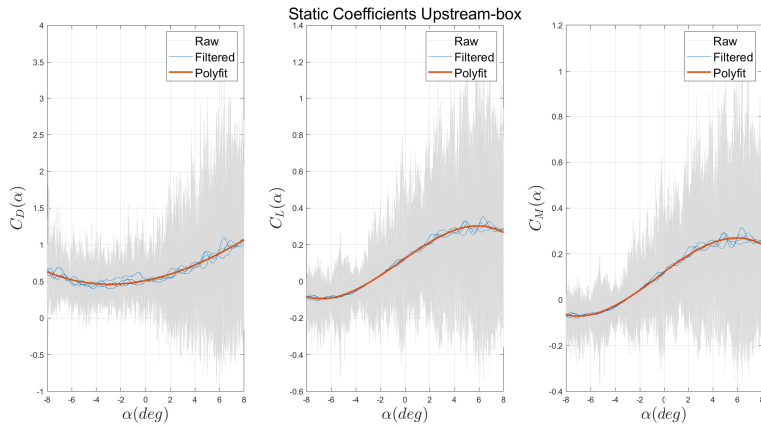
Figure 5.6: Static coefficients Upstream-box
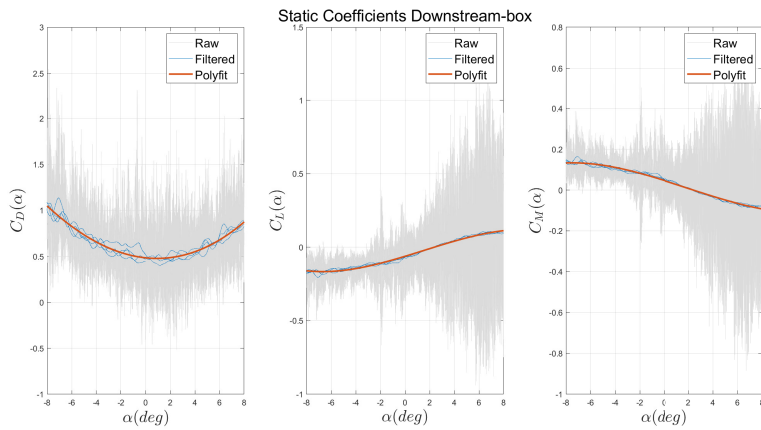
Figure 5.7: Static coefficients Downstream-box

From the plots, in figure 5.5 and 5.7, of the static coefficients, a clear nonlinear relationship can be seen between the angle, α, and the drag coefficient. A more linear relationship is seen for the lift and moment coefficients, especially at the downstream box, but some non-linearity can be seen for greater angles. In order to prevent the section from rotating when exposed to wind, C_M should be close to zero for $\alpha = 0$. This is not the case for the tested model and can lead to some unsteadiness of the model. A reason for this may be that there has not been focused on optimisation of the cross-sections shape.

The drag, lift and moment slopes, $dC_L/d\alpha$, $dC_D/d\alpha$ and $dC_M/d\alpha$, are plotted in figure 5.8. The slopes are defined as the rate of change in the static coefficients with respect to the angle of attack. It should be noted that the angle, α, is measured in radians when

finding the slopes. The static coefficients and corresponding slopes are given in table 5.3 to 5.6. The value at $\alpha=0$ is highlighted and will be used for further comparison of static coefficients obtained from the pressure measurements.
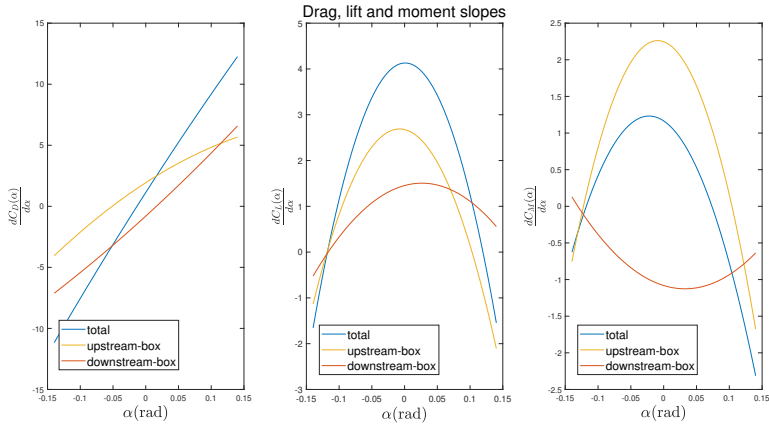
Figure 5.8: Drag, lift and moment slopes for bridge model, upstream-box and downstream-box

Total			
Angle	C_D	C_L	C_M
-8	1.683	-0.2424	0.0678
-4	1.121	-0.1884	0.08671
0	**0.9949**	**0.05851**	**0.1653**
4	1.273	0.3189	0.2182
8	1.949	0.3787	0.148

Table 5.3: Static coefficient from bridge model

Angle	Upstream-box			Downstream-box		
	C_D	C_L	C_M	C_D	C_L	C_M
-8	0.6329	-0.0825	-0.0649	1.05	-0.1600	0.1327
-4	0.4694	-0.0437	-0.0237	0.6538	-0.1446	0.1104
0	**0.5092**	**0.1219**	**0.1171**	**0.4857**	**-0.0634**	**0.0482**
4	0.7323	0.2784	0.2484	0.5502	0.0406	-0.0301
8	1.071	0.2657	0.2409	0.8779	0.1130	-0.0929

Table 5.4: Static coefficient from upstream- and downstream-box

Angle	Total		
	$dC_D/d\alpha$	$dC_L/d\alpha$	$dC_M/d\alpha$
-8	-11.16	-1.657	-0.6257
-4	-4.793	2.699	0.9369
0	**1.031**	**4.129**	**1.173**
4	6.798	2.753	0.1016
8	12.26	-1.548	-2.313

Table 5.5: Derivative of static coefficient for bridge model

Angle	Upstream-box			Downstream-box		
	$dC_D/d\alpha$	$dC_L/d\alpha$	$dC_M/d\alpha$	$dC_D/d\alpha$	$dC_L/d\alpha$	$dC_M/d\alpha$
-8	-4.0440	-1.133	-0.7532	-7.1150	-0.5234	-0.1397
-4	-0.7403	1.8640	1.6270	-4.0530	0.8346	-0.6900
0	**1.8910**	**2.6800**	**2.241**	**-0.8596**	**1.4600**	**-1.0860**
4	4.0690	1.3830	1.1700	2.7290	1.3700	-1.0680
8	5.6720	-2.105	-0.1402	6.587	0.5579	-0.6367

Table 5.6: Derivative of static coefficient for upstream- and downstream-box

Pressure Measurements

The calculation of the static coefficient based on measurements from the pressure scanners were found for three different mean wind velocities at 3.5m/s, 6.7 m/s and 10.1 m/s. All tests are done without the stiffening system and rotation of the model. For this reason, it is only possible to find the static coefficient at $\alpha = 0$ and the slope cannot be found. The coefficients from corresponding measurements from the load cells were also found for comparison and presented in table 5.7.

Mean wind (V)	C_D		C_L		C_M	
	MPS	Load cells	MPS	Load cells	MPS	Load cells
3.5 m/s	0.7179	1.2863	0.0205	0.0163	0.048	0.842
6.7 m/s	0.6455	0.9939	0.0264	0.0426	0.0541	0.0824
10.1 m/s	0.6185	0.9490	0.0348	0.0466	0.0560	0.0800

Table 5.7: Global Static Coefficient from pressure measurements and load cells

Next, the static coefficients for the upstream- and downstream-box were found separately and presented in table 5.8 and 5.9. It can be seen that the static coefficients obtained from the pressure measurements were lower than those from the load cells with roughly 30%. However, when comparing the measurements from the load cells and the static tests for the same mean wind speed, a deviation was observed. All the static coefficients are

lower for the static test, but the deviation between the drag coefficients are not as significant as for moment and lift. The reason for this can be that the tests were implemented differently in terms of rotation, or that the polyfit function is not as precise as expected. Furthermore, the static coefficients of the upstream-box are generally larger than those from the downstream-box which indicates that the upstream-box contributes most to the global static coefficient. The static coefficient's found by the pressure measurements and loads cells are closer in value for the downstream-box compared to the upstream-box.

Upstream box						
Mean wind (V)	C_D		C_L		C_M	
	MPS	Load cells	MPS	Load cells	MPS	Load cells
3.5 m/s	0.3615	0.6348	0.0819	0.1091	0.0337	0.0579
6.7 m/s	0.3235	0.5076	0.0971	0.1229	0.0384	0.0597
10.1 m/s	0.3078	0.4946	0.1036	0.1203	0.0406	0.0590

Table 5.8: Static coefficient for upstream box

Downstream box						
Mean wind (V)	C_D		C_L		C_M	
	MPS	Load cells	MPS	Load cells	MPS	Load cells
3.5 m/s	0.3564	0.6514	-0.0615	-0.0928	0.0143	0.0263
6.7 m/s	0.3220	0.4864	-0.0706	-0.0793	0.0157	0.0227
10.1 m/s	0.3107	0.4544	-0.0688	-0.0737	0.0154	0.0211

Table 5.9: Static coefficient for downstream box

As already discussed in section 5.2, the forces obtained from pressure measurements are generally lower than those obtained by the load cells, and will result in lower static coefficients. Based on these observations, it was decided that the static coefficients obtained from the static test will be the best representation when estimating the aerodynamic admittance functions. In addition, only the static test provides the slope of the coefficients, which is a parameter used in the estimation of the admittance functions.

5.4 Pressure Distribution

In this section, the pressure distributions from the wind tunnel tests are given. The distribution is represented by the mean value from the time series of each pressure hole. A complete representation, for all six correlation lines, will be presented for one test. For the remaining tests, the distribution is given by the first correlation line, due to its dense distribution of pressure holes. As mentioned in section 4.4.1, positive pressure is defined as pushing and pointing outward of the cross-section, while negative pressure data is defined as suction and faced inward. In addition, the dynamic pressure, $P_d = \frac{1}{2}\rho V^2$, where $\rho = 1.17kg/m^3$, will be given for each wind velocity. The definitions of the surfaces (S1-S10), given in figure 4.10, are used to explain the pressure acting on the various surfaces of the cross-section.

5.4.1 Uniform Wind Flow

The pressure distribution from the wind tunnel tests in uniform wind flow with mean velocity: 4.6 m/s, 5.7 m/s and 8.4 m/s, are presented below. Each wind velocity will be represented by point pressure at each pressure hole and distributed pressure around the cross-section. In these tests, the model was supported by the stiffening system.
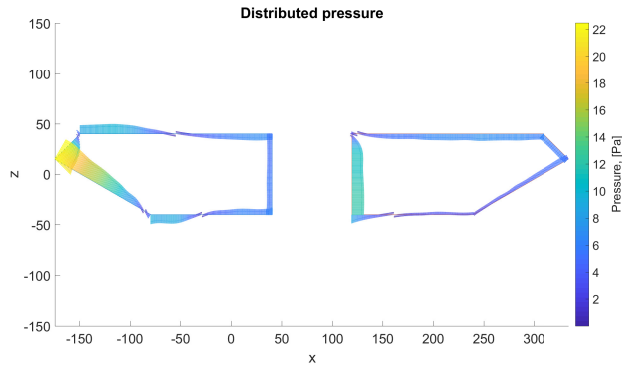
Figure 5.9: Uniform wind flow, $RPM = 220$, $V = 4.6m/s$, $P_d = 12.92Pa$
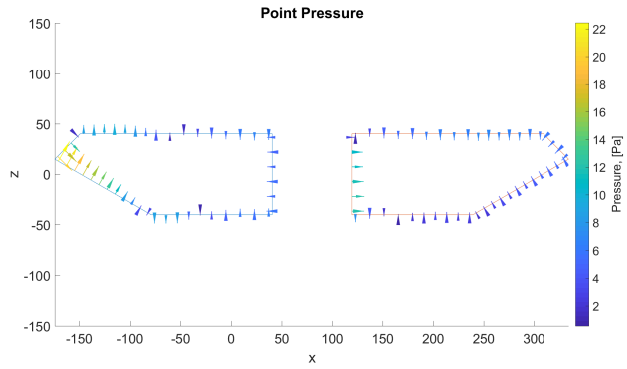
Figure 5.10: Uniform wind flow, $RPM = 220$, $V = 4.6m/s$, $P_d = 12.92Pa$
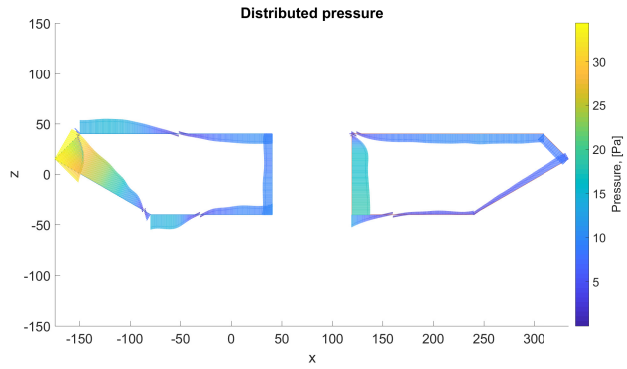
Figure 5.11: Uniform wind flow, $RPM = 271$, $V = 5.7m/s$, $P_d = 19.01Pa$
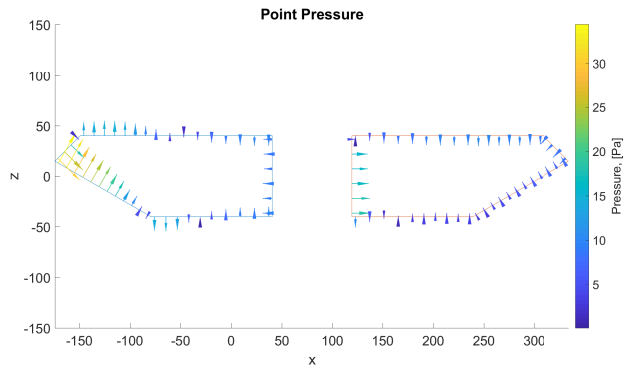
Figure 5.12: Uniform wind flow, $RPM = 271$, $V = 5.7m/s$, $P_d = 19.01Pa$
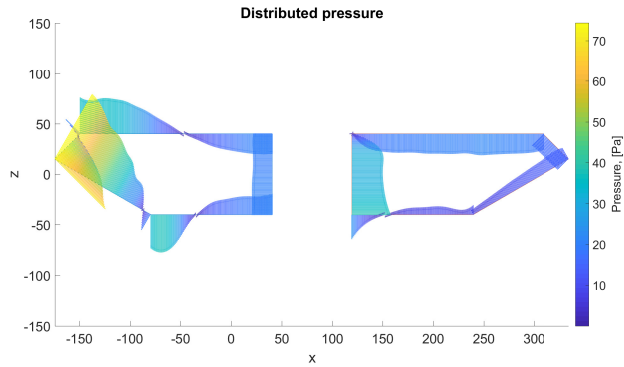
Figure 5.13: Uniform wind flow, $RPM = 397$, $v = 8.4m/s$, $P_d = 41.28Pa$
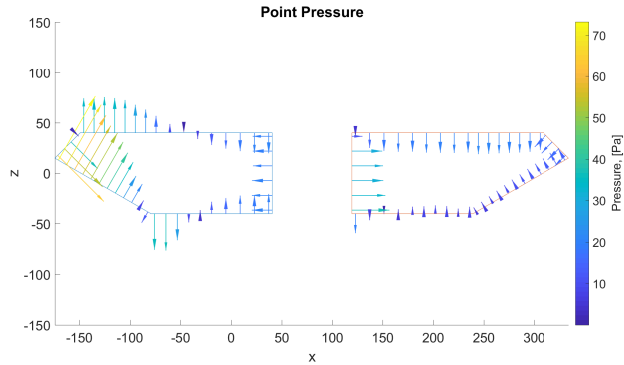
Figure 5.14: Uniform wind flow, $RPM = 397$, $V = 8.4m/s$, $P_d = 41.28Pa$

As predicted, pressure increases with the increasing wind flow. In addition to a higher magnitude, the pressure distributions show similarities for the three wind flows. Positive pressure can be seen at the windward sides of the upstream-box, S3 and S2. When the flow hits the corner between S2 and S1, the corner causes flow separation. The result is a separation bubble on S1, giving negative pressure. Further, the flow reattaches at S1 and the pressure turns positive. The same trend can be seen on the corner between S3 and S4, where the turbulence causes negative pressure around the corner before the flow reattaches at S4 and the pressure turns positive.

On the downstream-box, the wind flow gives positive pressure on S10. For the low wind flows, a separation bubble causing negative pressure can be seen on the corner between S10 and S6. While for the highest wind flow, the pressure remains positive around this corner. The same can be seen on the corner between S10 and S9. The pressure is positive on the surfaces S6, S7 and S8.

5.4.2 Turbulent Wind Flow

For the turbulent wind flow, the tests were run with and without the stiffening system.

Without Stiffening System

The tests without stiffening system were run with the wind velocities 3.5 m/s, 6.7 m/s and 10.1 m/s. Each wind velocity will be represented by point pressure at each pressure hole and distributed pressure around the cross-section. In these tests, the model was supported by the stiffening system. In addition, the pressure distribution of all the six correlation lines are shown for wind velocity 10.1 m/s.
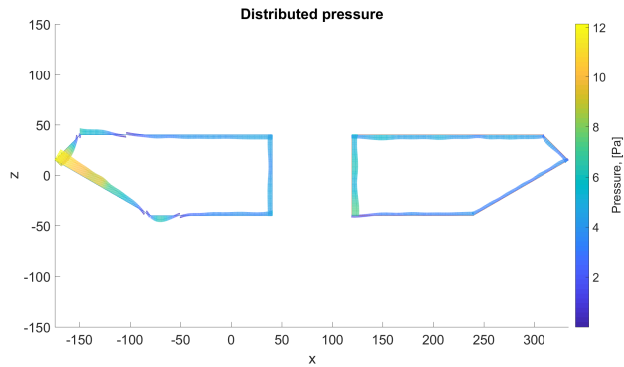
Figure 5.15: Turbulent wind flow, $RPM = 180$, $V = 3.5m/s$, $P_d = 7.17Pa$
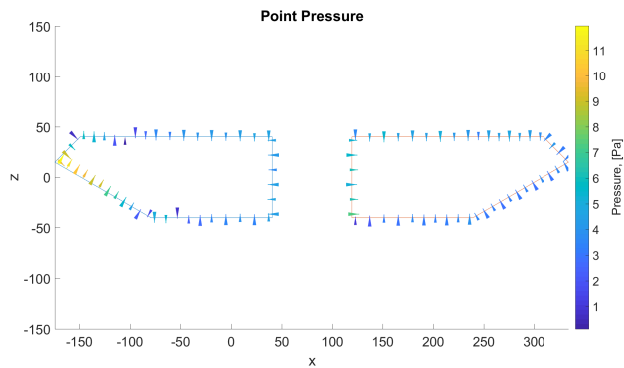
Figure 5.16: Turbulent wind flow, $RPM = 180$, $V = 3.5m/s$, $P_d = 7.17Pa$
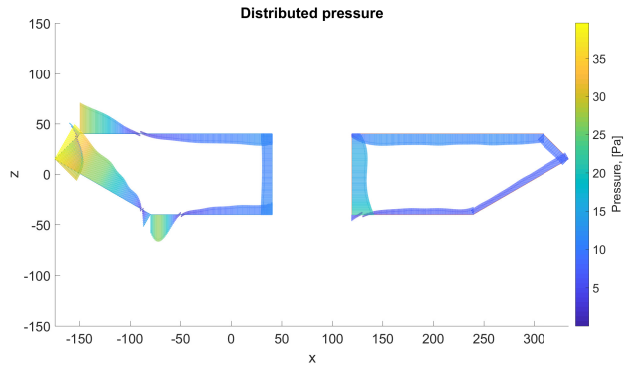
Figure 5.17: Turbulent wind flow, $RPM = 320$, $V = 6.7m/s$, $P_d = 26.26Pa$
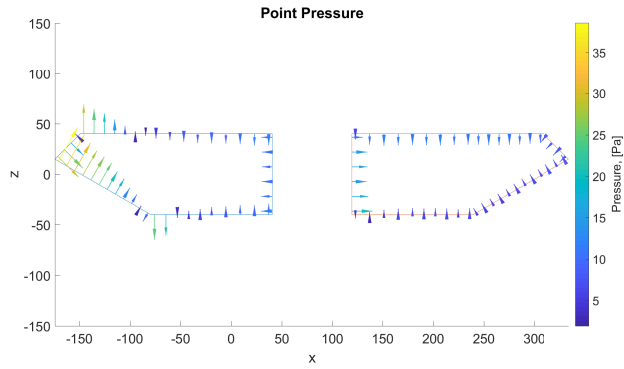
Figure 5.18: Turbulent wind flow, $RPM = 320$, $V = 6.7m/s$, $P_d = 26.26Pa$
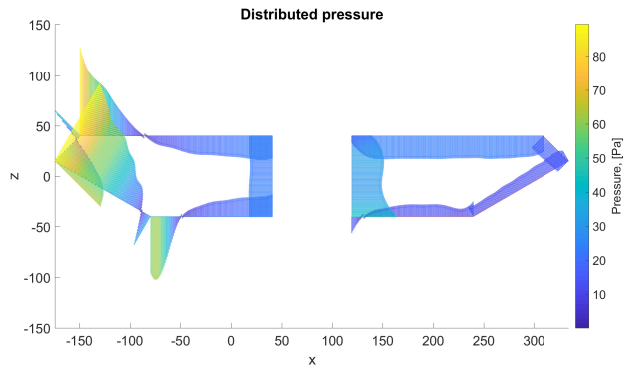
Figure 5.19: Turbulent wind flow, $RPM = 490$, $V = 10.1m/s$, $P_d = 59.68Pa$
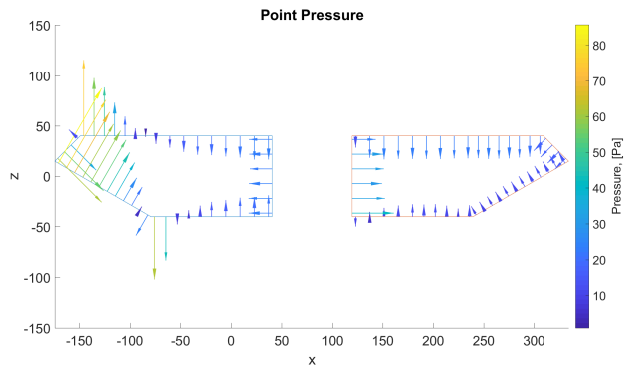
Figure 5.20: Turbulent wind flow, $RPM = 490$, $V = 10.1 m/s$, $P_d = 59.68 Pa$

The pressure distribution for the turbulent flows has the same trend as the uniform flow. It is no significant differences, except that the pressure remains positive around the corner between S10 and S6, similar to the highest wind velocity in the uniform flow test.

Figure 5.21 shows the pressure distribution for six correlation lines. A slight increase in the pressure magnitude was observed as the separation distance increased. This could indicate that the pressure increases in the span-wise direction. On the other hand, due to the sparse separation of tubes on correlation lines 2-6, the pressures may be more inaccurate compared to the pressure at correlation line 1.

(a) Correlation line 1.

(b) Correlation line 2.

(c) Correlation line 3.

(d) Correlation line 4.

(e) Correlation line 5.

(f) Correlation line 6.
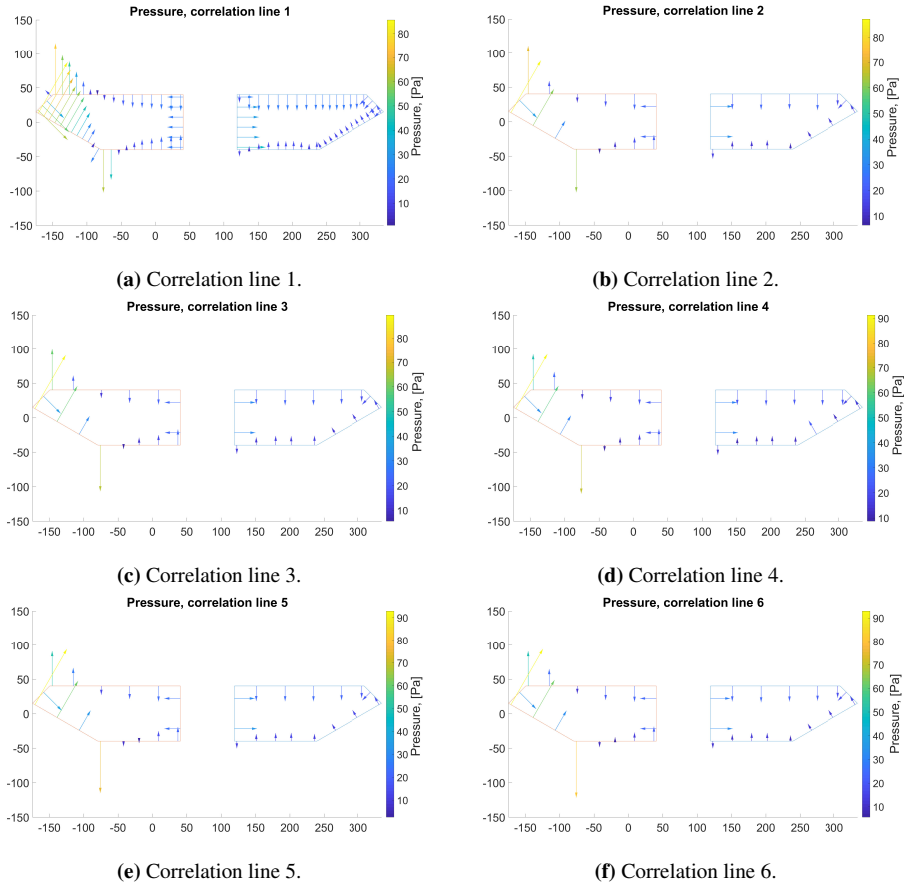
Figure 5.21: Pressure distribution for correlation line 1-6, $V = 10.1 m/s$, $P_d = 59.68 Pa$.

With Stiffening System

The test with stiffening system were run with wind velocities 3.9 m/s, 5.4 m/s and 8.3 m/s. Due to the almost identical distribution pattern, only distributed pressure is shown for these tests.
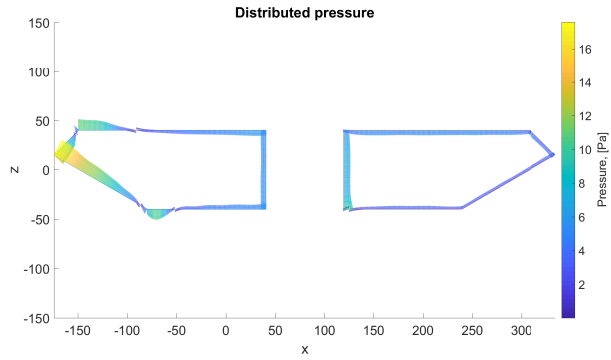
Figure 5.22: Turbulent wind flow, $RPM = 220$, $V = 3.9m/s$, $P_d = 8.9Pa$
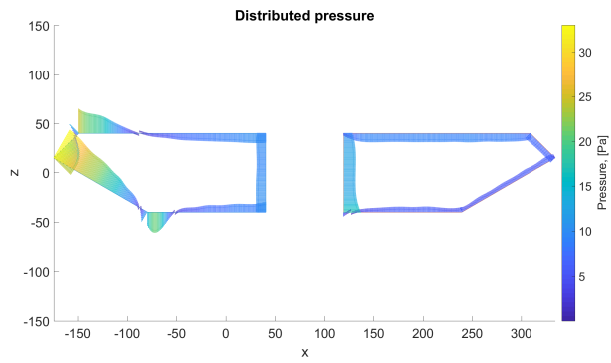
Figure 5.23: Turbulent wind flow, $RPM = 300$, $V = 5.4m/s$, $P_d = 17.06Pa$
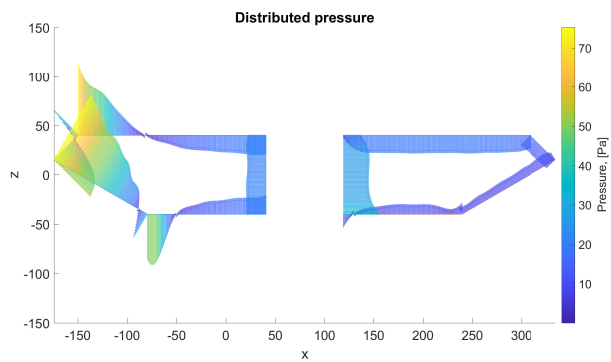
Figure 5.24: Turbulent wind flow, $RPM = 450$, $V = 8.3m/s$, $P_d = 40.30Pa$

The pressure distribution for the turbulent flow with the stiffening system are similar to the distribution for the turbulent flow without the stiffening system.

Comparison and validation of pressure distribution

Based on the knowledge of flow characteristics and results obtained from previous studies, on a twin-box bridge, the distributed pressure presented in this section showed an unexpected amount of positive pressure. This was especially observed for the downstream-box.

The pressure on the upstream-box shows a reasonable distribution at all surfaces except the leeward surface S5. In accordance with the study done by Wang et al. [28] the wind gives a positive pressure at the nose of the box, while a separation bubble changes the pressure direction on the onset of surface S1 and S4. As the flow reattaches after the separation bubble the pressure decreases yet stays negative even at surface S5. The same decrease is seen in the pressure distribution found by Wang et al, although the pressure changes direction towards the back of the box. The main reason for questioning the distribution on the upstream-box is the positive pressure on surface S5. Based on founding's by previous studies and the flow characteristics of bluff bodies a negative pressure was expected. A possible explanation of the positive pressure may be that the gap between the two sections is small and that the height of the model is relatively high. These factors can cause a stagnant pressure in the gap and causing the pressure on the surfaces in the gap to be equal.

At the downstream-box, the results show almost only positive pressure. This contrasts with the results obtained by Wang et al., where the pressure was negative around the entire box. The cross-section considered in this thesis has sharper edges and the height is relatively high compared to Wang et al., yet some negative pressure should be observed. Considering if the gap is too small, the twin-box will act more like a closed box and could explain the flow pattern. However, this does not explain the positive pressure on the leeward nose of the downstream-box. It is a known phenomenon that negative pressure is produced in the near wake area of a bluff body, due to the vortices shed from the trailing edge. This phenomenon gives reason to question the positive pressure on the leeward nose on the downstream box.

The unexpected pressure distributions gives reason to believe there is an overpressure in the wind tunnel, causing positive pressure on the bridge cross-section. This assumption is further investigated by subtracting a tentative overpressure from the mean value of the pressure from each pressure hole.
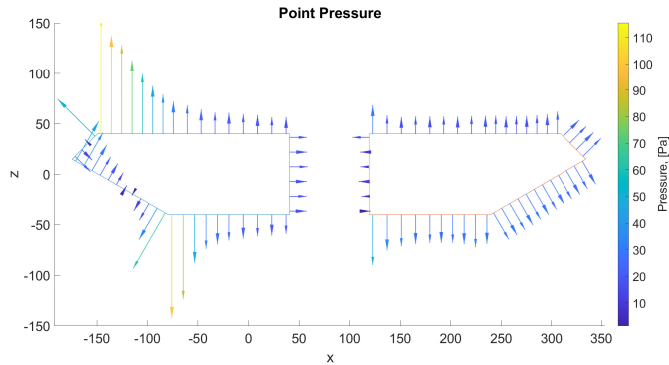
Figure 5.25: Pressure distribution in turbulent wind flow, RPM=490, V=10.1 m/s subtracting 40 Pa from each time series

Figure 5.25 shows the pressure distribution from the same test as figure 5.20 where 40 Pa are subtracted from every mean value. The flow pattern shows more consistency with results from other studies. However, the pressure on surface S10 is negative and considered unrealistic as the flow would enter the gap and generate positive pressure. For this reason, a tentative overpressure of 40 Pa can be an exaggeration. An overpressure of 20 Pa was then attempted and is shown in figure 5.26. The pressure is now negative at surface S10, as desired. Then again, the pressure on surface S4 becomes positive making it difficult to explain the wind field.
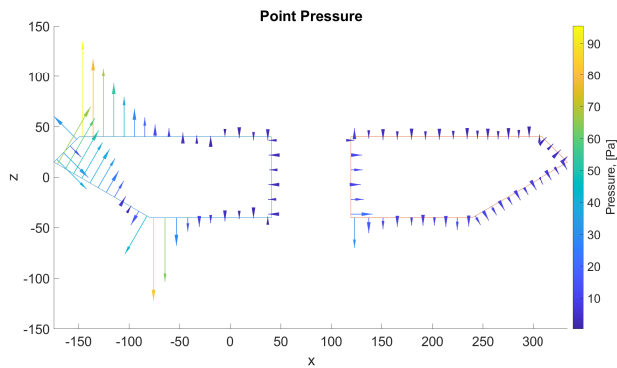
Figure 5.26: Pressure distribution in turbulent wind flow, RPM=490, V=10.1m/s subtracting 20 Pa from each time series

Last, it was discussed if the three detached pressure tubes mentioned in section 4.3 could be a source of error. Considering that the detached pressure tubes are inside the model, they could be used as a reference pressure and be subtracted from the mean values of the attached pressure holes. However, the mean value for the detached tubes was compared to the corresponding positioned tube at the other correlation lines. It was not detected any significant deviation, and the mean value of the pressure changes with the wind velocities.

The wind is probably penetrating the model and affecting the pressure signal in the detached tubes. Figure 5.27 presents the pressure distribution when the mean pressure from tube no. 1407 is subtracted. The pressure on the downstream-box becomes very small while the upper surface still only experiences positive pressure as for surface S5. However, there is positive pressure on surface S10, and a negative pressure at the lower surface of the downstream box, which seems reasonable compared to previous studies.
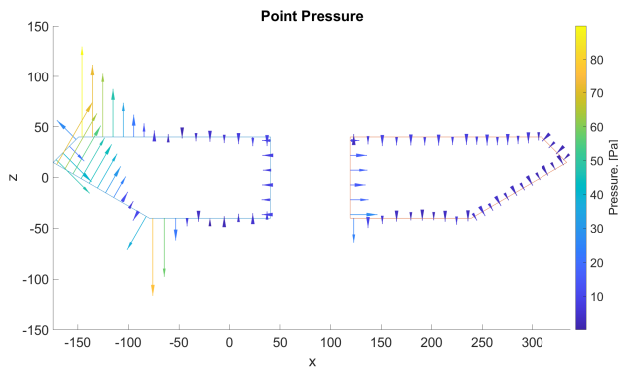
Figure 5.27: Pressure distrubution in tubulent wind flow, RPM =490, subtracting the mean pressure from tube nr 1407

The assumption of an overpressure in the wind tunnel will not affect the total moment and forces obtained by the integration of the pressure. This is expected, adding a constant pressure to all surfaces, will not change the forces since they are integrated around a closed circumference. Neither will the total moment change since the cross-section is single symmetrical about the y-axis and the moment is calculated around a point on this axis. However, when considering the boxes separately, it is no symmetry, and the moment on the downstream-box will decrease and increase at the upstream-box. Compared to the moments obtained from the load cells, the upstream-box will be closer in values, while the downstream-box will deviate even more than before the subtraction.

In order to evaluate whether an overpressure is possible, the pressure at the windward nose of the upstream-box was compared to the dynamic pressure and should be approximately equal. Table 5.10 shows the pressure obtained at the windward nose of the upstream-box for the three different cases discussed above, the original and the dynamic pressure. When an overpressure of 20 and 40 Pa was considered, the pressure at tube 1120 was significantly lower than the dynamic pressure. When the mean value of the detached tube was subtracted, the pressure was closer to the dynamic pressure, but still not as close as the original pressure at the nose.

Dynamic pressure V = 10.1m/s in wind tunnel	Pressure at tube no. 1120			
	Original	subtracted		
		40Pa	20Pa	mean pressure tube no.1407
59.68 Pa	61.48 Pa	21.48 Pa	41.48 Pa	47.06 Pa

Table 5.10: Comparison of pressure at tube nr.1120

It is obvious that the pressure distribution obtained from the test done in this thesis are questionable compared to previous studies. Plausible reasons for the deviations are discussed above. However, wind characteristics and the flow field are a complex and difficult topic and further investigations are needed to validate the results. Due to these uncertainties and the similarity between the original and the dynamic pressure, it was decided to use the original pressure signal the estimation of the aerodynamic admittance functions.

5.5   Force Spectra

Based on the pressure measurement data, the buffeting forces and spectra were calculated for each correlation line. The spectral densities were calculated with the forces obtained from the piece-wise load method, described in section 4.4.1. This method is preferable as it gives faster calculations and the results match the interpolated load method.

(a) Drag Force Spectra

(b) Lift Force Spectra

(c) Moment Spectra
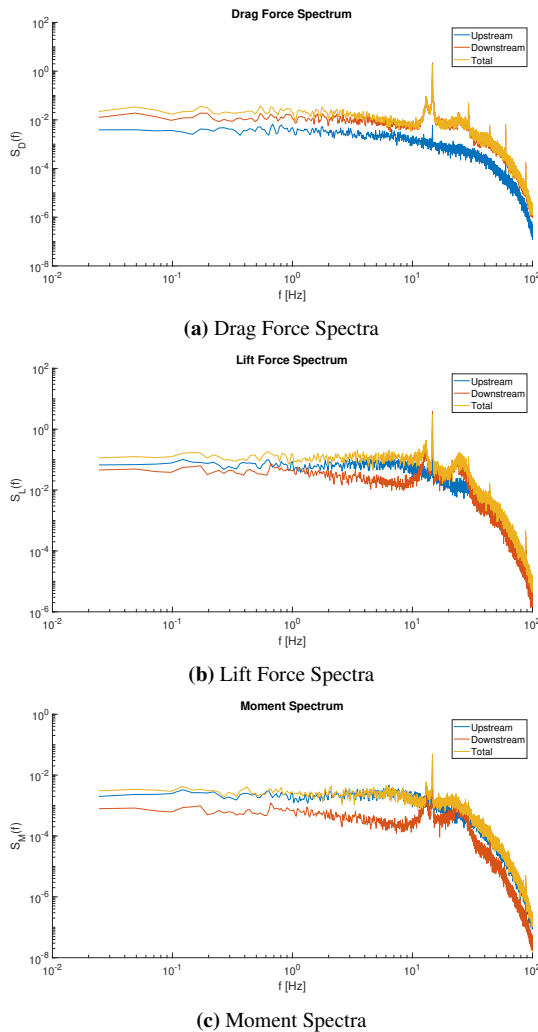
Figure 5.28: Buffeting Force spectra, $V = 10.1m/s$, without stiffening system.

Figure 5.28 shows the buffeting force spectra in turbulent wind flow without the stiffening system. Two peaks are distinct in the lift force spectrum at frequencies 13 Hz and 26 Hz. While the moment and drag force spectra shows one distinct peak at frequency 13 Hz. The

peaks are mainly caused by the downstream-box and may be due to the vortex shedding effect. The same effect was observed in the lift and moment spectra presented by Wang et al. [28].

(a) Drag Force Spectra

(b) Lift Force Spectra

(c) Moment Spectra
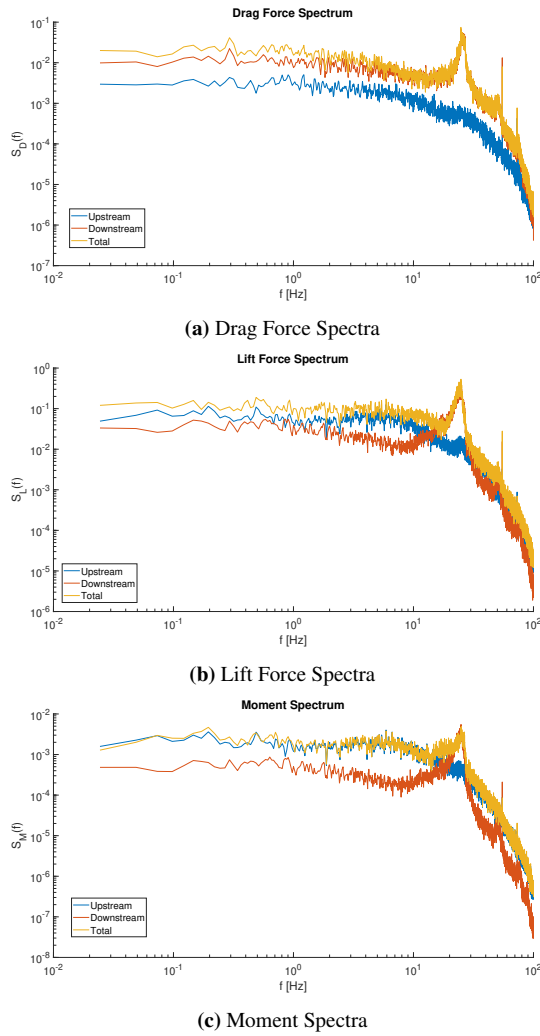
Figure 5.29: Buffeting Force spectra, $V = 8.3m/s$, $RPM = 450$, with stiffening system

(a) Drag Force Spectra

(b) Lift Force Spectra
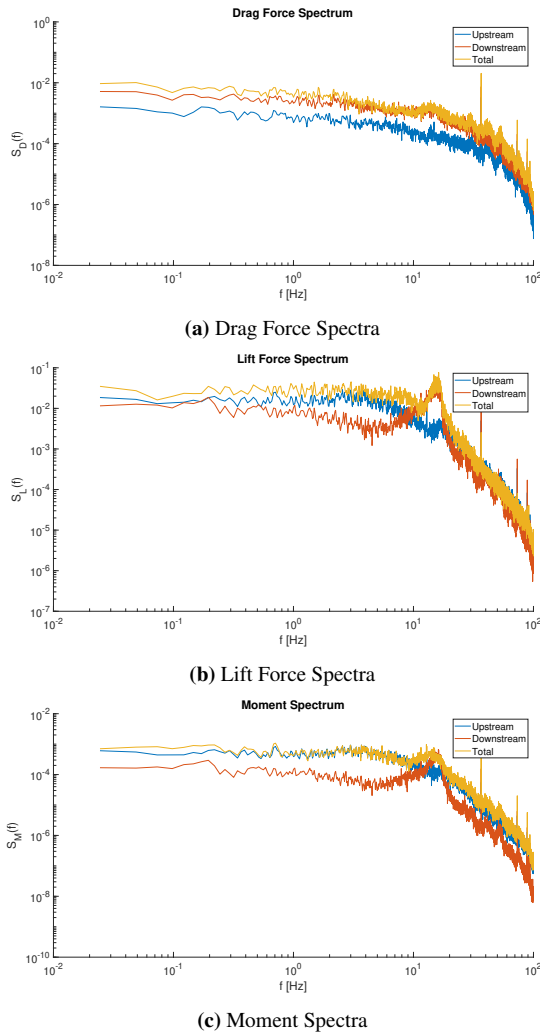
(c) Moment Spectra

Figure 5.30: Buffeting Force spectra, $V = 5.4m/s$, with stiffening system

Figure 5.29 and 5.30 show the buffeting force spectra in turbulent wind flow with the stiffening system. Only one distinct peak at 26 Hz is observed in the lift and moment force spectra.

For the drag force spectrum,in figure 5.29a and 5.28a, it is clear that the main contribution to the total drag force is from the downstream-box. While the lift and moment force spectra, seen in figure 5.28c, 5.28b, 5.29c and 5.29b, are mainly provided by the upstream-box. The downstream-box may be affected by the vortex shed from the upstream box, which could be formed by a mix of incoming turbulence and unsteady vortexes. This can explain why the forces acting on the downstream-box are different from the upstream-box, and

why the lift on the downstream-box deviates significantly from the upstream-box. More-over, when looking at the buffeting force spectra for uniform flow, shown in figure 5.31, it can be seen that the downstream-box contributes most to all three spectra, and indicates that the signature turbulence formed by the cross-section contributes to extra lift- and moment forces on the downstream-box.
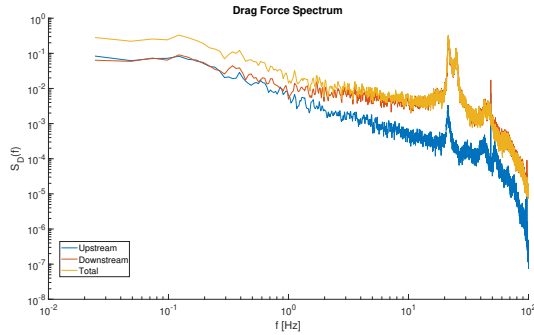
(a) Drag Force Spectra
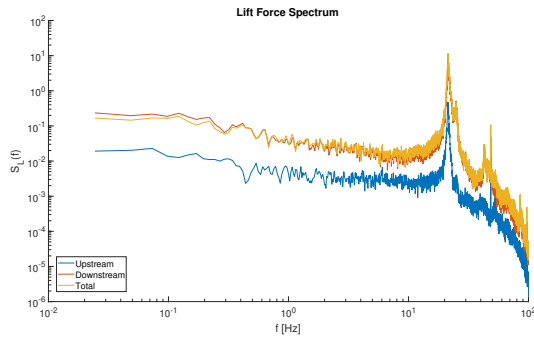
(b) Lift Force Spectra
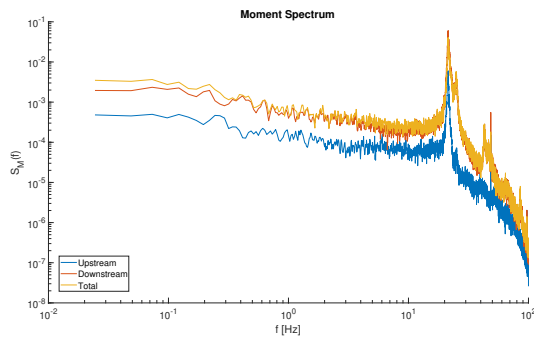
(c) Moment Spectra

Figure 5.31: Buffeting Force spectra, uniform flow, $V = 8, 4 m/s$, $RPM = 397$, with stiffening system

Figure 5.32 shows the force spectra of lift, drag and moment for all the six correlation lines on the twin-box in a turbulent flow. The high similarity of lift-, drag- and moment- spectra can be seen for the six lines and confirms the two-dimensionality of the mean flow and the reliability of the measurements.

(a) No stiffening system

(b) Stiffening system
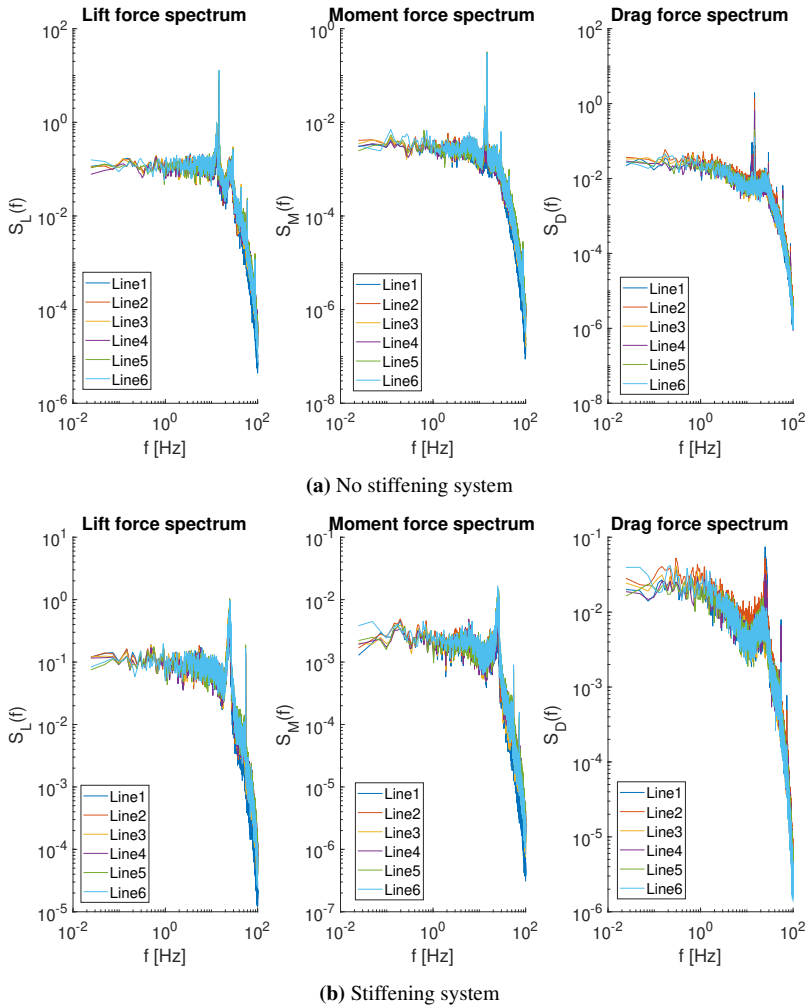
Figure 5.32: Buffeting Force spectra from all strips on the model.

5.6 Coherence

Based on the buffeting forces found by integration of the pressure on each correlation line the spanwise coherence was found. The spanwise coherence is based on the auto- and cross-spectra between two correlation lines with distance Δy and is calculated according to equation 2.87. An investigation of the force coherence was done for every test conducted in the wind tunnel. Figure 5.33 and 5.34 show the coherence for lift, drag and moment for five different separation distances at mean wind 3.9 m/s and 8.3 m/s for the total model, the upstream-box and the downstream-box. It is clear that the coherence of lift, drag and moment decreases as the distance, Δy, increases.

Beginning with the coherence for lift an moment, it can be seen that at low frequencies the downstream-box has lower coherence than the upstream-box. This gap seems to increase as the distance increases, meaning that the coherence of the downstream-box decreases more rapidly than the upstream-box. The total coherence is mainly affected by the upstream-box at low frequencies. Besides, the downstream-box gets higher coherence at high frequencies compared to the upstream-box. This is plausibly caused by the impinged vortices shed from the leeward edge of the upstream-box on the downstream-box. Xia et al. [38] also found that the downstream-box force coherence at high frequencies is stronger than the upstream-box before periodical vortices get suppressed by high turbulence intensity. This tendency seems to be more eminent for higher velocities, as seen in figure 5.34. Another remark for the higher velocities is the multiple peaks appearing with increasing frequency. Most peaks appear in the coherence of the downstream-box and can probably be explained by vortex shedding. Comparing low and high wind velocities, the slope of the coherence tends to decrease as the wind increase. As a result, the coherence is greater at high frequencies for higher wind velocities.

Further, the drag-coherence of the upstream-box is constantly higher than the downstream-box. However, the shape of the total drag-coherence tends to follow the drag-coherence of the downstream-box indicating that the downstream-box has the greatest influence on the drag-coherence.
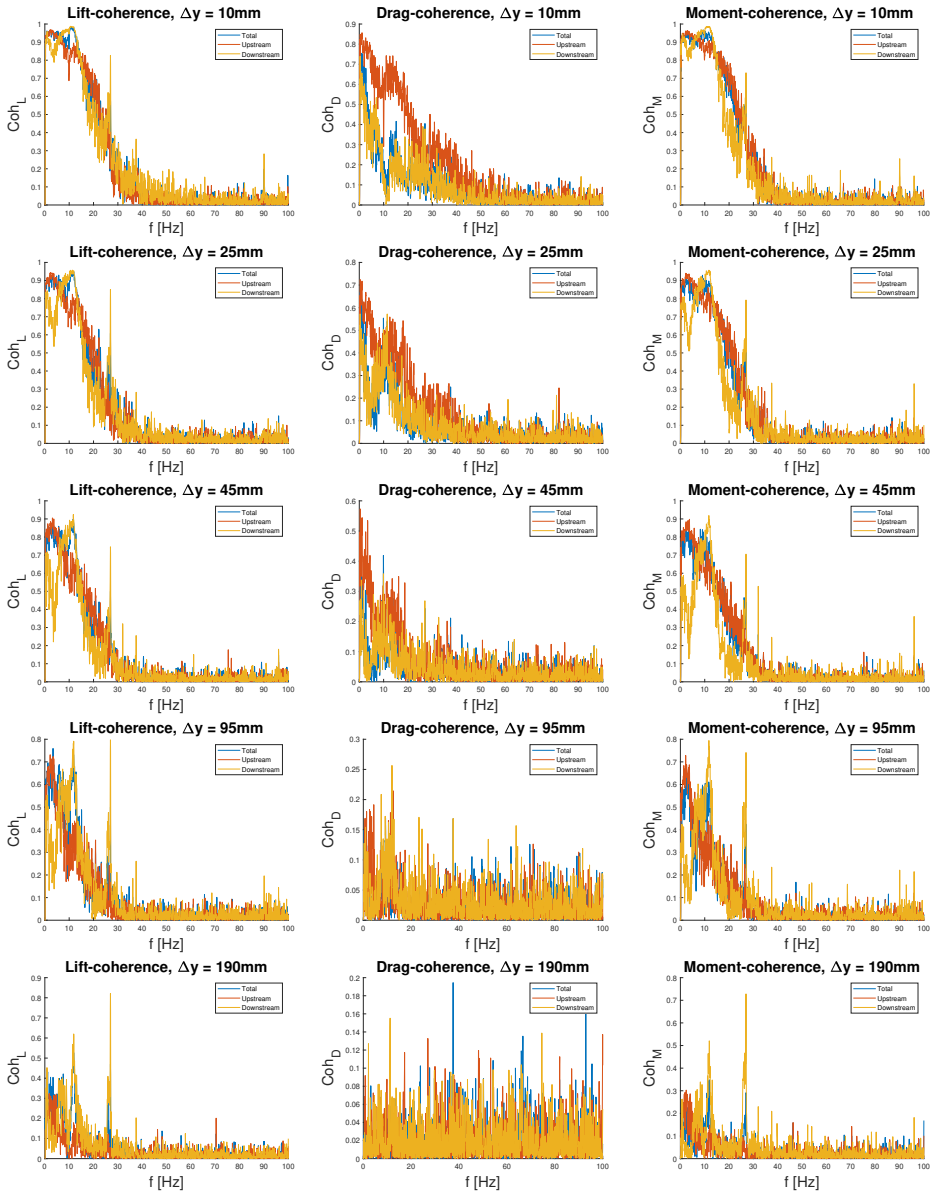
Figure 5.33: Spanwise coherence at $V = 3.9m/s$, turbulent flow.
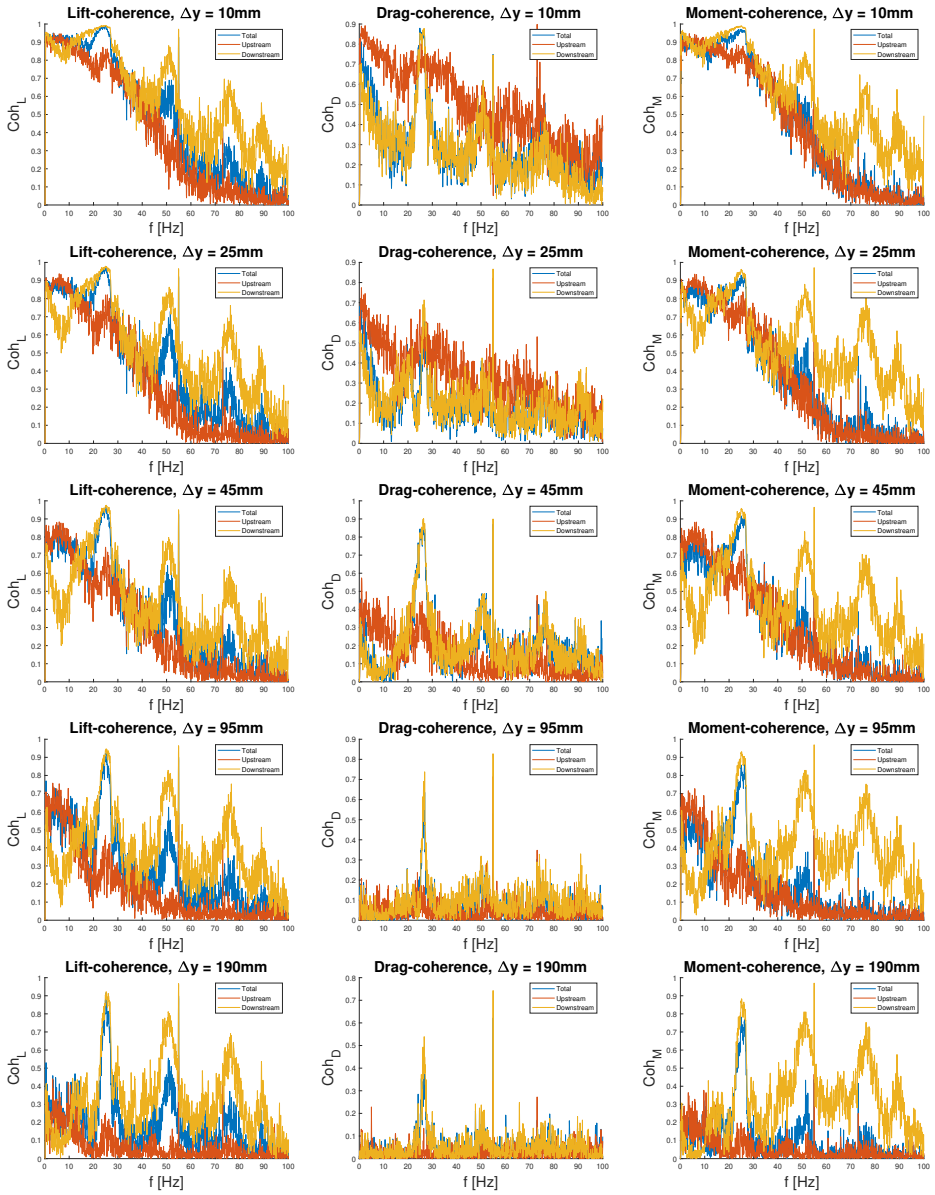
Figure 5.34: Spanwise coherence at $V = 8.3m/s$, turbulent flow.

5.7 Aerodynamic Admittance Functions

The admittance function transfers the wind spectra to a load spectra and accounts for the reduction in bridge response due to unsteadiness in the gust. Various methods for finding the aerodynamic admittance functions have been presented throughout chapter 2 resulting in the methods given in section 2.10. The first approach is the general admittance function found by equation 2.94, relating one turbulence spectra to one force spectra. The second approach, given in equation 2.96, gives the equivalent aerodynamic admittance relating the force spectra to both vertical and horizontal turbulence components. The last approach is the cross-spectral method which considers the cross-spectra between the buffeting forces and the turbulence components. Cross-spectral admittance's are estimated by equation 2.99. A comparison of the total model with the upstream- and downstream-box will also be presented for the equivalent method.

5.7.1 General Admittance Function

Figure 5.35 and 5.36 shows the general admittance functions for different mean wind velocities in turbulent flow, with and without the stiffness system.

(a) $V = 3.5m/s$

(b) $V = 6.7m/s$

(c) $V = 10.1m/s$
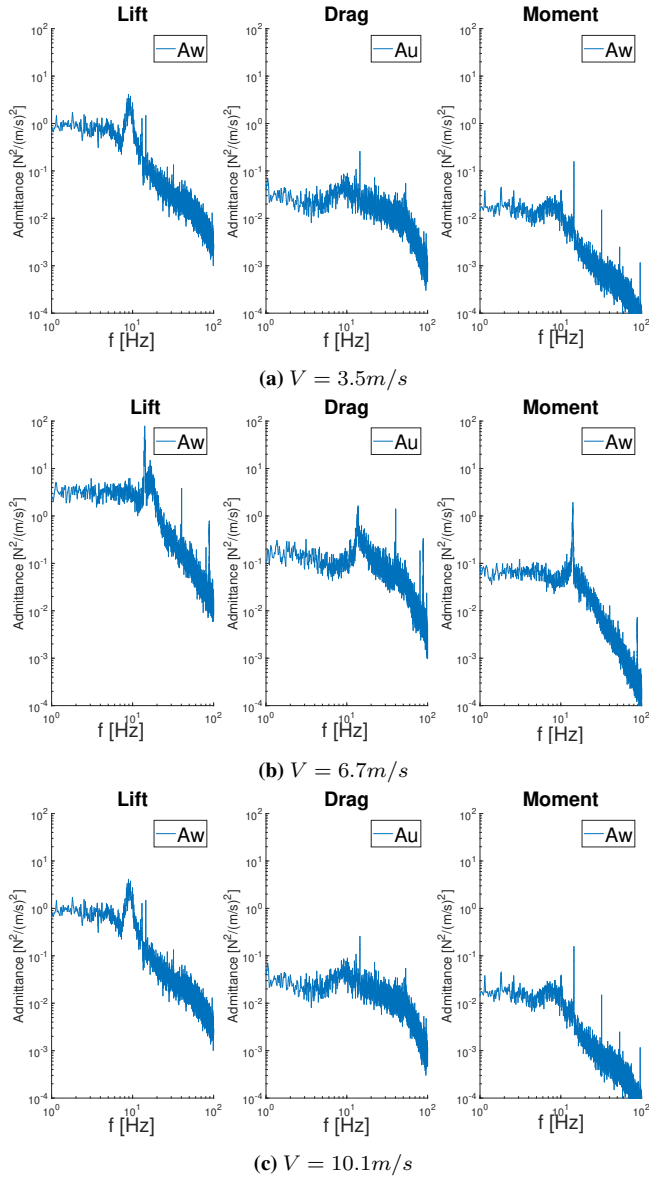
Figure 5.35: General admittance functions for test run without stiffening system.

(a) $V = 3.9 m/s.$

(b) $V = 5.4 m/s.$

(c) $V = 8.3 m/s.$
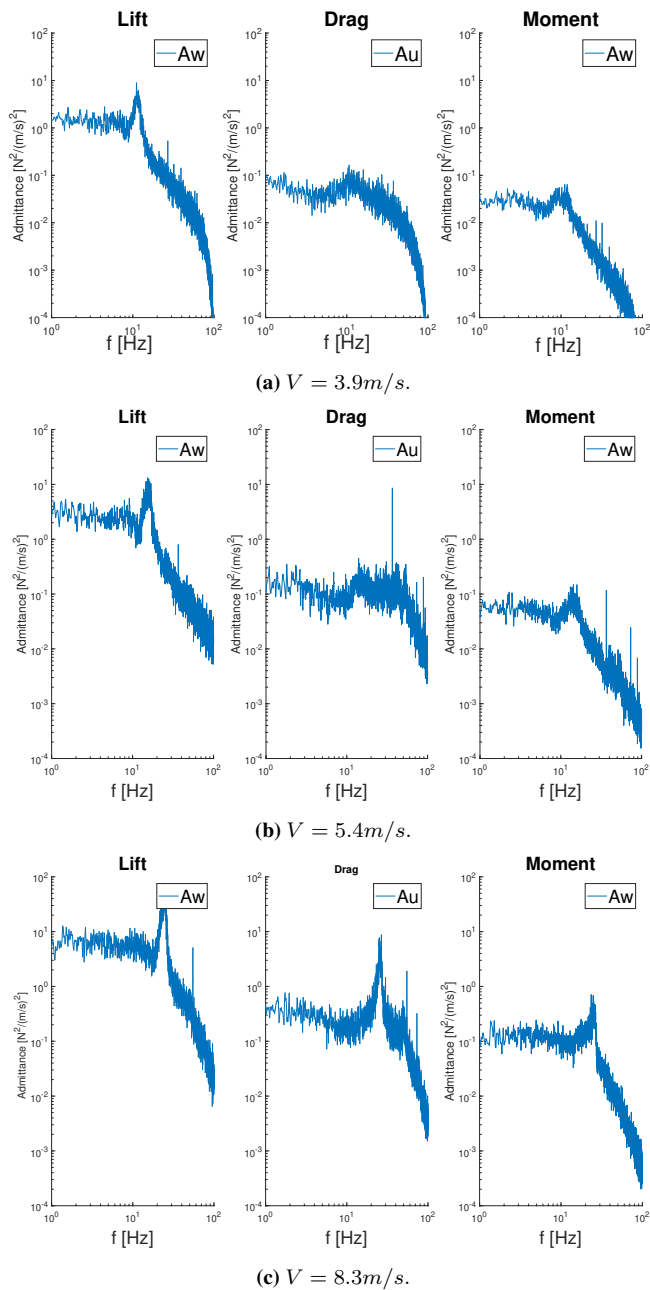
Figure 5.36: General admittance functions for tests run with stiffening system.

The admittance function is a general function transferring the velocity spectra to a force spectra. Consequently, the admittance's should be close to similar for all velocities. However, from the plots, it is seen that the admittance functions vary with the wind velocity. In general, when the wind speed increases the admittance functions increase. The variation in magnitude for the various velocities could also be due to the functions not being normalized. Another remark is that the lift admittance is between 10-20 times higher than the admittance for the drag and moment. In addition, the data reveals distinct peaks in the plots. These peaks are located at the same frequency as in the force spectra, in section 5.5, caused by the vibrations of the bridge deck. As noted, the vibrations are mainly caused by the downstream-box. Moreover, the shape seems reasonable since the function decreases whit increasing frequency.

5.7.2 Equivalent- and Cross-spectral Admittance Function

Figure 5.37 to 5.39, shows the admittance function estimated with the cross-spectral approach, A_{Fu} and A_{Fw} ($F = L, D, M$), and the equivalent method, A_F. In order to compare the result with other studies, Sears function is plotted with the estimated admittance functions. In addition, the admittance functions are found separately for the upstream- and downstream-box in order to investigate the contribution of each box. The admittance functions are shown for different wind velocities in turbulent flow and plotted against the reduced frequency.

(a) $V = 3.5m/s$, without stiffening system.

(b) $V = 3.9m/s$, with stiffening system.

(c) $V = 6.7m/s$, without stiffening system.

(d) $V = 5.4m/s$, with stiffening system.

(e) $V = 10.1m/s$, without stiffening system.

(f) $V = 8.3m/s$, with stiffening system
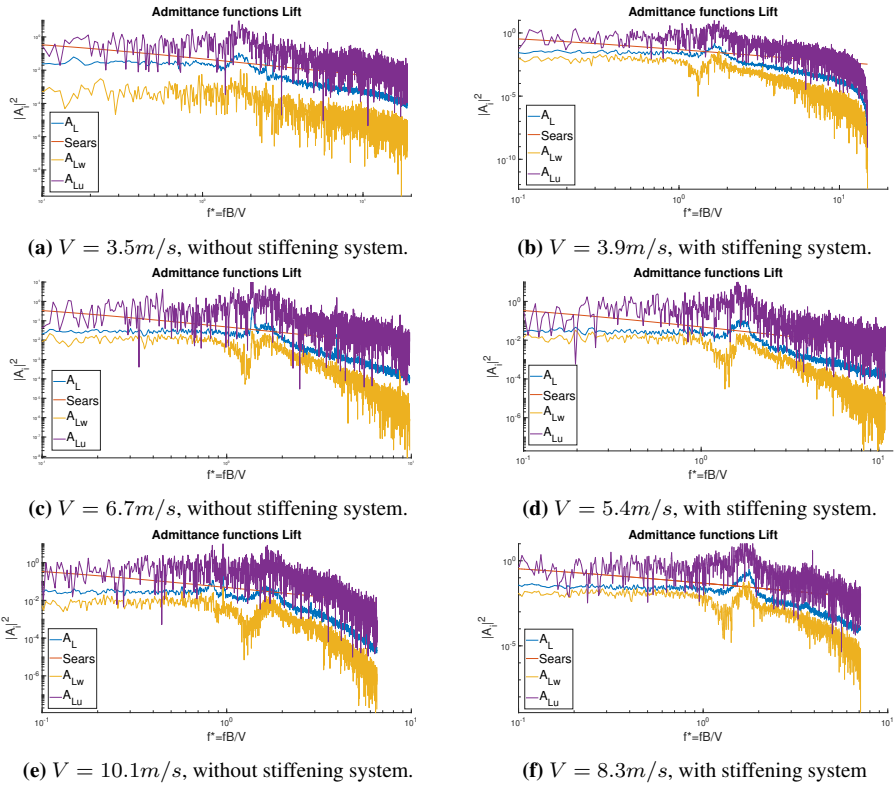
Figure 5.37: Admittance functions for lift estimated with the cross-spectral approach A_{Lu} and A_{Lw}, and with the equivalent method A_L for turbulent flow.

(a) $V = 3.5 m/s$, without stiffening system.

(b) $V = 3.9 m/s$, with stiffening system.

(c) $V = 6.7 m/s$, without stiffening system.

(d) $V = 5.4 m/s$, with stiffening system.

(e) $V = 10.1 m/s$, without stiffening system.

(f) $V = 8.3 m/s$, with stiffening system.
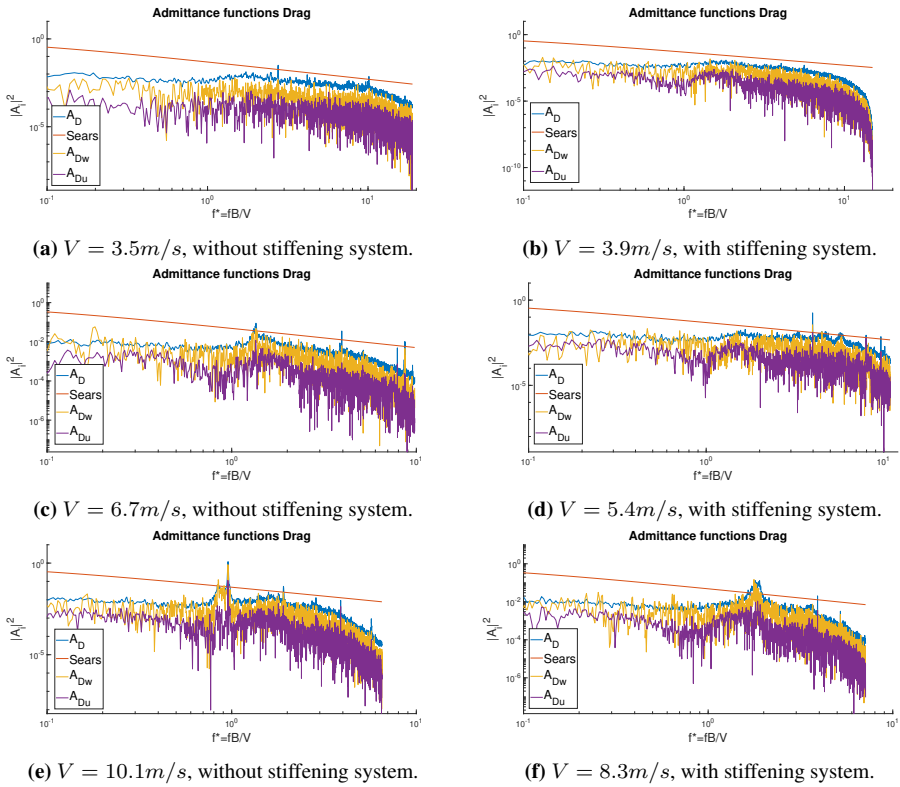
Figure 5.38: Admittance functions for drag estimated with the cross-spectral approach A_{Du} and A_{Dw}, and with the equivalent method A_D for turbulent flow.

(a) $V = 3.5m/s$, without stiffening system.

(b) $V = 3.9m/s$, with stiffening system.

(c) $V = 6.7m/s$, without stiffening system.

(d) $V = 5.4m/s$, with stiffening system.

(e) $V = 10.1m/s$. without stiffening system.

(f) $V = 9.8m/s$, with stiffening system.
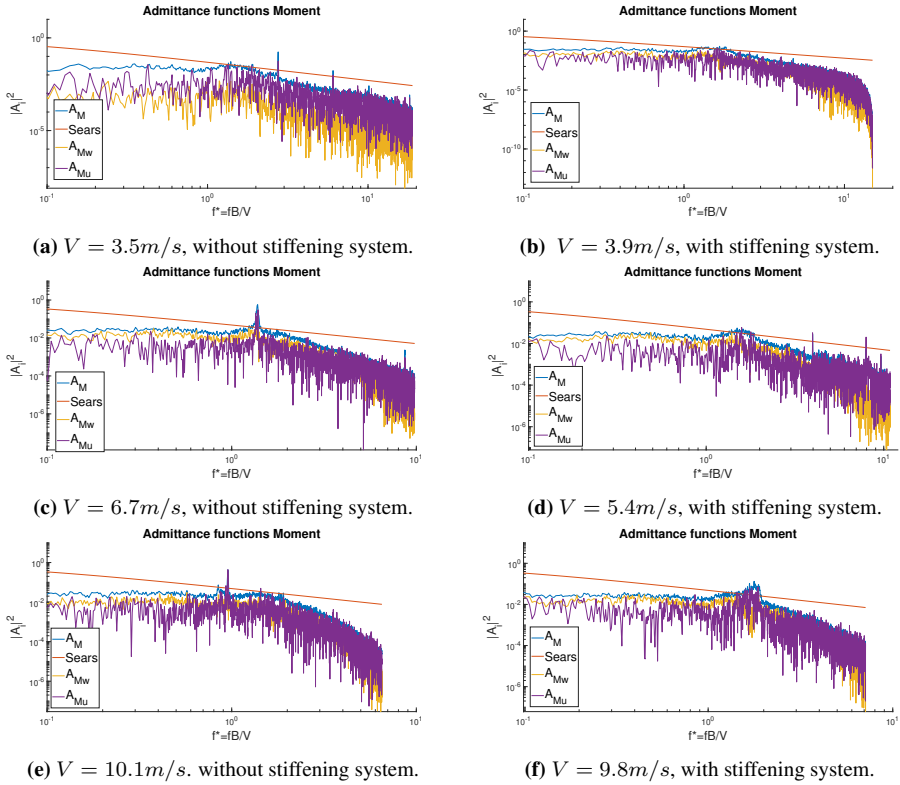
Figure 5.39: Admittance functions for moment estimated with the cross-spectral approach A_{Mu} and A_{Mw}, and with the equivalent method A_M for turbulent flow.

Figure 5.37 shows the estimated admittance functions for lift. In the equivalent lift admittance, a peak is distinct at small reduced frequencies for all tests. When the wind speed increases the slope to the AAF decreases more rapidly. Considering the cross-spectral AAF's, it is evident that $|A_{Lu}|^2$ and $|A_{Lw}|^2$ deviates significantly. Moreover, $|A_L|^2$ lays between $|A_{Lw}|^2$ and $|A_{Lu}|^2$ and considered reasonable as the equivalent AAF is a weighted average of these two. Due to the small value of the static coefficient, C_L, the equivalent AFF, $|A_L|^2$, is closer to $|A_{Lw}|^2$ than $|A_{Lu}|^2$.

The estimated admittance functions for drag are presented in figure 5.38. A smooth behaviour is seen for the equivalent drag admittance at low wind velocities. As the velocity increases more peaks appear. Besides, when the wind velocity increases the slope decreases faster. The equivalent admittance $|A_D|^2$ should be closer to $|A_{Du}|^2$ since the horizontal component, u, is the main contribution to the drag admittance. Considering that $|A_D|^2$ is closer to $|A_{Dw}|^2$, and laying above both $|A_{Du}|^2$ and $|A_{Dw}|^2$, implies that the equivalent approach overestimates the admittance function. Therefore, the true value of the equivalent drag admittance function may be closer to $|A_{Du}|^2$ found by the cross-spectral approach.

Figure 5.39 shows the estimates for the moment admittance functions. As for lift and drag, the slope decreases faster for higher velocities and one distinct peak appears. It is seen that $|A_M|^2$ lays above both $|A_{Mw}|^2$ and $|A_{Mu}|^2$. The equivalent admittance function, $|A_M|^2$, is closer to $|A_{Mw}|^2$ since the value of the static coefficient C_M is small compared to C'_M. A deviation can be seen in figure 5.39 (a) where $|A_M|^2$ is closer to $|A_{Mu}|^2$.

Compering the tests with and without the stiffening system shows no significant deviations between the equivalent admittance functions. In general, the estimated AAF's for various wind speed are similar in shape and decreases for increasing reduced frequencies.

Upstream- and Downstream-Deck

Figure 5.40 to 5.42 shows the equivalent admittance functions for the downstream- and upstream-box.

(a) $V = 3.54 m/s$, upstream deck

(b) $V = 3.54 m/s$, downstream deck

(c) $V = 6.68 m/s$, upstream deck

(d) $V = 6.68 m/s$, downstream deck

(e) $V = 10.11 m/s$, upstream deck

(f) $V = 10.11 m/s$, downstream deck
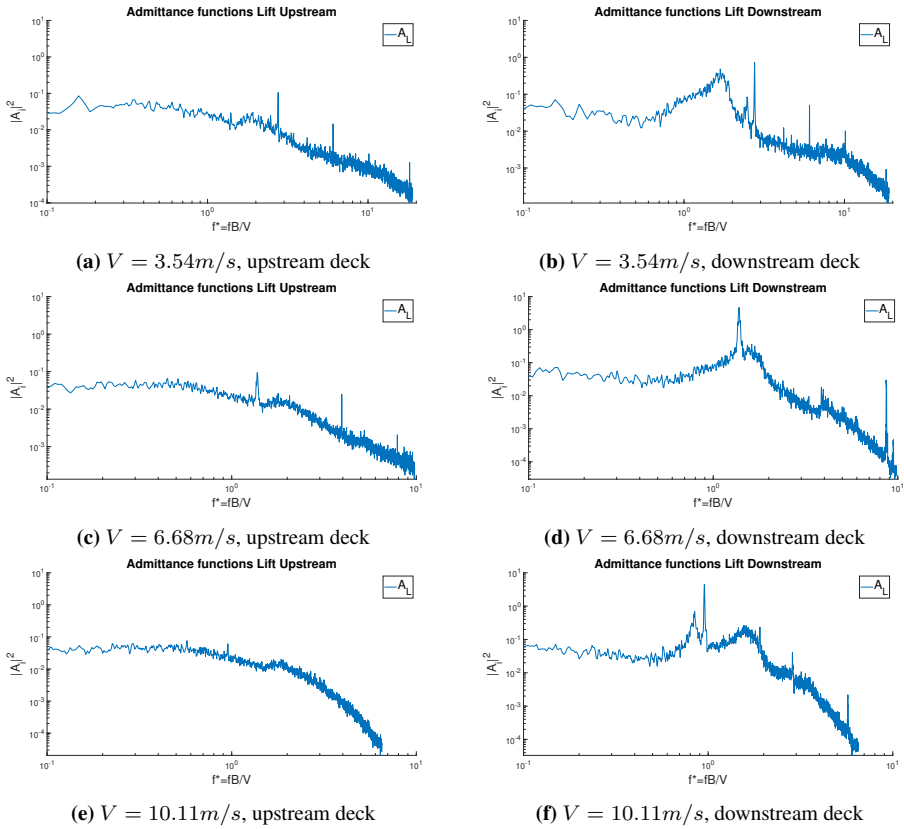
Figure 5.40: Equivalent lift admittance functions for upstream and downstream deck, without stiffening system, turbulent flow

(a) $V = 3.54m/s$, upstream deck

(b) $V = 3.54m/s$, downstream deck

(c) $V = 6.68m/s$, upstream deck

(d) $V = 6.68m/s$, downstream deck

(e) $V = 10.11m/s$, upstream deck

(f) $V = 10.11m/s$, downstream deck
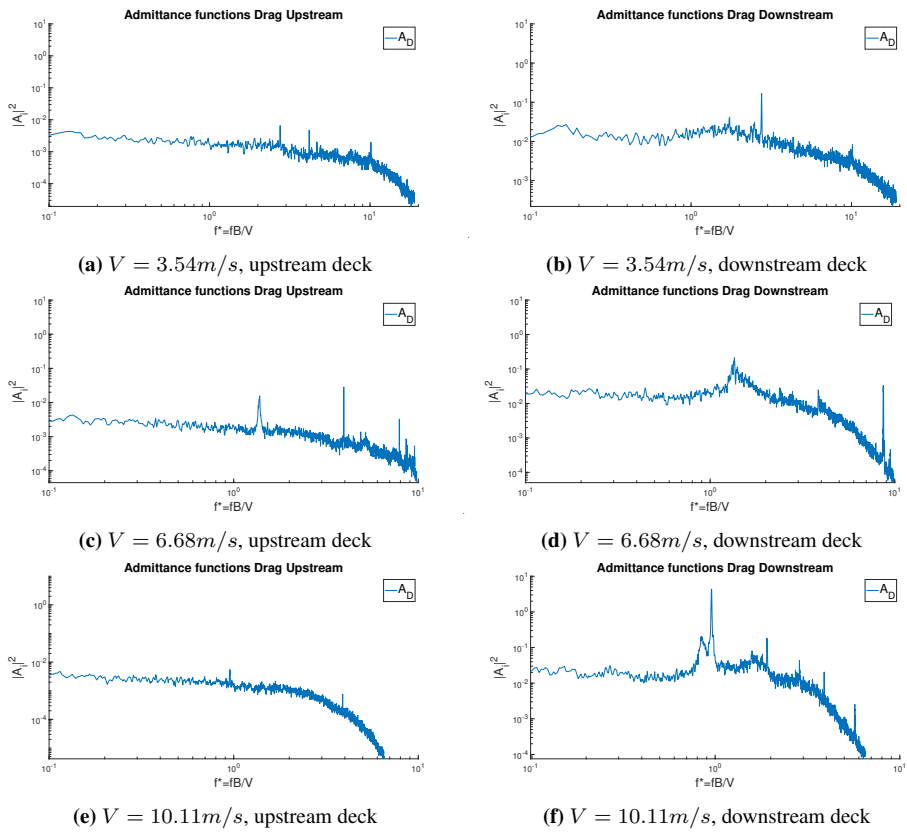
Figure 5.41: Equivalent drag admittance functions for upstream and downstream deck, without stiffening system, turbulent flow.

(a) $V = 3.54m/s$, upstream deck

(b) $V = 3.54m/s$, downstream deck

(c) $V = 6.68m/s$, upstream deck

(d) $V = 6.68m/s$, downstream deck

(e) $V = 10.11m/s$, upstream deck

(f) $V = 10.11m/s$, downstream deck
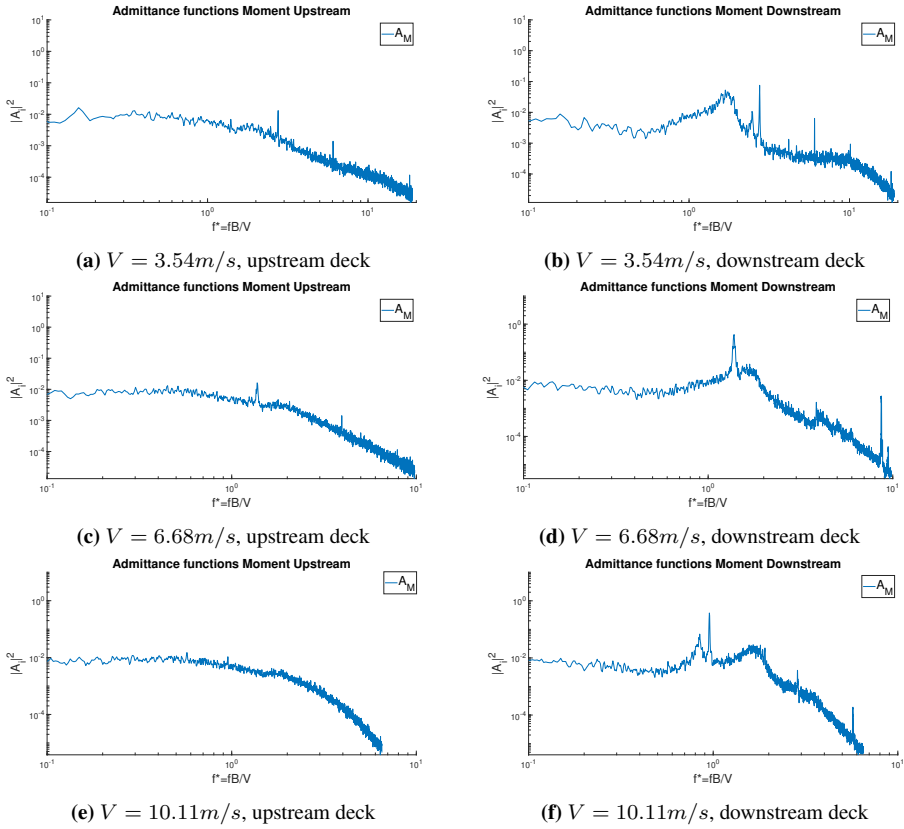
Figure 5.42: Equivalent moment admittance functions for upstream and downstream deck, without stiffening system, turbulent flow.

It is evident that the distinct peak in the total equivalent AAF, $|A_{L,D,M}|^2$, is caused by the downstream-box, similar to the force spectra in section 5.5. As discussed in section 5.2, this might be due to vortices shed from the upstream deck or vortices in the wake of the trailing edge of the downstream-box. Then again, the flow pattern and formation of vortices are complicated and nothing can be said for certain. The magnitude difference between upstream- and downstream-box is distinct for the drag admittance. The downstream-box has higher magnitudes, as expected considering the drag force spectra in section 5.5. Lastly, the lift admittance is slightly higher than the drag and moment admittance but not as significant as the general admittance functions.

Validation of the Aerodynamic Admittance Functions

From the results of the admittance functions is it evident that the admittance functions corresponding to the horizontal and vertical turbulence components deviates. This contradicts the assumption that the same effect is reached in each turbulence component. It emphasizes the importance of finding two admittance functions for each buffeting force. It also indicates that the equivalent AAF method gives inaccurate results.

As noted, the slope of the AAF's decreases faster with increasing wind velocity. A consequence is lower admittance functions for decreasing turbulence intensity which again leads to a greater reduction of buffeting forces when turbulence is present. The same effect was detected by Larose [9].

Further, it was detected that Sears function overestimates the equivalent AAF's for all reduced frequencies. Previous studies, Larose [9] and Wang et al. [28], shows similar results for low reduced frequencies, while Sears function underestimated at higher reduced frequencies. Sears function is an estimate for a thin plate/airfoil considering changes in the vertical turbulence component and therefore not applicable for bluff twin-box bridges. This especially applies for the drag AAF mainly affected by the horizontal turbulence component. The bluffness of the model could also be a cause to the deviation between the estimates and Sears function.

The equivalent and the cross-spectral AAF's have similarities in shape, but the magnitude deviates. Yan et al. [33] studied the same methods for moment and lift, in addition to the colligated least square method based on the colligated residue of the auto- and cross spectra (CRLSMACS), described in section 2.7.2. Their results showed that the equivalent AAF was closer to the $|A_{Fw}|^2$ (F=L,M) obtained from CRLSMACS, while the cross-spectral $|A_{Fw}|^2$ was significantly smaller than both the equivalent method and the CRLSMACS. This could indicate that the cross-spectral method underestimates $|A_{Fw}|^2$. The lift admittance functions obtained in this thesis showed consistency with these results. Therefore, the true value of $|A_{Lw}|^2$, from the cross-spectral method, should be closer to $|A_L|^2$. The same consistency was not detected in the moment AAF's. Figure 5.39 showed that the equivalent $|A_M|^2$ lays above both the cross-spectral moment admittance's. Whereas Yan et al. found that the equivalent admittance was between those from the cross-spectral method. Although the admittance functions for moment deviates from those estimated by Yan et al., it is important to point out that they examined a closed-box bridge. A twin-box bridge has a more complex wind field due to its geometry and the gap between the sections. This will have an impact on the results. However, Wang et al. showed that the cross-spectral approach gave inaccurate results compared to the CRLSMACS. The cross-spectral approach neglects the auto-spectral equations and the correlation between the buffeting forces and the fluctuating wind is generally weak, resulting in inaccurate estimations. At last, few previous studies have focused on estimating drag AFFs, and therefore it is difficult to conclude decisively about the results, expect that $|A_D|^2$ should be closer to $|A_{Du}|^2$ than $|A_{Dw}|^2$.

In the estimation methods presented in this thesis, the span-wise correlation effects are ignored. This assumption is investigated, by evaluating the AAF's from two different correlation lines. Figure 5.43 shows the admittance's for lift, drag, and moment for lines 1 and 6. A deviation can be seen between line 1 and 6 for the moment and lift AAF's. Also, the slope is decreasing faster for line 1 compared to line 6. The coherence spectra, shown in figure 5.34, shows that the lift and moment forces vary in the span-wise direction. It was also detected that the pressure increased from line 1 to line 6. These observations indicate that it is incorrect to assume 2-dimensional turbulence and that the 3-dimensional effect should be considered when estimating admittance functions. Further, the deviation between the drag admittance for line 1 and line 6 is less evident. Considering that the drag force has less coherence compared to the lift force and moment, it is unexpected that the two correlation lines would give similar AAF's. It should be mentioned that the turbulence components are measured only in front of correlation line 1, and may not be a correct representation of the turbulence in front of line 6. Due to uncertainties of wind characterises, the flow field and estimation of the admittance's, the span-wise correlation and the 3-dimensional turbulence effect on the forces should be investigated further.

(a) Lift. **(b)** Drag. **(c)** Moment
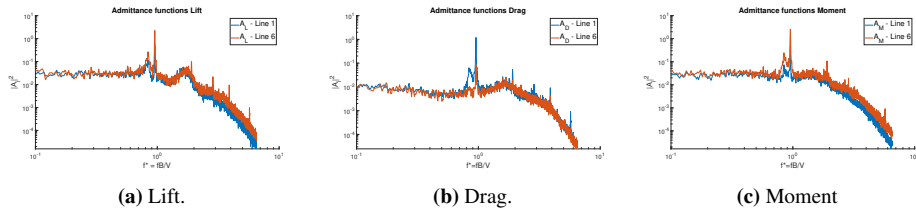
Figure 5.43: Equivalent admittance for line 1 and line 6, $V = 10.11 m/s$.

Considering that the cross-section tested in this thesis is not a model of a real bridge, there are no available data to compare and validate the values of the admittance functions. Hence, the only way to validate the admittance functions is to consider whether the shapes of the function has resemblance to previous research. Generally, aerodynamic admittance functions will gradually decrease as the frequencies increase. This trend can be seen in the admittance functions found in this thesis as well as showing similarities to the shape found by other studies. This indicates that the estimated admittance is relevant and can be used for a more accurate representation of the forces acting on a twin-box bridge.

Chapter 6

Conclusion and Further Work

6.1 Conclusion

This thesis places attention on the estimation of aerodynamic admittance functions for a twin-box bridge. The pressure distribution over the cross-section was also investigated. The twin-box model was tested in turbulent and laminar flow in the wind tunnel at NTNU. Pressure measurements were performed by using MSP4264 pressure scanners coupled with 256 pressure tubes distributed over 6 correlation lines on the two sections.

Based on the pressure measurements, the forces were found by using the piece-wise point load method and the interpolated method. It was discovered that these forces were slightly underestimated compared to the forces measured by the load cells. Further, the static coefficients were found by a static test and from the admittance tests. Due to the underestimated forces from the pressure measurements in the admittance tests, the coefficients and corresponding slope from the static test were used in the estimation of the admittance function.

A presentation of the pressure distributions was produced for all tests. The results showed inconsistency with previous research due to an unexpected amount of positive pressure, particularly at the downstream-box. Possible reasons for the unexpected pressure distribution may be due to the bluffness of the cross-section and that the gap between the sections is too small. In the building process, several irregularities were detected. This could cause penetration of the wind into the model and giving inaccurate results. In addition, the possibility for an overpressure was considered. It was found that the pressure acting on the cross-section, when subtracting an overpressure, did not match the dynamic pressure in the wind tunnel. Hence, the original pressure was further used in the estimation of admittance functions.

The turbulence spectra gave valid results and showed good alignment with the Kaimal spectra. Moreover, the force spectra, based on the pressure measurement, were examined. Several peaks were detected and were mainly caused by the downstream-box, either caused by the the vortices shed from the upstream-box or from the wake of the downstream-box.

Admittance functions were estimated using three different methods, the general, the equivalent and the cross-spectral. The functions decreased for increasing frequency and were considered valid. All functions had a distinct peak mainly caused by vortex shedding of the downstream-box. It was also detected that the slope decreased faster when the wind velocity increased, resulting in a higher buffeting response for high turbulence intensity. The methods showed higher magnitudes for the lift admittance, this was particularly evident in the general method.

Further, it was found that the admittance functions estimated with the cross-spectral method, $|A_{D,L,M,u}|^2$, $|A_{D,L,M,w}|^2$, deviated significantly. This implies that it is necessary to estimate all six admittance functions and that the equivalent method gives inaccurate results. On the other hand, the cross-spectral method neglects the auto spectral density and the correlation between the buffeting forces and the turbulence is generally weak. For this reason, the method may give inaccurate results for the six admittance functions and should be investigated further.

Comparison of the equivalent and cross-spectra method showed that the lift admittance matched previous studies, where the equivalent admittance lays above $|A_{Lu}|^2$ and below $|A_{Lw}|^2$. The same similarities cannot be seen for the moment and drag admittance functions. For the drag AAF's, the equivalent admittance lay above both $|A_{Du}|^2$ and $|A_{Dw}|^2$, but closer to $|A_{Dw}|^2$. Since the horizontal turbulence component is the main contribution to the drag force, the equivalent AAF should be closer to $|A_{Du}|^2$. This indicates that the equivalent AAF for drag is overestimated. The same trend was observed for the estimated admittance functions for moment, but here the equivalent admittance was closer to $|A_{Mw}|^2$. In addition, it was found that Sears function overestimates for all reduced frequencies and is not applicable for the twin-box bridge deck. Finally, the admittance functions for two separate correlations lines were compared and showed that the admittance function deviated. These observations give reason to question the 2-dimensional turbulence effect and that the span-wise correlation should be considered.

The estimated admittance functions found in this thesis show an acceptable shape that decreases with increasing frequency. The admittance functions are important for predicting the buffeting forces, and will lead to a reduction in the bridge response, compared to the quasi-steady theory.

6.2   Further Work

Due to the the unexpected pressure distribution detected for the twin-box model and that a optimized cross-section has not been the main focus in this thesis. Further work regarding and the model and cross-section should involve:

- Optimization of the model geometry.

- Improve the mid-section of the model where the pressure tubes are attached. The transition between the Lexan plates should be better executed, hence irregularities and holes affecting the flow should be avoided. In addition, the tubes should be attached better to prevent them from falling off.

- Test different gap widths to investigate its effects on the pressure distribution and the vortex shedding.

Further, evaluation regarding the pressure distribution and the aerodynamic admittance function should involve:

- A wider range of tests to validate the measurements from the MSP4264 pressure scanners. In addition to rotational tests of the model to investigate the influence of the angle of attack.

- Investigate the Strouhal number to get a better understanding of the incoming flow, and how it is influence the peaks appearing in the force spectra caused by the downstream-box. Investigation of the coherence between a tube on the downstream- and the upstream-box to detect at what distance the coherence equals zero. This will also give a better understanding of the turbulent flow.

- The cross-spectral approach was not considered as optimal for estimating the six admittance functions. Therefore should the CRLSMACS method be conducted to investigate the reliability of the admittance functions. Besides, the span-wise correlation is neglected and should be investigated further to state that this is an accurate assumption.

Bibliography

[1] Einar N Strømmen. *Theory of Bridge Aerodynamics*. Springer Berlin Heidelberg, Berlin, Heidelberg, 2006.

[2] Svend Erik Horg and Sigurd Berg Aas. Wind tunnel testing of bridge decks, 2016.

[3] TFI n.d. Getting started - series 100 cobra probe. http://www.turbulentflow.com.au/Products/CobraProbe/CobraProbe.php.

[4] Haojun Tang, K.M. Shum, and Yongle Li. Investigation of flutter performance of a twin-box bridge girder at large angles of attack. *Journal of Wind Engineering and Industrial Aerodynamics*, 186:192 – 203, 2019.

[5] K.C.S. Kwok, X.R. Qin, C.H. Fok, and P.A. Hitchcock. Wind-induced pressures around a sectional twin-deck bridge model: Effects of gap-width on the aerodynamic forces and vortex shedding mechanisms. *Journal of Wind Engineering and Industrial Aerodynamics*, 110:50 – 61, 2012.

[6] *Advanced Structural Wind Engineering*. Springer Japan, Tokyo, 2013 edition, 2013.

[7] José Ángel Jurado Albarracín J. A. Jurado. Bridge aeroelasticity : sensitivity analysis and optimal design, 2011.

[8] 2 - vibration induced by cross-flow. In Shigehiko Kaneko, Tomomichi Nakamura, Fumio Inada, and Minoru Kato, editors, *Flow Induced Vibrations*, pages 29 – 106. Elsevier, Amsterdam, 2008.

[9] Guy Louis Larose. The response of a suspension bridge deck to turbulent wind:the taut strip model approach. 1992.

[10] H Tanaka. Similitude and modelling in wind tunnel testing of bridges. *Journal of Wind Engineering Industrial Aerodynamics*, 33(1-2):283–300, 1990.

[11] M Matsumoto. Vortex shedding of bluff bodies: A review. *Journal of Fluids and Structures*, 13(7-8):791–811, 1999.

[12] Geurts C. n.d. The use of wind tunnel experiments for wind loads on structures. *TNO Built Environment and Geosciences, Delft, The Netherlands.*

[13] K Matsuda, K.R Cooper, H Tanaka, M Tokushige, and T Iwasaki. An investigation of reynolds number effects on the steady and unsteady aerodynamic forces on a 1 : 10 scale bridge deck section model. *Journal of Wind Engineering Industrial Aerodynamics*, 89(7-8):619–632, 2001.

[14] Chris Geurts and Carine van Bentum. Wind loading on buildings: Eurocode and experimental approach. In *Wind Effects on Buildings and Design of Wind-Sensitive Structures*, volume 493 of *CISM International Centre for Mechanical Sciences*, pages 31–65. Springer Vienna, Vienna, 2007.

[15] K. Takeda and M. Kato. Wind tunnel blockage effects on drag coefficient and wind-induced vibration. *Journal of Wind Engineering and Industrial Aerodynamics*, 42(1):897 – 908, 1992.

[16] Y Kubo, M Miyazaki, and K Kato. Effects of end plates and blockage of structural members on drag forces. *Journal of Wind Engineering Industrial Aerodynamics*, 32(3):329–342, 1989.

[17] Lianjie Liu, Liangliang Zhang, Bo Wu, and Ben Chen. Numerical and experimental studies on grid - generated turbulence in wind tunnel. *Journal of Engineering Science and Technology Review*, 10(3):159–169, 2017.

[18] Riccardo Tresso and David R. Munoz. Homogeneous, isotropic flow in grid generated turbulence. *Journal of Fluids Engineering*, 122(1):51, 2000.

[19] N400 bruprosjektering. Technical report, 2015.

[20] Taylor G.I. The spectrum of tubulence. 1938.

[21] Guy L. Larose. The dynamic action of gusty winds on long-span bridges, 1997.

[22] E.D Jancauskas and W.H Melbourne. The aerodynamic admittance of two-dimensional rectangular section cylinders in smooth flow. *Journal of Wind Engineering Industrial Aerodynamics*, 23(C):395–408, 1986.

[23] Yan Han, Z. Chen, and Xugang Hua. New estimation methodology of six complex aerodynamic admittance functions. *Wind and Structures*, 13, 05 2010.

[24] Ledong Zhu, Qi Zhou, Quanshun Ding, and Ziran Xu. Identification and application of six-component aerodynamic admittance functions of a closed-box bridge deck. *Journal of Wind Engineering Industrial Aerodynamics*, 172:268–279, 2018.

[25] Wim [van Drongelen]. 6 - continuous, discrete, and fast fourier transform. In Wim [van Drongelen], editor, *Signal Processing for Neuroscientists*, pages 91 – 105. Academic Press, Burlington, 2007.

[26] Cory Maklin. Fast fourier transform, 2019.

[27] IASBE (WG-10). Super-long span bridge aerodynamics, input for step 1.1a, 2016.

[28] Junxin Wang, Cunming Ma, Hongmiao Jing, Cheng Pei, and Elena Dragomirescu. Experimental study on aerodynamic admittance of twin-box bridge decks. *Journal of Wind Engineering Industrial Aerodynamics*, 198, 2020.

[29] Wen-Li Chen, Hui Li, and Hui Hu. An experimental study on the unsteady vortices and turbulent flow structures around twin-box-girder bridge deck models with different gap ratios. *Journal of Wind Engineering Industrial Aerodynamics*, 132(C):27–36, 2014.

[30] Y.C. He, Q.S. Liang, Z. Li, J.Y. Fu, J.R. Wu, and T. Deng. Accurate estimation of tube-induced distortion effects on wind pressure measurements. *Journal of Wind Engineering and Industrial Aerodynamics*, 188:260 – 268, 2019.

[31] Xue WANG, Xunnian WANG, Xiaobo REN, Xiwei YIN, and Weihua WANG. Effects of tube system and data correction for fluctuating pressure test in wind tunnel. *Chinese Journal of Aeronautics*, 31(4):710 – 718, 2018.

[32] Haosu Liu, Junqing Lei, and Li Zhu. Identification and application of the aerodynamic admittance functions of a double-deck truss girder. *Applied Sciences*, 9:1818, 05 2019.

[33] Lei Yan, Le-Dong Zhu, and Richard Flay. Identification of aerodynamic admittance functions of a flat closed-box deck in different grid-generated turbulent wind fields. *Advances in Structural Engineering*, 21:136943321771898, 02 2018.

[34] Vegard Antonsen and Ragne Røstbakken. Modelling of nonlinear self-excited aerodynamic forces for twin-deck bridge girders, 2019.

[35] Horg S. E. Aas, S. B. Wind tunnel testing of bridge decks. *Master's thesis, Norwegian University of Science and Technology, Department of Structural Engineering, Trondheim, Norway.*, 06 2016.

[36] T. Argentini D. Rocchi and M. Sbrosi. Pressure distribution and global forces on a bridge deck section: Experimental and cfd analysis of static aerodynamic forces. *Journal of Bridge Engineering*, 20(9), 2015.

[37] Scanivale. Mps4264 hardware software manual. `https://scanivalve.com/products/pressure-measurement/miniature-ethernet-pressure-scanners/mps4264/`.

[38] Jinlin Xia, Ke Li, and Yaojun Ge. Span-wise coherence of fluctuating forces on twin bridge decks and the turbulence effect. *Advances in Structural Engineering*, 22(15):3207–3221, 2019.

Appendix

A Pressure Transducer Connections

An overview of what channel on the pressure transducer the tubes at the surface of the section is connected to is presented below.

DOWNSTREAM-BOX										

SCANNER 1										
Channel no.	Tube no.		Channel no.	Tube no.		Channel no.	Tube no.		Channel no.	Tube no.
1	1101		2	1201		33	1502		34	1506
3	1102		4	1202		35	1503		36	1606
5	1103		6	1203		37	1504		38	1121
7	1104		8	1204		39	1505		40	1122
9	1105		10	1205		41	1601		42	1123
11	1106		12	1301		43	1602		44	1124
13	1107		14	1302		45	1603		46	1125
15	1108		16	1303		47	1604		48	1126
17	1109		18	1304		49	1605		50	1127
19	1110		20	1305		51	1117		52	1128
21	1111		22	1401		53	1118		54	1129
23	1112		24	1402		55	1119		56	1130
25	1113		26	1403		57	1120		58	1131
27	1114		28	1404		59	1206		60	1132
29	1115		30	1405		61	1306		62	1207
31	1116		32	1501		63	1406		64	1208

SCANNER 2										
Channel no.	Tube no.		Channel no.	Tube no.		Channel no.	Tube no.		Channel no.	Tube no.
1	1209		2	1136		33	1314		34	1143
3	1307		4	1137		35	1410		36	1144
5	1308		6	1138		37	1411		38	1145
7	1309		8	1139		39	1412		40	1146
9	1407		10	1140		41	1413		42	1147
11	1408		12	1141		43	1414		44	1148
13	1409		14	1142		45	1510		46	1215
15	1507		16	1210		47	1511		48	1216
17	1508		18	1211		49	1512		50	1315
19	1509		20	1212		51	1513		52	1316
21	1607		22	1213		53	1514		54	1415
23	1608		24	1214		55	1610		56	1416
25	1609		26	1310		57	1611		58	1515
27	1133		28	1311		59	1612		60	1516
29	1134		30	1312		61	1613		62	1615
31	1135		32	1313		63	1614		64	1616

UPSTREAM-BOX

SCANNER 3

Channel no.	Tube no.	Channel no.	Tube no.	Channel no.	Tube no.	Channel no.	Tube no.
1	2101	2	2201	33	2502	34	2506
3	2102	4	2202	35	2503	36	2606
5	2103	6	2203	37	2504	38	2121
7	2104	8	2204	39	2505	40	2122
9	2105	10	2205	41	2601	42	2123
11	2106	12	2301	43	2602	44	2124
13	2107	14	2302	45	2603	46	2125
15	2108	16	2303	47	2604	48	2126
17	2109	18	2304	49	2605	50	2127
19	2110	20	2305	51	2117	52	2128
21	2111	22	2401	53	2118	54	2129
23	2112	24	2402	55	2119	56	2130
25	2113	26	2403	57	2120	58	2131
27	2114	28	2404	59	2206	60	2132
29	2115	30	2405	61	2306	62	2207
31	2116	32	2501	63	2406	64	2208

SCANNER 4

Channel no.	Tube no.	Channel no.	Tube no.	Channel no.	Tube no.	Channel no.	Tube no.
1	2209	2	2136	33	2314	34	2143
3	2307	4	2137	35	2410	36	2144
5	2308	6	2138	37	2411	38	2145
7	2309	8	2139	39	2412	40	2146
9	2407	10	2140	41	2413	42	2147
11	2408	12	2141	43	2414	44	2148
13	2409	14	2142	45	2510	46	2215
15	2507	16	2210	47	2511	48	2216
17	2508	18	2211	49	2512	50	2315
19	2509	20	2212	51	2513	52	2316
21	2607	22	2213	53	2514	54	2415
23	2608	24	2214	55	2610	56	2416
25	2609	26	2310	57	2611	58	2515
27	2133	28	2311	59	2612	60	2516
29	2134	30	2312	61	2613	62	2615
31	2135	32	2313	63	2614	64	2616

B   Matlab scrips for Pressure Scanners Data Processing

Piece-wise Point Load Method

Matlab script for the piece-wise point load method.

```matlab
%% Time Series of Point Loads
% transforming pressure into loads and plotting the pressures
clc
clear all
close all
%corrline = 1
corrline = 2

%% importing pressure and sorting it
load('C:\Users\theah\Documents\NTNU\master\TESTER2\WindTunnelSystemMain\Dat
aCutted\Master2020TD_10_00_904_000.mat')
p=WT.Data.ProcessedData(8).Data; %pressure from scanners
[p1_1, p1_2, p1_3, p1_4, p1_5, p1_6, p2_1, p2_2, p2_3, p2_4, p2_5, p2_6] =
SortPressure2(p);
p1=p1_1; %downstream box pressure on corrline 1
p2=p2_1; %upstream box pressure on corrline 1.


%% importing coordinates
[x_taps, y_taps, x_taps2, y_taps2, x_coord, y_coord, x_coord2, y_coord2,
dist, A,...
    x_taps_16, y_taps_16, x_taps2_16, y_taps2_16, x_coord_16, y_coord_16,
x_coord2_16, y_coord2_16] = ImportingCoordinatesFunc;
%x_taps2, y_taps2 = coordinates for taps only on upstream box corrline 1.
%x_taps, y_taps = coordinates for taps only on downstream box corrline 1.
%x_coord2, y_coord2 = coordinates for taps and corners on upstream box
corrline 1.
%x_coord, y_coord = coordinates for taps and corners on downstream box
corrline 1.
%x_taps2_16, y_taps2_16 = coordinates for taps only on upstream box
corrline 2-6.
%x_taps_16, y_taps_16 = coordinates for taps only on downstream box
corrline 2-6.
%x_coord2_16, y_coord2_16 = coordinates for taps and corners on upstream
box corrline 2-6.
%x_coord_16, y_coord_16 = coordinates for taps and corners on downstream
box corrline 2-6.


%% ------------ Correlation line 1-----------------
%% normal vectors of the surfaces on the cross-section
a = zeros(6,2); %upstream box = box 2
a(1,:) = [x_coord2(1), y_coord2(1)];
a(2,:) = [x_coord2(18), y_coord2(18)];
a(3,:) = [x_coord2(24), y_coord2(24)];
a(4,:) = [x_coord2(38), y_coord2(38)];
a(5,:) = [x_coord2(50), y_coord2(50)];
a(6,:) = [x_coord2(1), y_coord2(1)];

b = zeros(6,2); %downstream box = box 1
b(1,:) = [x_coord(1), y_coord(1)];
b(2,:) = [x_coord(18), y_coord(18)];
b(3,:) = [x_coord(24), y_coord(24)];
b(4,:) = [x_coord(38), y_coord(38)];
b(5,:) = [x_coord(50), y_coord(50)];
b(6,:) = [x_coord(1), y_coord(1)];

%distance between two edges
dxdy=zeros(5,2); %upstream box
dxdy(1,:)= abs(a(2,:)-a(1,:));
dxdy(2,:)=abs(a(3,:)-a(2,:));
```

```
dxdy(3,:)=abs(a(4,:)-a(3,:));
dxdy(4,:)=abs(a(5,:)-a(4,:));
dxdy(5,:)=abs(a(6,:)-a(5,:));


dxdy2=zeros(5,2); %downstream box
dxdy2(1,:)= abs(b(2,:)-b(1,:));
dxdy2(2,:)=abs(b(3,:)-b(2,:));
dxdy2(3,:)=abs(b(4,:)-b(3,:));
dxdy2(4,:)=abs(b(5,:)-b(4,:));
dxdy2(5,:)=abs(b(6,:)-b(5,:));

%normal vectors
n1 = dxdy(1,:)/norm(dxdy(1,:)); %upstream
n2 = dxdy(2,:)/norm(dxdy(2,:)); %upstream
n3 = dxdy(3,:)/norm(dxdy(3,:)); %upstream
n4 = dxdy(4,:)/norm(dxdy(4,:)); %upstream
n5 = dxdy(5,:)/norm(dxdy(5,:)); %upstream
n6 = dxdy2(1,:)/norm(dxdy2(1,:)); %downstream
n7 = dxdy2(2,:)/norm(dxdy2(2,:)); %downstream
n8 = dxdy2(3,:)/norm(dxdy2(3,:)); %downstream
n9 = dxdy2(4,:)/norm(dxdy2(4,:)); %downstream
n10 = dxdy2(5,:)/norm(dxdy2(5,:)); %downstream

if corrline == 1;
%% decomponents of pressure
% the pressure points normal inward at the surface.

%upstream box = box2
%side1
Pressure_x2(:,1:16) = p2(:,1:16).*-n1(2);
Pressure_y2(:,1:16) = p2(:,1:16)*-n1(1);
%side2
Pressure_x2(:,17:20) = p2(:,17:20).*n2(2);
Pressure_y2(:,17:20) = p2(:,17:20).*(-n2(1));
%side3
Pressure_x2(:,21:32) =p2(:,21:32).*(n3(2));
Pressure_y2(:,21:32) = p2(:,21:32).*(n3(1));
%side4
Pressure_x2(:,33:42) = p2(:,33:42).*n4(2);
Pressure_y2(:,33:42) = p2(:,33:42).*(n4(1));
%side5
Pressure_x2(:,43:48) = p2(:,43:48).*-n5(2);
Pressure_y2(:,43:48) = p2(:,43:48).*+n5(1);

%downstream box = box1
%side6
Pressure_x(:,1:16) = p1(:,1:16).*-n6(2);
Pressure_y(:,1:16) = p1(:,1:16).*-n6(1);
%side 7
Pressure_x(:,17:20) = p1(:,17:20).*-n7(2);
Pressure_y(:,17:20)= p1(:,17:20).*-n7(1);
%side 8
Pressure_x(:,21:32) = p1(:,21:32).*-n8(2);
Pressure_y(:,21:32) = p1(:,21:32).*n8(1);
%side 9
Pressure_x(:,33:42) = p1(:,33:42).*n9(2);
Pressure_y(:,33:42) = p1(:,33:42).*n9(1);
%side 10
Pressure_x(:,43:48) = p1(:,43:48).*n10(2);
Pressure_y(:,43:48) = p1(:,43:48).*n10(1);
```

```matlab
%% plotting pressure
%using mean value of pressure from time series.
MeanP_x2 = mean(Pressure_x2);
MeanP_y2 = mean(Pressure_y2);
MeanP_x = mean(Pressure_x);
MeanP_y = mean(Pressure_y);

x_new2 = x_taps2 + MeanP_x2';
y_new2 = y_taps2 + MeanP_y2';
x_new = x_taps + MeanP_x';
y_new = y_taps + MeanP_y';

xy = zeros(48*2,2);
xy_new = zeros(48*2,2);
xy(1:48,:) = [x_taps, y_taps];
xy(49:end,:) = [x_taps2, y_taps2];
xy_new(1:48,:) = [x_new, y_new];
xy_new(49:end,:) = [x_new2, y_new2];

figure(); hold on
plot(x_coord2, y_coord2)
plot(x_coord, y_coord)
axis equal
hn=arrow3(xy, xy_new, '|-1',[0, 0]);
c=colorbar;
title('Point Pressure')
xlabel('x')
ylabel('z')
set(gca, 'fontsize',20)
xlabel(c,'Pressure, [Pa]')
ylim([-150 150])
%% ---------- Transforming pressure to loads ---------------------
w=1; %width [m]
Area = w.*A*10^-3; %[m^2]
for n = 1:size(p2,2)
        Load_x(:,n) = Pressure_x(:,n)*Area(n); %downstream
        Load_y(:,n) = Pressure_y(:,n)*Area(n); %downstream
        Load_x2(:,n) = Pressure_x2(:,n)*Area(n); %upstream
        Load_y2(:,n) = Pressure_y2(:,n)*Area(n); %upstream
end


%% Transforming pressure to moments
centerX = (x_coord2(1)+x_coord(1))/2; centerY=0;
%(y_coord2(1)+y_coord(1))/2;
distX=zeros(1,length(x_taps)); distY=zeros(1,length(y_taps));
distX2=zeros(1, length(x_taps)); distY2=zeros(1,length(y_taps));
for i = 1:length(x_taps)
    distX(i) = x_taps(i)-centerX;
    distY(i) = y_taps(i)-centerY;
    distX2(i) = x_taps2(i)-centerX;
    distY2(i) = y_taps2(i)-centerY;
end

abs_distX = abs(distX*10^-3);
abs_distY = abs(distY*10^-3);
abs_distX2 = abs(distX2*10^-3);
abs_distY2 = abs(distY2*10^-3);
a=0; b=0; c=0; d=0;
```

```matlab
for i=1:length(x_taps2) %upstream box nr 2
    if x_taps2(i)<=centerX && y_taps2(i)>=centerY %taps nr 1-24 and 48,47,
46 box 2
        if i>=21 %21,22,23,24
            PS_moment2(:,i) = Load_y2(:,i).*abs_distX2(i) +
Load_x2(:,i).*abs_distY2(i);
            a = a+1;
        elseif i>=17 && i<=20 %17-20
            PS_moment2(:,i) = Load_y2(:,i).*abs_distX2(i) +
Load_x2(:,i).*abs_distY2(i);
            a = a+1;
        elseif i<=16 && i>=1 %1-16
            PS_moment2(:,i) = Load_y2(:,i).*abs_distX2(i);
            a = a+1;
        else %46-48
            PS_moment2(:,i) = Load_x2(:,i).*abs_distY2(i);
            a = a+1;
        end
    elseif x_taps2(i)<=centerX && y_taps2(i) <=centerY %taps nr 25-45
        if i>=25 && i<=32 %taps 25-32
            PS_moment2(:,i) = Load_y2(:,i).*abs_distX2(i)-
Load_x2(:,i).*abs_distY2(i);
            b=b+1;
        elseif i>=33 && i<=42
            PS_moment2(:,i) = Load_y2(:,i).*abs_distX2(i);
            b=b+1;
        else %43-45
            PS_moment2(:,i) = -Load_x2(:,i).*abs_distY2(i);
            b=b+1;
        end
    end
end

for i=1:length(x_taps) %downstream box, nr.1
    if x_taps(i)>= centerX && y_taps(i)>=centerY %%upstream box, nr.2
        if i>=21 && i<=24 %21,22,23,24
            PS_moment(:,i) = -Load_y(:,i).*abs_distX(i) +
Load_x(:,i).*abs_distY(i);
            c = c+1;
        elseif i>=17 && i<=20 %17-20
            PS_moment(:,i) = -Load_y(:,i).*abs_distX(i) +
Load_x(:,i).*abs_distY(i);
            c = c+1;
        elseif i<=16 && i>=1 %1-16
            PS_moment(:,i) = -Load_y(:,i).*abs_distX(i);
            c = c+1;
        else %46-4842)
            PS_moment(:,i) = Load_x(:,i).*abs_distY(i);
            c = c+1;
        end
    else x_taps(i)>=centerX && y_taps(i)<=centerY; %taps nr 25-45
        if i>=25 && i<=32 %taps 25-32
            PS_moment(:,i) = -Load_y(:,i).*abs_distX(i)-
Load_x(:,i).*abs_distY(i);
            d=d+1;
        elseif i>=33 && i<=42 %33-42
            PS_moment(:,i) = -Load_y(:,i).*abs_distX(i);
            d=d+1;
        else %43-45
            PS_moment(:,i) = -Load_x(:,i).*abs_distY(i);
            d=d+1;
```

```matlab
        end
    end
end


%% saving time series
TSPointLoad(1).Fz1 = Load_y;
TSPointLoad(1).Fz2 = Load_y2;
TSPointLoad(1).Fx1 = Load_x;
TSPointLoad(1).Fx2 = Load_x2;
TSPointLoad(1).M1 = PS_moment;
TSPointLoad(1).M2 = PS_moment2;

%save('C:\Users\theah\Documents\NTNU\master\TESTER2\WindTunnelSystemMain\Po
stProccessing\Time Series Pont Load\TS10_00_904_000', 'TSPointLoad')

else %%corrline = 2
%% ---------- Line 2:6------------------------------------------------%%

%% Decomponents of pressure
p1=zeros(size(p1_2,1),16,5);
p2=zeros(size(p1_2,1),16,5);
p1(:,:,1) = p1_2; p1(:,:,2) = p1_3; p1(:,:,3) = p1_4; p1(:,:,4) = p1_5;
p1(:,:,5) = p1_6;
p2(:,:,1) = p2_2; p2(:,:,2) = p2_3; p2(:,:,3) = p2_4; p2(:,:,4) = p2_5;
p2(:,:,5) = p2_6;


Pressure_x2=zeros(size(p1_2,1),16,5);
for n=1:5
%upstream box = box2
%side1
Pressure_x2(:,1:5,n) = p2(:,1:5,n).*-n1(2);
Pressure_y2(:,1:5,n) = p2(:,1:5,n)*-n1(1);
%side2
Pressure_x2(:,6,n) = p2(:,6,n).*n2(2);
Pressure_y2(:,6,n) = p2(:,6,n).*(-n2(1));
%side3
Pressure_x2(:,7:9,n) =p2(:,7:9,n).*(n3(2));
Pressure_y2(:,7:9,n) = p2(:,7:9,n).*(n3(1));
%side4
Pressure_x2(:,10:14,n) = p2(:,10:14,n).*n4(2);
Pressure_y2(:,10:14,n) = p2(:,10:14,n).*(n4(1));
%
Pressure_x2(:,15:16,n) = p2(:,15:16,n).*-n5(2);
Pressure_y2(:,15:16,n) = p2(:,15:16,n).*+n5(1);
%downstream box = box1
%side6
Pressure_x(:,1:5,n) = p1(:,1:5,n).*-n6(2);
Pressure_y(:,1:5,n) = p1(:,1:5,n).*-n6(1);
%side 7
Pressure_x(:,6,n) = p1(:,6,n).*-n7(2);
Pressure_y(:,6,n)= p1(:,6,n).*-n7(1);
%side 8
Pressure_x(:,7:9,n) = p1(:,7:9,n).*-n8(2);
Pressure_y(:,7:9,n) = p1(:,7:9,n).*n8(1);
%side 9
Pressure_x(:,10:14,n) = p1(:,10:14,n).*n9(2);
Pressure_y(:,10:14,n) = p1(:,10:14,n).*n9(1);
%side 10
```

```matlab
    Pressure_x(:,15:16,n) = p1(:,15:16,n).*n10(2);
    Pressure_y(:,15:16,n) = p1(:,15:16,n).*n10(1);
end

for n=1:5
    MeanP_x2 = mean(Pressure_x2(:,:,n));
    MeanP_y2 = mean(Pressure_y2(:,:,n));
    MeanP_x = mean(Pressure_x(:,:,n));
    MeanP_y = mean(Pressure_y(:,:,n));

    x_new2 = x_taps2_16 + MeanP_x2';
    y_new2 = y_taps2_16 + MeanP_y2';
    x_new = x_taps_16 + MeanP_x';
    y_new = y_taps_16 + MeanP_y';

    xy = zeros(16*2,2);
    xy_new = zeros(16*2,2);
    xy(1:16,:) = [x_taps_16, y_taps_16];
    xy(17:end,:) = [x_taps2_16, y_taps2_16];
    xy_new(1:16,:) = [x_new, y_new];
    xy_new(17:end,:) = [x_new2, y_new2];

    figure(n); hold on
    plot(x_coord2_16, y_coord2_16)
    plot(x_coord_16, y_coord_16)
    axis equal
    hn=arrow3(xy, xy_new, '|-1',[0, 0]);
    c=colorbar;
    title('Point Pressure')
    xlabel('x')
    ylabel('z')
    set(gca, 'fontsize',20)
    xlabel(c,'Pressure, [Pa]')
    ylim([-150 150])

end

%% ------------Tranforming into Loads--------------------
A = Distance16Taps;
w=1; %width [m]
Area = w.*A*10^-3; %[m^2]
for n=1:5
    for i = 1:16
        Load_x(:,i,n) = Pressure_x(:,i,n).*Area(i); %downstream
        Load_y(:,i,n) = Pressure_y(:,i,n).*Area(i); %downstream
        Load_x2(:,i,n) = Pressure_x2(:,i,n).*Area(i); %upstream
        Load_y2(:,i,n) = Pressure_y2(:,i,n).*Area(i); %upstream
    end
end

centerX = (x_coord2_16(1)+x_coord_16(1))/2; centerY=0;
%(y_coord2(1)+y_coord(1))/2;
% distX=zeros(1,length(x_taps_16)); distY=zeros(1,length(y_taps_16));
% distX2=zeros(1, length(x_taps_16)); distY2=zeros(1,length(y_taps_16));
for i = 1:length(x_taps_16)
    distX(i) = x_taps_16(i)-centerX;
    distY(i) = y_taps_16(i)-centerY;
    distX2(i) = x_taps2_16(i)-centerX;
    distY2(i) = y_taps2_16(i)-centerY;
end
```

```matlab
abs_distX = abs(distX*10^-3);
abs_distY = abs(distY*10^-3);
abs_distX2 = abs(distX2*10^-3);
abs_distY2 = abs(distY2*10^-3);
a=0; b=0; c=0; d=0;

for n=1:5
    for i=1:length(x_taps_16);
            if x_taps2_16(i)<=centerX && y_taps2_16(i)>=centerY %
                if i>=7
                    PS_moment2(:,i,n) = Load_y2(:,i,n).*abs_distX2(i) +
Load_x2(:,i,n).*abs_distY2(i);
                    a = a+1;
                elseif i==6
                 PS_moment2(:,i,n) = Load_y2(:,i,n).*abs_distX2(i) +
Load_x2(:,i,n).*abs_distY2(i);
                    a = a+1;
                elseif i<=5 && i>=1 %1-5
                    PS_moment2(:,i,n) = Load_y2(:,i,n).*abs_distX2(i);
                    a = a+1;
                else %16
                    PS_moment2(:,i,n) = Load_x2(:,i,n).*abs_distY2(i);
                    a = a+1;
                end
            elseif x_taps2_16(i)<=centerX && y_taps2_16(i) <=centerY %taps
nr 25-45
                if i>=8 && i<=9 %taps 8,9
                    PS_moment2(:,i,n) = Load_y2(:,i,n).*abs_distX2(i)-
Load_x2(:,i,n).*abs_distY2(i);
                    b=b+1;
                elseif i>=10 && i<=14
                    PS_moment2(:,i,n) = Load_y2(:,i,n).*abs_distX2(i);
                    b=b+1;
                else %15
                    PS_moment2(:,i,n) = -Load_x2(:,i,n).*abs_distY2(i);
                    b=b+1;
                end
            end
    end
end
%%
for n=1:5
    for i=1:length(x_taps_16) %downstream box, nr.1
        if x_taps_16(i)>= centerX && y_taps_16(i)>=centerY %%upstream box,
nr.2
            if i>=7 %21,22,23,24
                PS_moment(:,i,n) = -Load_y(:,i,n).*abs_distX(i) +
Load_x(:,i,n).*abs_distY(i);
                c = c+1;
            elseif i==6
                PS_moment(:,i,n) = -Load_y(:,i,n).*abs_distX(i) +
Load_x(i,n).*abs_distY(i);
                c = c+1;
            elseif i<=5 && i>=1 %1-16
                PS_moment(:,i,n) = -Load_y(:,i,n).*abs_distX(i);
                c = c+1;
            else %46-4842)
                PS_moment(:,i,n) = Load_x(:,i,n).*abs_distY(i);
                c = c+1;
            end
        else x_taps_16(i)>=centerX && y_taps_16(i)<=centerY; %taps nr 25-45
```

```matlab
                if i>=8 && i<=9 %8,9
                    PS_moment(:,i,n) = -Load_y(:,i,n).*abs_distX(i)-
Load_x(:,i,n).*abs_distY(i);
                    d=d+1;
                elseif i>=10 && i<=14 %33-42
                    PS_moment(:,i,n) = -Load_y(:,i,n).*abs_distX(i);
                    d=d+1;
                else %43-45
                    PS_moment(:,i,n) = -Load_x(:,i,n).*abs_distY(i);
                    d=d+1;
                end
            end
        end
end
H = [2 3 4 5 6]; %%Corrline names
for n=1:5
    TSPointLoadCorrline(n).Corrline = H(n);
    TSPointLoadCorrline(n).Fz1 = Load_y(:,:,n);
    TSPointLoadCorrline(n).Fz2 = Load_y2(:,:,n);
    TSPointLoadCorrline(n).Fx1 = Load_x(:,:,n);
    TSPointLoadCorrline(n).Fx2 = Load_x2(:,:,n);
    TSPointLoadCorrline(n).M1 = PS_moment(:,:,n);
    TSPointLoadCorrline(n).M2 = PS_moment2(:,:,n);
end


%save('C:\Users\theah\Documents\NTNU\master\TESTER2\WindTunnelSystemMain\Po
stProccessing\Time Series Pont Load\TS_Corrline10_00_903_000',
'TSPointLoadCorrline')


end %if corrline
```

Interpolated load Method

Matlab script for the interpolated load method.

```matlab
%% distributed forces on correlation line 1
clc
clear all
close all

filename = '10_00_906_000_Line1.jpg';
filenamePressure = '10_00_906_000_Line1.jpg';

fname = 'C:\Users\theah\NTNU\Gruppeområde - General\10 testing\05 Distributed
Load plot';
fnamePressure = 'C:\Users\theah\NTNU\Gruppeområde - General\10 testing\06
Distributed Pressure Plot';
%importing pressure and sorting it
load('C:\Users\theah\Documents\NTNU\master\TESTER2\WindTunnelSystemMain\DataCu
tted\Master2020TD_10_00_906_000.mat')
p=WT.Data.ProcessedData(8).Data; %pressure from scanners
[p1_1, p1_2, p1_3, p1_4, p1_5, p1_6, p2_1, p2_2, p2_3, p2_4, p2_5, p2_6] =
SortPressure2(p);
p1_1 =mean(p1_1,1);
p2_1 = mean(p2_1,1);

%% importing coordinates
[x_taps, y_taps, x_taps2, y_taps2, x_coord, y_coord, x_coord2, y_coord2,
dist, A,...
    x_taps_16, y_taps_16, x_taps2_16, y_taps2_16, x_coord_16, y_coord_16,
x_coord2_16, y_coord2_16] = ImportingCoordinatesFunc;
%x_taps2, y_taps2 = coordinates for taps only on upstream box corrline 1.
%x_taps, y_taps = coordinates for taps only on downstream box corrline 1.
%x_coord2, y_coord2 = coordinates for taps and corners on upstream box
corrline 1.
%x_coord, y_coord = coordinates for taps and corners on downstream box
corrline 1.
%x_taps2_16, y_taps2_16 = coordinates for taps only on upstream box corrline
2-6.
%x_taps_16, y_taps_16 = coordinates for taps only on downstream box corrline
2-6.
%x_coord2_16, y_coord2_16 = coordinates for taps and corners on upstream box
corrline 2-6.
%x_coord_16, y_coord_16 = coordinates for taps and corners on downstream box
corrline 2-6.
figure(1); hold on;
plot(x_coord,y_coord, 'displayname', 'downstream')
plot(x_coord2,y_coord2, 'displayname', 'upstream')
legend show
axis equal


%% new coordinates box 1 = downstream box
Ncord = [191, 36, 110, 121, 81]; %number of coordinates on each side
x_start = [x_coord(1), x_coord(19), x_coord(25), x_coord(39), x_coord(51)];
y_start = [y_coord(1), y_coord(19), y_coord(25), y_coord(39), y_coord(51)];
dt = 1; %spacing of coordinates [mm]
angle=[0 45.0 30.0 0 90];
%creates new coordinates with spacing dt
%Xcoord = zeros(sum(Ncord),1);
```

```matlab
[Xcoord6, Ycoord6] = NewCoordinates(x_start(1), y_start(1), dt, 180-angle(1),
Ncord(1));
[Xcoord7, Ycoord7] = NewCoordinates(x_start(2), y_start(2), dt, 180-angle(2),
Ncord(2));
[Xcoord8, Ycoord8] = NewCoordinates(x_start(3), y_start(3), dt, angle(3),
Ncord(3));
[Xcoord9, Ycoord9] = NewCoordinates(x_start(4), y_start(4), dt, angle(4),
Ncord(4));
[Xcoord10, Ycoord10] = NewCoordinates(x_start(5), y_start(5), dt,
180+angle(5), Ncord(5));

% %% new coordinates box 2 = upstream box
x_start2 = [x_coord2(1), x_coord2(19), x_coord2(25), x_coord2(39),
x_coord2(51)];
y_start2 = [y_coord2(1), y_coord2(19), y_coord2(25), y_coord2(39),
y_coord2(51)];
dt = 1; %spacing of coordinates [mm]
%creates new coordinates with spacing dt
%Xcoord = zeros(sum(Ncord),1);
[Xcoord1, Ycoord1] = NewCoordinates(x_start2(1), y_start2(1), dt, angle(1),
Ncord(1));
[Xcoord2, Ycoord2] = NewCoordinates(x_start2(2), y_start2(2), dt, angle(2),
Ncord(2));
[Xcoord3, Ycoord3] = NewCoordinates(x_start2(3), y_start2(3), dt, 180-
angle(3), Ncord(3));
[Xcoord4, Ycoord4] = NewCoordinates(x_start2(4), y_start2(4), dt, 180-
angle(4), Ncord(4));
[Xcoord5, Ycoord5] = NewCoordinates(x_start2(5), y_start2(5), dt,
180+angle(5), Ncord(5));

Xcoord_2 = [Xcoord1, Xcoord2, Xcoord3, Xcoord4, Xcoord5];
%Xcoord(end+1)=Xcoord(1);
Ycoord_2 = [Ycoord1, Ycoord2, Ycoord3, Ycoord4, Ycoord5];
%Ycoord(end+1)=Ycoord(1);

Xcoord = [Xcoord6, Xcoord7, Xcoord8, Xcoord9, Xcoord10];
%Xcoord(end+1)=Xcoord(1);
Ycoord = [Ycoord6, Ycoord7, Ycoord8, Ycoord9, Ycoord10];
%Ycoord(end+1)=Ycoord(1);


%% converting point loads to distributed loads
%by using spline interpolation function
for k=1:10
        if k==1 %Side 1 upstream box = box 2
            s_x1 = x_coord2(1:18);
            s_y1 = y_coord2(1:18);
            s_x=s_x1;
            s_y=s_y1;
            s_taps1 = p2_1(1:16);
            s_taps=s_taps1;
        elseif k==2 %side2
            s_x2 = x_coord2(19:24);
            s_y2 = y_coord2(19:24);
            s_x=s_x2;
            s_y=s_y2;
            s_taps2 = p2_1(17:20);
```

```matlab
        s_taps=s_taps2;
    elseif k==3 %side3
        s_x3 = x_coord2(25:38);
        s_y3 = y_coord2(25:38);
        s_x = s_x3;
        s_y=s_y3;
        s_taps3 = p2_1(21:32);
        s_taps=s_taps3;
    elseif k==4 %side4
        s_x4 = x_coord2(39:50);
        s_y4 = y_coord2(39:50);
        s_x=s_x4; s_y=s_y4;
        s_taps4 = p2_1(33:42);
        s_taps=s_taps4;
    elseif k==5 %side5
        s_x5 = x_coord(51:58);
        s_y5 = y_coord(51:58);
        s_x=s_x5; s_y=s_y5;
        s_taps5 = p2_1(43:48);
        s_taps=s_taps5;
    elseif k==6 %Side 1 box 1 = downstream box
        s_x6 = x_coord(1:18);
        s_y6 = y_coord(1:18);
        s_x=s_x6;
        s_y=s_y6;
        s_taps6 = p1_1(1:16);
        s_taps=s_taps6;
    elseif k==7 %side2 box 1 = downstream box
        s_x7 = x_coord(19:24);
        s_y7 = y_coord(19:24);
        s_x=s_x7;
        s_y=s_y7;
        s_taps7 = p1_1(17:20);
        s_taps=s_taps7;
    elseif k==8 %side3 box 1 = downstream box
        s_x8 = x_coord(25:38);
        s_y8 = y_coord(25:38);
        s_x = s_x8;
        s_y=s_y8;
        s_taps8 = p1_1(21:32);
        s_taps=s_taps8;
    elseif k==9 %side4 box 1 = downstream box
        s_x9 = x_coord(39:50);
        s_y9 = y_coord(39:50);
        s_x=s_x9; s_y=s_y9;
        s_taps9 = p1_1(33:42);
        s_taps=s_taps9;
    elseif k==10 %side5 box 1 = downstram box
        s_x10 = x_coord(51:58);
        s_y10 = y_coord(51:58);
        s_x=s_x10; s_y=s_y10;
        s_taps10 = p1_1(43:48);
        s_taps=s_taps10;
    end

    S_L = zeros(1,length(s_x));
    for i=2:(length(s_x))
```

```matlab
                S_L(i)=S_L(i-1)+sqrt((s_x(i)-s_x(i-1))^2+(s_y(i)-s_y(i-1))^2);
            end
            X_s = S_L(2:end-1);
            xx_s = S_L(1):dt:S_L(end);
            yy_s = spline(X_s, s_taps,xx_s);

%           figure; hold on;
%           plot(X_s, s_taps, 'o', xx_s, yy_s)
%           plot(xx_s, yy_s, 'r', 'Displayname', 'yy_s')
%           %plot(Xcoord, Ycoord, 'r')
%           axis equal
%           legend show

            if k==1
                PS_1 = yy_s;
                S_LS1 = S_L;
            elseif k==2
                PS_2 = yy_s;
                S_LS2 = S_L;
            elseif k==3
                PS_3 = yy_s;
                S_LS3 = S_L;
                tap_end3 = yy_s(end);
            elseif k==4
                PS_4 = yy_s;
                S_LS4 = S_L;
            elseif k==5
                PS_5 = yy_s;
                S_LS5 = S_L;
            elseif k==6
                 PS_6 = yy_s;
                S_LS6 = S_L;
            elseif k==7
                PS_7 = yy_s;
                S_LS7 = S_L;
            elseif k==8
                PS_8 = yy_s;
                S_LS8 = S_L;
            elseif k==9
                PS_9 = yy_s;
                S_LS9 = S_L;
            elseif k==10
                PS_10 = yy_s;
                S_LS10 = S_L;

            end
    end


%% deocomponents of pressures
%edges on the cross section
a = zeros(6,2); %upstream box = box 2
a(1,:) = [x_coord2(1), y_coord2(1)];
a(2,:) = [x_coord2(18), y_coord2(18)];
a(3,:) = [x_coord2(24), y_coord2(24)];
a(4,:) = [x_coord2(38), y_coord2(38)];
a(5,:) = [x_coord2(50), y_coord2(50)];
```

```matlab
a(6,:) = [x_coord2(1), y_coord2(1)];

b = zeros(6,2); %downstream box = box 1
b(1,:) = [x_coord(1), y_coord(1)];
b(2,:) = [x_coord(18), y_coord(18)];
b(3,:) = [x_coord(24), y_coord(24)];
b(4,:) = [x_coord(38), y_coord(38)];
b(5,:) = [x_coord(50), y_coord(50)];
b(6,:) = [x_coord(1), y_coord(1)];

%distance between two edges
dxdy=zeros(5,2); %upstream box
dxdy(1,:)= abs(a(2,:)-a(1,:));
dxdy(2,:)=abs(a(3,:)-a(2,:));
dxdy(3,:)=abs(a(4,:)-a(3,:));
dxdy(4,:)=abs(a(5,:)-a(4,:));
dxdy(5,:)=abs(a(6,:)-a(5,:));

dxdy2=zeros(5,2); %downstream box
dxdy2(1,:)= abs(b(2,:)-b(1,:));
dxdy2(2,:)=abs(b(3,:)-b(2,:));
dxdy2(3,:)=abs(b(4,:)-b(3,:));
dxdy2(4,:)=abs(b(5,:)-b(4,:));
dxdy2(5,:)=abs(b(6,:)-b(5,:));

%normal vectors
n1 = dxdy(1,:)/norm(dxdy(1,:)); %upstream
n2 = dxdy(2,:)/norm(dxdy(2,:)); %upstream
n3 = dxdy(3,:)/norm(dxdy(3,:)); %upstream
n4 = dxdy(4,:)/norm(dxdy(4,:)); %upstream
n5 = dxdy(5,:)/norm(dxdy(5,:)); %upstream
n6 = dxdy2(1,:)/norm(dxdy2(1,:)); %downstream
n7 = dxdy2(2,:)/norm(dxdy2(2,:)); %downstream
n8 = dxdy2(3,:)/norm(dxdy2(3,:)); %downstream
n9 = dxdy2(4,:)/norm(dxdy2(4,:)); %downstream
n10 = dxdy2(5,:)/norm(dxdy2(5,:)); %downstream

%% upstream deck, PS_x1,PS_y1-PS_x5,PS_y5
PS_x = PS_1.*-n1(2);
PS_y = PS_1*-n1(1);
PS = PS_1;
PS_y1 = PS_y; PS_x1=PS_x;
name=sprintf('S%d.mat',1);
save(name, 'PS_y', 'PS_x', 'PS');

PS_x = PS_2.*n2(2);
PS_y = PS_2.*-n2(1);
PS = PS_2;
PS_xy2=[PS_x; PS_y]';
PS_y2 = PS_y; PS_x2=PS_x;
name=sprintf('S%d.mat',2);
save(name, 'PS_y', 'PS_x', 'PS');

PS_x =PS_3.*n3(2);
PS_y = PS_3.*n3(1);
PS = PS_3;
PS_y3 = PS_y; PS_x3=PS_x;
```

```matlab
name=sprintf('S%d.mat',3);
save(name, 'PS_y', 'PS_x', 'PS');


PS_x = PS_4.*n4(2);
PS_y = PS_4.*n4(1);
PS = PS_4;
PS_y4 = PS_y; PS_x4=PS_x;
name=sprintf('S%d.mat',4);
save(name, 'PS_y', 'PS_x', 'PS');


PS_x = PS_5.*-n5(2);
PS_y = PS_5.*n5(1);
PS = PS_5(1:end);
PS_y5 = PS_y; PS_x5=PS_x;
name=sprintf('S%d.mat',5);
save(name, 'PS_y', 'PS_x', 'PS');

%% upstream deck, PS_x6,PS_y6-PS_x10,PS_y10
PS_x = PS_6.*-n6(2);
PS_y = PS_6.*-n6(1);
PS = PS_6;
PS_y6 = PS_y; PS_x6=PS_x;
name=sprintf('S%d.mat',6);
save(name, 'PS_y', 'PS_x', 'PS');


PS_x = PS_7.*-n7(2);
PS_y = PS_7.*-n7(1);
PS = PS_7;
PS_y7 = PS_y; PS_x7=PS_x;
name=sprintf('S%d.mat',7);
save(name, 'PS_y', 'PS_x', 'PS');


PS_x = PS_8.*-n8(2);
PS_y = PS_8.*n8(1);
PS = PS_8(1:end);
PS_y8 = PS_y; PS_x8=PS_x;
name=sprintf('S%d.mat',8);
save(name, 'PS_y', 'PS_x', 'PS');


PS_x = PS_9.*n9(2);
PS_y = PS_9.*n9(1);
PS = PS_9(1:end);
PS_y9 = PS_y; PS_x9=PS_x;
name=sprintf('S%d.mat',9);
save(name, 'PS_y', 'PS_x', 'PS');


PS_x = PS_10.*n10(2);
PS_y = PS_10.*n10(1);
PS = PS_10(1:end);
PS_y10 = PS_y; PS_x10=PS_x;
name=sprintf('S%d.mat',10);
save(name, 'PS_y', 'PS_x', 'PS');


%% plotting pressure distribution
P_x1 = (Xcoord1+PS_x1);
P_y1 = (Ycoord1+PS_y1);
```

```matlab
P_x2 = Xcoord2+PS_x2;
P_y2 = Ycoord2+PS_y2;
P_x3 = Xcoord3+PS_x3;
P_y3 = Ycoord3+PS_y3;
P_x4 = Xcoord4+PS_x4;
P_y4 = Ycoord4+PS_y4;
P_x5 = Xcoord5+PS_x5;
P_y5 = Ycoord5+PS_y5;

P_x6 = (Xcoord6+PS_x6);
P_y6 = (Ycoord6+PS_y6);
P_x7 = Xcoord7+PS_x7;
P_y7 = Ycoord7+PS_y7;
P_x8 = Xcoord8+PS_x8;
P_y8 = Ycoord8+PS_y8;
P_x9 = Xcoord9+PS_x9;
P_y9 = Ycoord9+PS_y9;
P_x10 = Xcoord10+PS_x10;
P_y10 = Ycoord10+PS_y10;

Pressure_x_2 = [P_x1, P_x2, P_x3, P_x4, P_x5];
Pressure_y_2 = [P_y1, P_y2, P_y3, P_y4, P_y5];
Pressure_x = [P_x6, P_x7, P_x8, P_x9, P_x10];
Pressure_y = [P_y6, P_y7, P_y8, P_y9, P_y10];


xy = zeros(length(Xcoord)*2,2);
xy_pressure = zeros(length(Xcoord)*2,2);
xy(1:length(Xcoord),:) = [Xcoord', Ycoord'];
xy(length(Xcoord)+1:end,:) = [Xcoord_2', Ycoord_2'];
xy_pressure(1:length(Xcoord),:) = [Pressure_x', Pressure_y'];
xy_pressure(length(Xcoord)+1:end,:) = [Pressure_x_2', Pressure_y_2'];


%plotting distributed pressure
figure(); hold on
plot(x_coord2, y_coord2)
plot(x_coord, y_coord)
axis equal
hn=arrow3(xy, xy_pressure, '|-1',[0.1,0.1]);
c=colorbar ;
title('Distributed pressure')
xlabel('x')
ylabel('z')
ylim([-150 150])
set(gca, 'fontsize',20)
xlabel(c,'Pressure, [Pa]')
saveas(gca, fullfile(fnamePressure, filenamePressure), 'fig');
saveas(gca, fullfile(fnamePressure, filenamePressure), 'jpg');



%% convert pressure to loads
w=2.68; Dt=dt*10^-3;
for i=1:10
    name = sprintf('S%d.mat', i);
    load(name);
```

```matlab
    F = zeros(1, length(PS));
    Fy = zeros(1, length(PS_y));
    Fx = zeros(1,length(PS_x));

    F(2:end-1)=PS(2:end-1).*Dt*w;
    F(1)=PS(1)*Dt*w/2;
    F(end)=PS(end)*Dt*w/2;

    Fy(2:end-1)=PS_y(2:end-1).*Dt*w;
    Fy(1)=PS_y(1).*Dt*w/2;
    Fy(end)=PS_y(end).*Dt*w/2;

    Fx(2:end-1)=PS_x(2:end-1).*Dt*w;
    Fx(1)=PS_x(1).*Dt*w/2;
    Fx(end)=PS_x(end).*Dt*w/2;

    name = sprintf('S%d_loads.mat', i);
    save(name, 'Fx', 'Fy', 'F');
end
%Load 1-5, upstream deck and load 6-10 downstream deck.
name = sprintf('S%d_loads.mat', 1);
load(name);
Fy_1 = Fy;
Fx_1 = Fx;
F_1 = F;

name = sprintf('S%d_loads.mat', 2);
load(name);
Fy_2 = Fy;
Fx_2 = Fx;
F_2 = F;

name = sprintf('S%d_loads.mat', 3);
load(name);
Fy_3 = Fy;
Fx_3 = Fx;
F_3 = F;

name = sprintf('S%d_loads.mat', 4);
load(name);
Fy_4 = Fy;
Fx_4 = Fx;
F_4 = F;

name = sprintf('S%d_loads.mat', 5);
load(name);
Fy_5 = Fy;
Fx_5 = Fx;
F_5 = F;

name = sprintf('S%d_loads.mat', 6);
load(name);
Fy_6 = Fy;
Fx_6 = Fx;
F_6 = F;
```

```matlab
name = sprintf('S%d_loads.mat', 7);
load(name);
Fy_7 = Fy;
Fx_7 = Fx;
F_7 = F;

name = sprintf('S%d_loads.mat', 8);
load(name);
Fy_8 = Fy;
Fx_8 = Fx;
F_8 = F;

name = sprintf('S%d_loads.mat', 9);
load(name);
Fy_9 = Fy;
Fx_9 = Fx;
F_9 = F;

name = sprintf('S%d_loads.mat', 10);
load(name);
Fy_10 = Fy;
Fx_10 = Fx;
F_10 = F;

Fx2 = [Fx_1, Fx_2, Fx_3, Fx_4, Fx_5]; %upstream
Fy2 = [Fy_1, Fy_2, Fy_3, Fy_4, Fy_5]; %upstream
Fx = [Fx_6, Fx_7, Fx_8, Fx_9, Fx_10]; %downstream
Fy = [Fy_6, Fy_7, Fy_8, Fy_9, Fy_10]; %downstream

SumFx2=sum(Fx_1)+sum(Fx_2)+sum(Fx_3)+sum(Fx_4)+sum(Fx_5);
SumFx1=sum(Fx_6)+sum(Fx_7)+sum(Fx_8)+sum(Fx_9)+sum(Fx_10);

SumFz2=sum(Fy_1)+sum(Fy_2)+sum(Fy_3)+sum(Fy_4)+sum(Fy_5);
SumFz1=sum(Fy_6)+sum(Fy_7)+sum(Fy_8)+sum(Fy_9)+sum(Fy_10);
%% plotting loads F;
scale=100;
Load_x1 = (Xcoord1+Fx_1*scale);
Load_y1 = (Ycoord1+Fy_1*scale);
Load_x2 = Xcoord2+Fx_2*scale;
Load_y2 = Ycoord2+Fy_2*scale;
Load_x3 = Xcoord3+Fx_3*scale;
Load_y3 = Ycoord3+Fy_3*scale;
Load_x4 = Xcoord4+Fx_4*scale;
Load_y4 = Ycoord4+Fy_4*scale;
Load_x5 = Xcoord5+Fx_5*scale;
Load_y5 = Ycoord5+Fy_5*scale;

Load_x6 = (Xcoord6+Fx_6*scale);
Load_y6 = (Ycoord6+Fy_6*scale);
Load_x7 = Xcoord7+Fx_7*scale;
Load_y7 = Ycoord7+Fy_7*scale;
Load_x8 = Xcoord8+Fx_8*scale;
Load_y8 = Ycoord8+Fy_8*scale;
Load_x9 = Xcoord9+Fx_9*scale;
Load_y9 = Ycoord9+Fy_9*scale;
Load_x10 = Xcoord10+Fx_10*scale;
Load_y10 = Ycoord10+Fy_10*scale;
```

```matlab
Loadx2 = [Load_x1, Load_x2, Load_x3, Load_x4, Load_x5];
Loady2 = [Load_y1, Load_y2, Load_y3, Load_y4, Load_y5];
Loadx = [Load_x6, Load_x7, Load_x8, Load_x9, Load_x10];
Loady = [Load_y6, Load_y7, Load_y8, Load_y9, Load_y10];


xy = zeros(length(Xcoord)*2,2);
xy_Load = zeros(length(Xcoord)*2,2);
xy(1:length(Xcoord),:) = [Xcoord', Ycoord'];
xy(length(Xcoord)+1:end,:) = [Xcoord_2', Ycoord_2'];
xy_Load(1:length(Xcoord),:) = [Loadx', Loady'];
xy_Load(length(Xcoord)+1:end,:) = [Loadx2', Loady2'];


% %plotting distributed load
% figure(); hold on
% plot(x_coord2, y_coord2)
% plot(x_coord, y_coord)
% axis equal
% hn=arrow3(xy, xy_Load, '|-1',0);
% c=colorbar;
% title('Distributed Load')
% xlabel('x')
% ylabel('z')
% set(gca, 'fontsize',20)
% ylim([-100 100])
% xlabel(c,'Force, [N]\cdot10^{-2}')

% saveas(gca, fullfile(fname, filename), 'fig');
%saveas(gca, fullfile(fname, filename), 'jpg');
%
%% moment forces
centerX = (x_coord2(1)+x_coord(1))/2; centerY=0;
%(y_coord2(1)+y_coord(1))/2;
distX=zeros(1, length(Ncord)); distY=zeros(1,length(Xcoord));
for i = 1:length(Xcoord)
    distX(i) = Xcoord(i)-centerX;
    distY(i) = Ycoord(i)-centerY;
    distX2(i) = Xcoord_2(i)-centerX;
    distY2(i) = Ycoord_2(i)-centerY;
end
m1=length(Xcoord1); m2=length(Xcoord2); m3=length(Xcoord3);
m4=length(Xcoord4); m5=length(Xcoord5);

% figure(16); hold on
% plot(x_coord, y_coord)
% plot(x_coord2, y_coord2)
% plot(centerX, centerY, 'o')
% plot(x_taps, y_taps, 'o')
% plot(x_taps2, y_taps2, 'o')
% plot(10)
% axis equal

%absoulte vale of moment arm and converting from mm to m.
abs_distX=abs(distX*10^(-3));
```

```matlab
abs_distY=abs(distY*10^(-3));
abs_distX2=abs(distX2*10^(-3));
abs_distY2=abs(distY2*10^(-3));

a=0;b=0;c=0;d=0;
PS_moment2=zeros(1,length(Xcoord));
for i=1:length(Xcoord_2) % upstream box, box 2
    if Xcoord_2(i)<=centerX && Ycoord_2(i)>=centerY %taps nr 1-24 and 48,47,
46 box 2
        if i>=(m1+m2+1) %21,22,23
            PS_moment2(i) = Fy2(i).*abs_distX2(i) + Fx2(i).*abs_distY2(i);
            a = a+1;
        elseif i>=(m1+1) && i<=(m1+m2) %17-20
            PS_moment2(i) = Fy2(i).*abs_distX2(i) + Fx2(i).*abs_distY2(i);
            a = a+1;
        elseif i<=m1 %1-16
            PS_moment2(i) = Fy2(i).*abs_distX2(i);
            a = a+1;
        else %46-48
            PS_moment2(i) = Fx2(i).*abs_distY2(i);
            a = a+1;
        end
    elseif Xcoord_2(i)<=centerX && Ycoord_2(i) <=centerY %taps nr 24-45
        if i>=(m1+m2+4) && i<=(m1+m2+m3) %taps 25-32
            PS_moment2(i) = Fy2(i).*abs_distX2(i)-Fx2(i).*abs_distY2(i);
            b=b+1;
        elseif i>=(m1+m2+m3+1) && i<=(m1+m2+m3+m4) %%
            PS_moment2(i) = Fy2(i).*abs_distX2(i);
            b=b+1;
        else %43-45
            PS_moment2(i) = -Fx2(i).*abs_distY2(i);
            b=b+1;
        end
    end
end
moment=zeros(1,length(Xcoord));
for i=1:length(Xcoord) %downstream box, nr.1
    if Xcoord(i)>= centerX && Ycoord(i)>=centerY %%downstream box, nr.2
        if i>=(m1+m2+1) %21,22,23
            moment(i) = -Fy(i).*abs_distX(i) + Fx(i).*abs_distY(i);
            c = c+1;
        elseif i>(m1) && i<=(m1+m2) %17-20
            moment(i) = -Fy(i).*abs_distX(i) + Fx(i).*abs_distY(i);
            c = c+1;
        elseif i<=m1 %1-16
            moment(i) = -Fy(i).*abs_distX(i);
            c = c+1;
        else %46-48
            moment(i) = Fx(i).*abs_distY(i);
            c = c+1;
        end
    else  %Ycoord(i)<=centerY && Xcoord(i)>=centerX; %taps nr 24-45
        if  i<=(m1+m2+m3) %taps 24-32 i>=(m1+m2+5) &&
            moment(i) = -Fy(i).*abs_distX(i)-Fx(i).*abs_distY(i);
            d=d+1;
        elseif i>(m1+m2+m3) && i<=(m1+m2+m3+m4) %33-42
            moment(i) = -Fy(i).*abs_distX(i);
```

```matlab
            d=d+1;
        else %43-45  Pressure_y_2
            moment(i) = -Fx(i).*abs_distY(i);
            d=d+1;
        end
    end
end

SumM1=sum(moment)
SumM2=sum(PS_moment2);
```

Functions

Functions used in both the piece-wise point load method and the interpolated load method.

- Function SortPressure: Finding the right value of each tube from the pressure transducer data.

- Function Distance16Taps: Finding surface area for correlation line 2-6, used in the calculation of forces.

- Function ImportingCoordinates: Imports the coordinates from the cross-section, finding the angles of the sides of the cross-section and finding the surface area for correlation line 1.

- Function NewCoordinates: Gives new coordinates/points on the cross-section with spacing dt. Used in the interpolated load method.

```matlab
%% pressure
% sorting the pressure from the pressure transducers


function [p1_1, p1_2, p1_3, p1_4, p1_5, p1_6, p2_1, p2_2,
p2_3, p2_4, p2_5, p2_6] = SortPressure2(p)
% function sorting pressure from pressure scanners after
correlation line
% and box
% p1_1 = correlation line 1 box 1 etc.
% p2_1 = correlation line 1 box 2 etc.

%% box 1, scanner 179 and 182, downstream box
%Corr line 1
p_corrline1=zeros(size(p,1), 48);
p_corrline1(:,1)  = p(:,193);
p_corrline1(:,2)  = p(:,195);
p_corrline1(:,3)  = p(:,197);
p_corrline1(:,4)  = p(:,199);
p_corrline1(:,5)  = p(:,201);
p_corrline1(:,6)  = p(:,203);
p_corrline1(:,7)  = p(:,205);
p_corrline1(:,8)  = p(:,207);
p_corrline1(:,9)  = p(:,209);
p_corrline1(:,10) = p(:,211);
p_corrline1(:,11) = p(:,213);
p_corrline1(:,12) = p(:,215);
p_corrline1(:,13) = p(:,217);
p_corrline1(:,14) = p(:,219);
p_corrline1(:,15) = p(:,221);
p_corrline1(:,16) = p(:,223);
p_corrline1(:,17) = p(:,243);
p_corrline1(:,18) = p(:,245);
p_corrline1(:,19) = p(:,247);
p_corrline1(:,20) = p(:,249);
p_corrline1(:,21) = p(:,230);
p_corrline1(:,22) = p(:,232);
p_corrline1(:,23) = p(:,234);
p_corrline1(:,24) = p(:,236);
p_corrline1(:,25) = p(:,238);
p_corrline1(:,26) = p(:,240);
p_corrline1(:,27) = p(:,242);
p_corrline1(:,28) = p(:,244);
p_corrline1(:,29) = p(:,246);
```

```
p_corrline1(:,30) = p(:,248);
p_corrline1(:,31) = p(:,250);
p_corrline1(:,32) = p(:,252);
p_corrline1(:,33) = p(:,27);
p_corrline1(:,34) = p(:,29);
p_corrline1(:,35) = p(:,31);
p_corrline1(:,36) = p(:,2);
p_corrline1(:,37) = p(:,4);
p_corrline1(:,38) = p(:,6);
p_corrline1(:,39) = p(:,8);
p_corrline1(:,40) = p(:,10);
p_corrline1(:,41) = p(:,12);
p_corrline1(:,42) = p(:,14);
p_corrline1(:,43) = p(:,34);
p_corrline1(:,44) = p(:,36);
p_corrline1(:,45) = p(:,38);
p_corrline1(:,46) = p(:,40);
p_corrline1(:,47) = p(:,42);
p_corrline1(:,48) = p(:,44);

%coorline 2
p_corrline2=zeros(size(p,1), 16);

p_corrline2(:,1) = p(:,194);
p_corrline2(:,2) = p(:,196);
p_corrline2(:,3) = p(:,198);
p_corrline2(:,4) = p(:,200);
p_corrline2(:,5) = p(:,202);
p_corrline2(:,6) = p(:,251);
p_corrline2(:,7) = p(:,254);
p_corrline2(:,8) = p(:,256);
p_corrline2(:,9) = p(:,1);
p_corrline2(:,10) = p(:,16);
p_corrline2(:,11) = p(:,18);
p_corrline2(:,12) = p(:,20);
p_corrline2(:,13) = p(:,22);
p_corrline2(:,14) = p(:,24);
p_corrline2(:,15) = p(:,46);
p_corrline2(:,16) = p(:,46);

%corrline3
p_corrline3=zeros(size(p,1), 16);
p_corrline3(:,1) = p(:,204);
p_corrline3(:,2) = p(:,206);
```

```matlab
p_corrline3(:,3)  = p(:,208);
p_corrline3(:,4)  = p(:,210);
p_corrline3(:,5)  = p(:,212);
p_corrline3(:,6)  = p(:,253);
p_corrline3(:,7)  = p(:,3);
p_corrline3(:,8)  = p(:,5);
p_corrline3(:,9)  = p(:,7);
p_corrline3(:,10) = p(:,26);
p_corrline3(:,11) = p(:,28);
p_corrline3(:,12) = p(:,30);
p_corrline3(:,13) = p(:,32);
p_corrline3(:,14) = p(:,33);
p_corrline3(:,15) = p(:,50);
p_corrline3(:,16) = p(:,52);

%corrline4
p_corrline4=zeros(size(p,1), 16);
p_corrline4(:,1)  = p(:,214);
p_corrline4(:,2)  = p(:,216);
p_corrline4(:,3)  = p(:,218);
p_corrline4(:,4)  = p(:,220);
p_corrline4(:,5)  = p(:,222);
p_corrline4(:,6)  = p(:,255);
p_corrline4(:,7)  = p(:,9);
p_corrline4(:,8)  = p(:,11);
p_corrline4(:,9)  = p(:,213);
p_corrline4(:,10) = p(:,35);
p_corrline4(:,11) = p(:,37);
p_corrline4(:,12) = p(:,39);
p_corrline4(:,13) = p(:,41);
p_corrline4(:,14) = p(:,43);
p_corrline4(:,15) = p(:,54);
p_corrline4(:,16) = p(:,56);


%corrline5
p_corrline5=zeros(size(p,1), 16);
p_corrline5(:,1)  = p(:,224);
p_corrline5(:,2)  = p(:,225);
p_corrline5(:,3)  = p(:,227);
p_corrline5(:,4)  = p(:,229);
p_corrline5(:,5)  = p(:,231);
p_corrline5(:,6)  = p(:,226);
p_corrline5(:,7)  = p(:,15);
```

```matlab
p_corrline5(:,8) = p(:,17);
p_corrline5(:,9) = p(:,19);
p_corrline5(:,10) = p(:,45);
p_corrline5(:,11) = p(:,47);
p_corrline5(:,12) = p(:,49);
p_corrline5(:,13) = p(:,51);
p_corrline5(:,14) = p(:,53);
p_corrline5(:,15) = p(:,58);
p_corrline5(:,16) = p(:,60);

%corrline6
p_corrline6=zeros(size(p,1), 16);
p_corrline6(:,1) = p(:,233);
p_corrline6(:,2) = p(:,235);
p_corrline6(:,3) = p(:,237);
p_corrline6(:,4) = p(:,239);
p_corrline6(:,5) = p(:,241);
p_corrline6(:,6) = p(:,228);
p_corrline6(:,7) = p(:,21);
p_corrline6(:,8) = p(:,23);
p_corrline6(:,9) = p(:,25);
p_corrline6(:,10) = p(:,55);
p_corrline6(:,11) = p(:,57);
p_corrline6(:,12) = p(:,59);
p_corrline6(:,13) = p(:,61);
p_corrline6(:,14) = p(:,53);
p_corrline6(:,15) = p(:,62);
p_corrline6(:,16) = p(:,64);


%% box 2, scanner 179 and 182
%Corr line 1
p_corrline7=zeros(size(p,1), 48);
p_corrline7(:,1) = p(:,129);
p_corrline7(:,2) = p(:,131);
p_corrline7(:,3) = p(:,133);
p_corrline7(:,4) = p(:,135);
p_corrline7(:,5) = p(:,137);
p_corrline7(:,6) = p(:,139);
p_corrline7(:,7) = p(:,141);
p_corrline7(:,8) = p(:,143);
p_corrline7(:,9) = p(:,145);
p_corrline7(:,10) = p(:,147);
p_corrline7(:,11) = p(:,149);
```

```matlab
p_corrline7(:,12) = p(:,151);
p_corrline7(:,13) = p(:,153);
p_corrline7(:,14) = p(:,155);
p_corrline7(:,15) = p(:,157);
p_corrline7(:,16) = p(:,159);
p_corrline7(:,17) = p(:,179);
p_corrline7(:,18) = p(:,181);
p_corrline7(:,19) = p(:,183);
p_corrline7(:,20) = p(:,185);
p_corrline7(:,21) = p(:,166);
p_corrline7(:,22) = p(:,168);
p_corrline7(:,23) = p(:,170);
p_corrline7(:,24) = p(:,172);
p_corrline7(:,25) = p(:,174);
p_corrline7(:,26) = p(:,176);
p_corrline7(:,27) = p(:,178);
p_corrline7(:,28) = p(:,180);
p_corrline7(:,29) = p(:,182);
p_corrline7(:,30) = p(:,184);
p_corrline7(:,31) = p(:,186);
p_corrline7(:,32) = p(:,188);
p_corrline7(:,33) = p(:,91);
p_corrline7(:,34) = p(:,93);
p_corrline7(:,35) = p(:,95);
p_corrline7(:,36) = p(:,66);
p_corrline7(:,37) = p(:,68);
p_corrline7(:,38) = p(:,70);
p_corrline7(:,39) = p(:,72);
p_corrline7(:,40) = p(:,74);
p_corrline7(:,41) = p(:,76);
p_corrline7(:,42) = p(:,78);
p_corrline7(:,43) = p(:,98);
p_corrline7(:,44) = p(:,100);
p_corrline7(:,45) = p(:,102);
p_corrline7(:,46) = p(:,104);
p_corrline7(:,47) = p(:,106);
p_corrline7(:,48) = p(:,108);

%coorline 8 aka corrline 2 box 2
p_corrline8=zeros(size(p,1), 16);

p_corrline8(:,1) = p(:,130);
p_corrline8(:,2) = p(:,132);
p_corrline8(:,3) = p(:,134);
```

```matlab
p_corrline8(:,4) = p(:,136);
p_corrline8(:,5) = p(:,138);
p_corrline8(:,6) = p(:,187);
p_corrline8(:,7) = p(:,190);
p_corrline8(:,8) = p(:,192);
p_corrline8(:,9) = p(:,65);
p_corrline8(:,10) = p(:,80);
p_corrline8(:,11) = p(:,82);
p_corrline8(:,12) = p(:,84);
p_corrline8(:,13) = p(:,86);
p_corrline8(:,14) = p(:,88);
p_corrline8(:,15) = p(:,110);
p_corrline8(:,16) = p(:,112);

%corrline9 aka corrline 3 box2
p_corrline9=zeros(size(p,1), 16);
p_corrline9(:,1) = p(:,140);
p_corrline9(:,2) = p(:,142);
p_corrline9(:,3) = p(:,144);
p_corrline9(:,4) = p(:,146);
p_corrline9(:,5) = p(:,148);
p_corrline9(:,6) = p(:,189);
p_corrline9(:,7) = p(:,67);
p_corrline9(:,8) = p(:,69);
p_corrline9(:,9) = p(:,71);
p_corrline9(:,10) = p(:,90);
p_corrline9(:,11) = p(:,92);
p_corrline9(:,12) = p(:,94);
p_corrline9(:,13) = p(:,96);
p_corrline9(:,14) = p(:,97);
p_corrline9(:,15) = p(:,114);
p_corrline9(:,16) = p(:,116);

%corrline10 aka corrline 4 box2
p_corrline10=zeros(size(p,1), 16);
p_corrline10(:,1) = p(:,150);
p_corrline10(:,2) = p(:,152);
p_corrline10(:,3) = p(:,154);
p_corrline10(:,4) = p(:,156);
p_corrline10(:,5) = p(:,158);
p_corrline10(:,6) = p(:,191);
p_corrline10(:,7) = p(:,73);
p_corrline10(:,8) = p(:,75);
p_corrline10(:,9) = p(:,77);
```

```matlab
p_corrline10(:,10) = p(:,99);
p_corrline10(:,11) = p(:,101);
p_corrline10(:,12) = p(:,103);
p_corrline10(:,13) = p(:,105);
p_corrline10(:,14) = p(:,107);
p_corrline10(:,15) = p(:,118);
p_corrline10(:,16) = p(:,120);


%corrline11 aka corrline 5 box2
p_corrline11=zeros(size(p,1), 16);
p_corrline11(:,1) = p(:,160);
p_corrline11(:,2) = p(:,161);
p_corrline11(:,3) = p(:,163);
p_corrline11(:,4) = p(:,165);
p_corrline11(:,5) = p(:,167);
p_corrline11(:,6) = p(:,162);
p_corrline11(:,7) = p(:,79);
p_corrline11(:,8) = p(:,81);
p_corrline11(:,9) = p(:,83);
p_corrline11(:,10) = p(:,109);
p_corrline11(:,11) = p(:,111);
p_corrline11(:,12) = p(:,113);
p_corrline11(:,13) = p(:,115);
p_corrline11(:,14) = p(:,117);
p_corrline11(:,15) = p(:,122);
p_corrline11(:,16) = p(:,124);

%corrline12 aka corrline 6 box2
p_corrline12=zeros(size(p,1), 16);
p_corrline12(:,1) = p(:,169);
p_corrline12(:,2) = p(:,171);
p_corrline12(:,3) = p(:,173);
p_corrline12(:,4) = p(:,175);
p_corrline12(:,5) = p(:,177);
p_corrline12(:,6) = p(:,164);
p_corrline12(:,7) = p(:,85);
p_corrline12(:,8) = p(:,87);
p_corrline12(:,9) = p(:,89);
p_corrline12(:,10) = p(:,119);
p_corrline12(:,11) = p(:,121);
p_corrline12(:,12) = p(:,123);
p_corrline12(:,13) = p(:,125);
p_corrline12(:,14) = p(:,127);
```

```matlab
p_corrline12(:,15) = p(:,126);
p_corrline12(:,16) = p(:,128);



%% saving pressure
p1_1 = p_corrline1;
p1_2 = p_corrline2;
p1_3 = p_corrline3;
p1_4 = p_corrline4;
p1_5 = p_corrline5;
p1_6 = p_corrline6;

p2_1 = p_corrline7;
p2_2 = p_corrline8;
p2_3 = p_corrline9;
p2_4 = p_corrline10;
p2_5 = p_corrline11;
p2_6 = p_corrline12;

end
```

```matlab
%%  Finding surface area for point loads for correlation line 2-6
%length between taps, first number is edge to tap, last number is tap to
edge

function [A] = Distance16Taps;

dist1 = [17.63, 42.38, 41.25, 44.39, 40.86, 3.5];
dist2 = [12.83, 22.66];
dist3 = [4, 37.20, 37.20, 31.40];
dist4 = [3.5, 22.60, 22.60, 25.42, 42.38, 3.5];
dist5 = [18.10, 43.80, 18.10];
dist = [dist1, dist2, dist3, dist4, dist5];


%% Surface area for point loads
%side 1
A(1) = dist(1)+dist(2)/2;
for i=2:4
    A(i) = (dist(i)+dist(i+1))/2;
end
A(5) = dist(5)/2+dist(6);
%side 2
A(6) = dist(7)+dist(8);
%side 3
A(7) = dist(9)+dist(10)/2;
A(8) = (dist(10)+dist(11))/2;
A(9) = dist(11)/2+dist(12);
%side 4
A(10) = dist(13)+dist(14)/2;
A(11) = (dist(14)+dist(15))/2;
A(12) = (dist(15)+dist(16))/2;
A(13) = (dist(16)+dist(17))/2;
A(14) = dist(17)/2 + dist(18);
%side 5
A(15)=dist(19)+dist(20)/2;
A(16) = dist(20)/2+dist(21);
A=A';
```

```matlab
%% importing coordinates and angles of the cross-section and finding the
surface area for line 1.

function [x_taps, y_taps, x_taps2, y_taps2, x_coord, y_coord, x_coord2,
y_coord2,  dist, A,...
    x_taps_16, y_taps_16, x_taps2_16, y_taps2_16, x_coord_16, y_coord_16,
x_coord2_16, y_coord2_16] = ImportingCoordinatesFunc
[Coordinates_cross, txt, raw] = xlsread('kordinater_edge.xlsx', 1);
[Pressure, txt, raw] = xlsread('kordinater_edge.xlsx', 3); %pressure
[Coordinates, txt1, raw1] = xlsread('kordinater_edge.xlsx', 4); %coordinates
to pressure taps only'
[Coordinates_16_cross, txt, raw] =xlsread('kordinater_edge.xlsx',2);
%coordinates cross-section corrline 2-6
[Coordinates_16, txt, raw1] =xlsread('kordinater_edge.xlsx',5); %coordinates
taps only corrline 2-6


%% box 2 = upstream box
x_taps2 = Coordinates(1:end,2);
y_taps2 = Coordinates(1:end,3);
pressure2 = Pressure(1:end,2);
x_coord2= Coordinates_cross(1:end,2);
y_coord2 = Coordinates_cross(1:end,3);

x_taps2_16 = Coordinates_16(1:end,2);
y_taps2_16 = Coordinates_16(1:end,3);
x_coord2_16 = Coordinates_16_cross(1:end,2);
y_coord2_16 = Coordinates_16_cross(1:end,3);

%% box 1 = downstream box
w=160; %distance between upstream and downstream box.
x_coord = -x_coord2+w; %mirro2 the coordinates to get the second box.
y_coord = y_coord2;
x_taps = -x_taps2+w;
y_taps = y_taps2;

x_coord_16 = -x_coord2_16+w; %mirro2 the coordinates to get the second box.
y_coord_16 = y_coord2_16;
x_taps_16 = -x_taps2_16+w;
y_taps_16 = y_taps2_16;


%angels box 1
a_S11 = atan(abs(y_coord(18)-y_coord(1))/abs(x_coord(18)-x_coord(1)))*180/pi;
a_S21 = atan(abs(y_coord(24)-y_coord(19))/abs(x_coord(24)-
x_coord(19)))*180/pi;
a_S31 = atan(abs(y_coord(38)-y_coord(25))/abs(x_coord(38)-
x_coord(25)))*180/pi;
a_S41 = atan(abs(y_coord(50)-y_coord(39))/abs(x_coord(50)-
x_coord(39)))*180/pi;
a_S51 = atan(abs(y_coord(58)-y_coord(51))/abs(x_coord(58)-
x_coord(51)))*180/pi;

angle1 = [a_S11, a_S21, a_S31, a_S41, a_S51];

%angles box 2
```

```matlab
a_S12 = atan(abs(y_coord2(18)-y_coord2(1))/abs(x_coord2(18)-
x_coord2(1)))*180/pi;
a_S22 = atan(abs(y_coord2(24)-y_coord2(19))/abs(x_coord2(24)-
x_coord2(19)))*180/pi;
a_S32 = atan(abs(y_coord2(38)-y_coord2(25))/abs(x_coord2(38)-
x_coord2(25)))*180/pi;
a_S42 = atan(abs(y_coord2(50)-y_coord2(39))/abs(x_coord2(50)-
x_coord2(39)))*180/pi;
a_S52 = atan(abs(y_coord2(58)-y_coord2(51))/abs(x_coord2(58)-
x_coord2(51)))*180/pi;

angle2 = [a_S12, a_S22, a_S32, a_S42, a_S52];

%length between taps, first number is edge to tap, last number is tap to edge
dist1 = [3.5, 14.125, 14.125, 14.125, 14.125, 13.749975, 13.749975, 13.749975,
13.749975,...
    10.21429971, 10.21429971, 10.21429971, 10.21429971, 10.21429971,
10.21429971, 10.21429971, 3.5];
dist2 = [3.5, 9.33, 9.33, 9.33, 4];
dist3 = [4, 9.30090909, 9.30090909, 9.30090909, 9.30090909, 9.30090909,
9.30090909, 9.30090909, 9.30090909, 9.30090909, 9.30090909, 9.30090909, 3.5];
dist4 = [3.5, 11.298, 11.298, 11.298, 11.298, 11.298, 14.125, 14.125, 14.125,
14.125, 3.51];
dist5 = [3.5, 14.6, 14.6, 14.6, 14.6, 14.6, 3.5];

dist = [dist1, dist2, dist3, dist4, dist5];

%% Surface area for point loads
%side 1
A(1) = dist(1)+dist(2)/2;
for i=2:15
    A(i) = (dist(i)+dist(i+1))/2;
end
A(16) = dist(16)/2+dist(17);
%side 2
A(17) = dist(18)+dist(19)/2;
A(18) = (dist(19)+dist(20))/2;
A(19) = (dist(20)+dist(21))/2;
A(20) = dist(21)/2+dist(22);
%side 3
A(21) = dist(23)+dist(24)/2;
for i=22:31
    A(i) = (dist(i+2)+dist(i+3))/2;
end
A(32) = dist(34)/2+dist(35);

%side 4
A(33) = dist(36)+dist(37)/2;
for i = 34:41
    A(i) = (dist(i+3)+dist(i+4))/2;
end
A(42) = dist(45)/2+dist(46);

%side 5
A(43) = dist(47)+dist(48)/2;
for i = 44:47
    A(i) = (dist(i+4)+dist(i+5))/2;
```

```
end
A(48) = dist(52)/2+dist(53);
A=A';
```

```matlab
%% new coordinates for the distributed pressure
%functions that makes new points/coordinates on the cross section with spacing
equal to dt.
function [Xcoord, Ycoord] = NewCoordinates(xcord, ycord, dt, angle, Ncord)

Xcoord=zeros(1,Ncord);
Ycoord=zeros(1, Ncord);
Xcoord(1)=xcord;
Ycoord(1)=ycord;
for i = 2:Ncord
    Xcoord(i) = -dt*cos((pi/180)*angle)+Xcoord(i-1);
    Ycoord(i) = -dt*sin((pi/180)*angle)+Ycoord(i-1);
end


end
```

C Matlab script for Admittance Functions

The Matlab scrip for the three methods, general, equivalent and cross-spectral, for the estimation of the Aerodynamic Admittance Functions are given below.

```matlab
%% Admittance functions

clc
clear all
close all
%loading time series of forces and turbulences
load('C:\Users\theah\Documents\NTNU\master\TESTER2\WindTunnelSystemMain\PostPr
occessing\Time Series Pont Load\TS10_00_903_000.mat')
load('C:\Users\theah\Documents\NTNU\master\TESTER2\WindTunnelSystemMain\DataCu
tted\Master2020TD_10_00_903_000.mat')
load('C:\Users\theah\Documents\NTNU\master\TESTER2\WindTunnelSystemMain\PostPr
occessing\Time Series Pont Load\TS_Corrline10_00_903_000.mat')
%file=005;

U = WT.Data.ProcessedData(1).Data; %Measured mean wind velocity
u = WT.Data.ProcessedData(2).Data; %Measured displacements
Fs=str2num(WT.Data.Root.Property(5).Value{1}(1:end-3)); %Sampling frequency
t=0:1/Fs:(size(u,1)-1)/Fs; % Time vector
rhostr=num2str(strrep(WT.Data.Root.Property(10).Value{1},',','.')); %Air
density
rho=str2num(rhostr(1:regexp(rhostr,' ')));
dt=t(2)-t(1);
T=t(end);
u=WT.Data.ProcessedData(7).Data(:,1);
v=WT.Data.ProcessedData(7).Data(:,2);
w=WT.Data.ProcessedData(7).Data(:,3);
U=mean(u); %mean wind flow
V=U;


B=0.59; %witdh
L=2.68; %length

%% LIFT
Fz_upstream = TSPointLoad.Fz2;
Fz_downstream = TSPointLoad.Fz1;
Fz_total=Fz_upstream+Fz_downstream;


%% DRAG
Fx_upstream = TSPointLoad.Fx2;
Fx_downstream = TSPointLoad.Fx1;
Fx_total = Fx_upstream+Fx_downstream;

%% Moment
M_upstream = TSPointLoad.M2;
M_downstream = TSPointLoad.M1;
M_total = M_upstream+M_downstream;

%--------------------
DragForce_upstream = zeros(size(Fz_upstream,1),1);
DragForce_downstream = zeros(size(Fz_upstream,1),1);
DragForce_total = zeros(size(Fz_upstream,1),1);
LiftForce_upstream = zeros(size(Fz_upstream,1),1);
LiftForce_downstream = zeros(size(Fz_upstream,1),1);
LiftForce_total = zeros(size(Fz_upstream,1),1);
Moment_upstream = zeros(size(Fz_upstream,1),1);
Moment_downstream = zeros(size(Fz_upstream,1),1);
```

```matlab
Moment_total = zeros(size(Fz_upstream,1),1);

for n=1:48
    DragForce_upstream = DragForce_upstream + Fx_upstream(:,n);
    DragForce_downstream = DragForce_downstream + Fx_downstream(:,n);
    DragForce_total = DragForce_total + Fx_total(:,n);

    LiftForce_upstream = LiftForce_upstream + Fz_upstream(:,n);
    LiftForce_downstream = LiftForce_downstream + Fz_downstream(:,n);
    LiftForce_total = LiftForce_total + Fz_total(:,n);

    Moment_upstream = Moment_upstream + M_upstream(:,n);
    Moment_downstream = Moment_downstream + M_downstream(:,n);
    Moment_total = Moment_total + M_total(:,n);
end


    DragForce_upstream = DragForce_upstream - mean(DragForce_upstream);
    DragForce_downstream = DragForce_downstream -mean(DragForce_downstream);
    DragForce_total = DragForce_total -mean(DragForce_total);

    LiftForce_upstream = LiftForce_upstream -mean(LiftForce_upstream);
    LiftForce_downstream = LiftForce_downstream - mean(LiftForce_downstream);
    LiftForce_total = LiftForce_total -mean(LiftForce_total);

    Moment_upstream = Moment_upstream -mean(Moment_upstream);
    Moment_downstream = Moment_downstream - mean(Moment_downstream);

    Moment_total = Moment_total -mean(Moment_total);

%% ---------- Buffeting force spectrum ---------------- %%
Nwelch=20;
Nwindow = round(length(t)/Nwelch);
nfft = 2^nextpow2(Nwindow);

[SL_upstream, f] = cpsd(LiftForce_upstream, LiftForce_upstream, ...
hanning(Nwindow), [], nfft, Fs, 'onesided');
[SL_downstream, f] = cpsd(LiftForce_downstream, LiftForce_downstream, ...
hanning(Nwindow), [], nfft, Fs, 'onesided');
[SL_total, f] = cpsd(LiftForce_total, LiftForce_total, hanning(Nwindow), [], ...
nfft, Fs, 'onesided');

[SD_upstream, f] = cpsd(DragForce_upstream, DragForce_upstream, ...
hanning(Nwindow), [], nfft, Fs, 'onesided');
[SD_downstream, f] = cpsd(DragForce_downstream, DragForce_downstream, ...
hanning(Nwindow), [], nfft, Fs, 'onesided');
[SD_total, f] = cpsd(DragForce_total, DragForce_total, hanning(Nwindow), [], ...
nfft, Fs, 'onesided');

[SM_upstream, f] = cpsd(Moment_upstream, Moment_upstream, hanning(Nwindow), ...
[], nfft, Fs, 'onesided');
[SM_downstream, f] = cpsd(Moment_downstream, Moment_downstream, ...
hanning(Nwindow), [], nfft, Fs, 'onesided');
[SM_total, f] = cpsd(Moment_total, Moment_total, hanning(Nwindow), [], nfft, ...
Fs, 'onesided');
%
%
```

```matlab
figure(); hold on
plot(f, SL_upstream, 'displayname', 'upstream');
plot(f, SL_downstream, 'displayname', 'downstream');
plot(f, SL_total, 'displayname', 'total');
title('lift spectra')
legend show
%% Corrline 2-6

for n=1:5
    %lift
    Fz_n_upstream(:,:,n) = TSPointLoadCorrline(n).Fz2;
    Fz_n_downstream(:,:,n) = TSPointLoadCorrline(n).Fz1;
    Fz_n_total = Fz_n_upstream+Fz_n_downstream;
    %drag
    Fx_n_upstream(:,:,n) = TSPointLoadCorrline(n).Fx2;
    Fx_n_downstream(:,:,n) = TSPointLoadCorrline(n).Fx1;
    Fx_n_total = Fx_n_upstream+Fx_n_downstream;
    %moment
    M_n_upstream(:,:,n) = TSPointLoadCorrline(n).M2;
    M_n_downstream(:,:,n) = TSPointLoadCorrline(n).M1;
    M_n_total = M_n_upstream+M_n_downstream;

end

DragForce_n_upstream = zeros(size(Fz_n_upstream,1),1,5);
DragForce_n_downstream = zeros(size(Fz_n_upstream,1),1,5);
DragForce_n_total = zeros(size(Fz_n_upstream,1),1,5);
LiftForce_n_upstream = zeros(size(Fz_n_upstream,1),1,5);
LiftForce_n_downstream = zeros(size(Fz_n_upstream,1),1,5);
LiftForce_n_total = zeros(size(Fz_n_upstream,1),1,5);
Moment_n_upstream = zeros(size(Fz_n_upstream,1),1,5);
Moment_n_downstream = zeros(size(Fz_n_upstream,1),1,5);
Moment_n_total = zeros(size(Fz_n_upstream,1),1,5);

for k=1:5
    for n=1:16
        DragForce_n_upstream(:,k) = DragForce_n_upstream(:,:,k) +
Fx_n_upstream(:,n,k);
        DragForce_n_downstream(:,k) = DragForce_n_downstream(:,:,k) +
Fx_n_downstream(:,n,k);
        DragForce_n_total(:,k) = DragForce_n_total(:,:,k) + Fx_n_total(:,n,k);

        LiftForce_n_upstream(:,k) = LiftForce_n_upstream(:,:,k) +
Fz_n_upstream(:,n,k);
        LiftForce_n_downstream(:,k) = LiftForce_n_downstream(:,:,k) +
Fz_n_downstream(:,n,k);
        LiftForce_n_total(:,k) = LiftForce_n_total(:,:,k) + Fz_n_total(:,n,k);

        Moment_n_upstream(:,k) = Moment_n_upstream(:,:,k) +
M_n_upstream(:,n,k);
        Moment_n_downstream(:,k) = Moment_n_downstream(:,:,k) +
M_n_downstream(:,n,k);
        Moment_n_total(:,k) = Moment_n_total(:,:,k) + M_n_total(:,n,k);
    end

end
for i=1:5
```

```matlab
    DragForce_m_upstream(:,i) = DragForce_n_upstream(:,:,i) -
mean(DragForce_n_upstream(:,:,i));
    DragForce_m_downstream(:,i) = DragForce_n_downstream(:,:,i) -
mean(DragForce_n_downstream(:,:,i));
    DragForce_m_total(:,i) = DragForce_n_total(:,:,i) -
mean(DragForce_n_total(:,:,i));

    LiftForce_m_upstream(:,i) = LiftForce_n_upstream(:,:,i) -
mean(LiftForce_n_upstream(:,:,i));
    LiftForce_m_downstream(:,i) = LiftForce_n_downstream(:,:,i) -
mean(LiftForce_n_downstream(:,:,i));
    LiftForce_m_total(:,i) = LiftForce_n_total(:,:,i) -
mean(LiftForce_n_total(:,:,i));

    Moment_m_upstream(:,i) = Moment_n_upstream(:,:,i) -
mean(Moment_n_upstream(:,:,i));
    Moment_m_downstream(:,i) = Moment_n_downstream(:,:,i) -
mean(Moment_n_downstream(:,:,i));
    Moment_m_total(:,i)= Moment_n_total(:,:,i) -mean(Moment_n_total(:,:,i));
end

%% ------------ Buffeting force spectrum for corrline 2-6--------------------
-------
for j=1:5
    [SL_n_upstream(j,:), f] = cpsd(LiftForce_m_upstream(:,j),
LiftForce_m_upstream(:,j), hanning(Nwindow), [], nfft, Fs, 'onesided');
    [SL_n_downstream(j,:), f] = cpsd(LiftForce_m_downstream(:,j),
LiftForce_m_downstream(:,j), hanning(Nwindow), [], nfft, Fs, 'onesided');
    [SL_n_total(j,:), f] = cpsd(LiftForce_m_total(:,j),
LiftForce_m_total(:,j), hanning(Nwindow), [], nfft, Fs, 'onesided');

    [SD_n_upstream(j,:), f] = cpsd(DragForce_m_upstream(:,j),
DragForce_m_upstream(:,j), hanning(Nwindow), [], nfft, Fs, 'onesided');
    [SD_n_downstream(j,:), f] = cpsd(DragForce_m_downstream(:,j),
DragForce_m_downstream(:,j), hanning(Nwindow), [], nfft, Fs, 'onesided');
    [SD_n_total(j,:), f] = cpsd(DragForce_m_total(:,j),
DragForce_m_total(:,j), hanning(Nwindow), [], nfft, Fs, 'onesided');

    [SM_n_upstream(j,:), f] = cpsd(Moment_m_upstream(:,j),
Moment_m_upstream(:,j), hanning(Nwindow), [], nfft, Fs, 'onesided');
    [SM_n_downstream(j,:), f] = cpsd(Moment_m_downstream(:,j),
Moment_m_downstream(:,j), hanning(Nwindow), [], nfft, Fs, 'onesided');
    [SM_n_total(j,:), f] = cpsd(Moment_m_total(:,j), Moment_m_total(:,j),
hanning(Nwindow), [], nfft, Fs, 'onesided');

end




%% --------------------Admittance Functions--------------------- %%
% Turbulence

u = u-mean(u);
w = w-mean(w);

%% ------------Turbulence spectrum------------------------------------
```

```matlab
[Su, f] = cpsd(u, u, hanning(Nwindow), [], nfft, Fs, 'onesided');
[Sw, f] = cpsd(w, w, hanning(Nwindow), [], nfft, Fs, 'onesided');
[Suw, f] = cpsd(w, u, hanning(Nwindow), [], nfft, Fs, 'onesided');
[Swu, f] = cpsd(u, w, hanning(Nwindow), [], nfft, Fs, 'onesided');

% figure(); hold on
% plot(f, Su, 'displayname', 'Su');
% plot(f, Sw, 'displayname', 'Sw');
% title('Turbulence spectra')
% legend show

%% -----------------Cross spectrum total------------------------------------
[SLu, f] = cpsd(LiftForce_total, u, hanning(Nwindow), [], nfft, Fs, ...
'onesided');
[SLw, f] = cpsd(LiftForce_total, w, hanning(Nwindow), [], nfft, Fs, ...
'onesided');

[SDu, f] = cpsd(DragForce_total, u, hanning(Nwindow), [], nfft, Fs, ...
'onesided');
[SDw, f] = cpsd(DragForce_total, w, hanning(Nwindow), [], nfft, Fs, ...
'onesided');

[SMu, f] = cpsd(Moment_total, u, hanning(Nwindow), [], nfft, Fs, 'onesided');
[SMw, f] = cpsd(Moment_total, w, hanning(Nwindow), [], nfft, Fs, 'onesided');


%% -----------------cross spectrum upstream---------------------------------
-
[SLu_up, f] = cpsd(LiftForce_upstream, u, hanning(Nwindow), [], nfft, Fs, ...
'onesided');
[SLw_up, f] = cpsd(LiftForce_upstream, w, hanning(Nwindow), [], nfft, Fs, ...
'onesided');

[SDu_up, f] = cpsd(DragForce_upstream, u, hanning(Nwindow), [], nfft, Fs, ...
'onesided');
[SDw_up, f] = cpsd(DragForce_upstream, w, hanning(Nwindow), [], nfft, Fs, ...
'onesided');

[SMu_up, f] = cpsd(Moment_upstream, u, hanning(Nwindow), [], nfft, Fs, ...
'onesided');
[SMw_up, f] = cpsd(Moment_upstream, w, hanning(Nwindow), [], nfft, Fs, ...
'onesided');

%% -----------------cross spectrum downstream-------------------------------
---
[SLu_down, f] = cpsd(LiftForce_downstream, u, hanning(Nwindow), [], nfft, Fs, ...
'onesided');
[SLw_down, f] = cpsd(LiftForce_downstream, w, hanning(Nwindow), [], nfft, Fs, ...
'onesided');

[SDu_down, f] = cpsd(DragForce_downstream, u, hanning(Nwindow), [], nfft, Fs, ...
'onesided');
[SDw_down, f] = cpsd(DragForce_downstream, w, hanning(Nwindow), [], nfft, Fs, ...
'onesided');
```

```matlab
[SMu_down, f] = cpsd(Moment_downstream, u, hanning(Nwindow), [], nfft, Fs, ...
'onesided');
[SMw_down, f] = cpsd(Moment_downstream, w, hanning(Nwindow), [], nfft, Fs, ...
'onesided');


%% ----------General admittance functions---------------------
Aw_lift=SL_total./Sw;
Au_drag=SD_total./Su;
Aw_moment=SM_total./Sw;


%% Equivalente admittance functions and cross-spectral admittance functions
%% ------------Total Box-------------------------------------------------
Cd=0.9949; Cl=0.05852; Cm=0.1653;
dCd=1.031; dCl=4.129; dCm=1.173;

%af
aD=2*Cd;
aL=2*Cl;
aM=2*Cm;

%bf
bD=(dCd-Cl);
bL=(dCl+Cd);
bM=dCm;
%Sears approximated function
fred=f.*B/(V);
for n=1:length(f)
    sears(n) = (1/(1+2*pi^2*fred(n))); %approximated sears function |ø(f*)|^2
end
%------------AL-------------------------------------------------------------
-
AL = SL_total./((0.5*rho*B*V).^2*(aL.^2*Su + bL.^2*Sw));
ALw = (Su.*SLw-Suw.*SLu)./((0.5*rho*B*V).^1*(bL*(Su.*Sw-Swu.*Suw)));
ALu = (Sw.*SLu-Suw.*SLw)./((0.5*rho*B*V).^1*(aL*(Su.*Sw-Swu.*Suw)));
%------------ AD-------------------------------------------------------------
-
AD = SD_total./((0.5*rho*B*V)^2*(aD.^2*Su +bD.^2*Sw));
ADw = (Su.*SDw-Suw.*SDu)./((0.5*rho*B*V).^1*(bD*(Su.*Sw-Swu.*Suw)));
ADu = (Sw.*SDu-Suw.*SDw)./((0.5*rho*B*V).^1*(aD*(Su.*Sw-Swu.*Suw)));
%------------AM-------------------------------------------------------------
AM = SM_total./((0.5*rho*B*B*V).^2*(aM.^2*Su +bM.^2*Sw));
AMw = (Su.*SMw-Suw.*SMu)./((0.5*rho*B*B*V).^1*(bM*(Su.*Sw-Swu.*Suw)));
AMu = (Sw.*SMu-Suw.*SMw)./((0.5*rho*B*B*V).^1*(aM*(Su.*Sw-Swu.*Suw)));


%----------------AL corrline 2:6---------------------------
AL6 = SL_n_total(5,:)'./((0.5*rho*B*V).^2*(aL.^2*Su + bL.^2*Sw));
AD6 = SD_n_total(5,:)'./((0.5*rho*B*V).^2*(aD.^2*Su + bD.^2*Sw));
AM6 = SM_n_total(5,:)'./((0.5*rho*B*B*V).^2*(aM.^2*Su + bM.^2*Sw));

figure(); hold on;
plot(fred, AL, 'displayname', 'A_L')
%plot(fred, AL6, 'displayname', 'A_L - Line 6')
plot(fred, sears,'displayname', 'Sears', 'linewidth', 2)
plot(fred,(abs(ALw)).^2, 'displayname', 'A_{Lw}')
plot(fred, (abs(ALu)).^2, 'displayname', 'A_{Lu}')
```

```matlab
set(gca, 'Yscale', 'log', 'Xscale', 'log')
%xlabel('f*=fB/V')
xlabel('f*=fB/V', 'fontsize', 30)
ylabel('|A_i|^2', 'fontsize', 30)
legend show
title('Admittance functions Lift', 'fontsize', 30)
ylim([0 10])
% saveas(gcf,sprintf('10_00_%d_000_Lift.jpg',file))
% saveas(gcf,sprintf('10_00_%d_000_Lift.fig',file))


figure(); hold on;
plot(fred, AD, 'displayname', 'A_D')
%plot(fred, AD6, 'displayname', 'A_D - Line 6')
plot(fred, sears,'displayname', 'Sears', 'linewidth', 2)
plot(fred,(abs(ADw)).^2, 'displayname', 'A_{Dw}')
plot(fred, (abs(ADu)).^2, 'displayname', 'A_{Du}')
set(gca, 'Yscale', 'log', 'Xscale', 'log')
xlabel('f*=fB/V', 'fontsize', 30)
ylabel('|A_i|^2', 'fontsize', 30)
legend show
title('Admittance functions Drag', 'fontsize', 30)
ylim([0 10])
% saveas(gcf,sprintf('10_00_%d_000_Drag.jpg',file))
% saveas(gcf,sprintf('10_00_%d_000_Drag.fig',file))



figure(); hold on;
plot(fred, AM, 'displayname', 'A_M')
%plot(fred, AM6, 'displayname', 'A_M - Line 6')
plot(fred, sears,'displayname', 'Sears', 'linewidth', 2)
plot(fred,(abs(AMw)).^2, 'displayname', 'A_{Mw}')
plot(fred, (abs(AMu)).^2, 'displayname', 'A_{Mu}')
set(gca,'Yscale', 'log', 'Xscale', 'log')
xlabel('f*=fB/V', 'fontsize', 30)
ylabel('|A_i|^2', 'fontsize', 30)
legend show
title('Admittance functions Moment', 'fontsize', 30)
ylim([0 10])
% saveas(gcf,sprintf('10_00_%d_000_Moment.jpg',file))
% saveas(gcf,sprintf('10_00_%d_000_Moment.fig',file))




%% --------------------Upstream box----------------------
CdU=0.5092; ClU=0.1219; CmU=0.1171;
dCdU=1.891; dClU=2.68; dCmU=2.24;
%af
aDU=2*CdU;
aLU=2*ClU;
aMU=2*CmU;

%bf
bDU=(dCdU-ClU);
bLU=(dClU+CdU);
```

```matlab
bMU=dCmU;

fredU=f*B/V;
Sears=1./(1+2*pi^2*fredU);

%------------AL---------------------------------------------------------
AL_up = SL_upstream./((0.5*rho*B*V).^2*(aLU.^2*Su + bLU.^2*Sw));
ALw_up = (Su.*SLw_up-Suw.*SLu_up)./((0.5*rho*B*V).^1*(bLU*(Su.*Sw-Swu.*Suw)));
ALu_up = (Sw.*SLu_up-Suw.*SLw_up)./((0.5*rho*B*V).^1*(aLU*(Su.*Sw-Swu.*Suw)));
%------------ AD---------------------------------------------------------
-
AD_up = SD_upstream./((0.5*rho*B*V)^2*(aDU.^2*Su +bDU.^2*Sw));
ADw_up = (Su.*SDw_up-Suw.*SDu_up)./((0.5*rho*B*V).^1*(bDU*(Su.*Sw-Swu.*Suw)));
ADu_up = (Sw.*SDu_up-Suw.*SDw_up)./((0.5*rho*B*V).^1*(aDU*(Su.*Sw-Swu.*Suw)));
%-----------AM----------------------------------------------------------
AM_up = SM_upstream./((0.5*rho*B*B*V).^2*(aMU.^2*Su +bMU.^2*Sw));
AMw_up = (Su.*SMw_up-Suw.*SMu_up)./((0.5*rho*B*B*V).^1*(bMU*(Su.*Sw-
Swu.*Suw)));
AMu_up = (Sw.*SMu_up-Suw.*SMw_up)./((0.5*rho*B*B*V).^1*(aMU*(Su.*Sw-
Swu.*Suw)));



figure(); hold on;
plot(fredU, AL_up, 'displayname', 'A_L')
%plot(fredU, sears,'displayname', 'Sears', 'linewidth', 2)
%plot(fredU,(abs(ALw_up)).^2, 'displayname', 'A_{Lw}')
%plot(fredU, (abs(ALu_up)).^2, 'displayname', 'A_{Lu}')
set(gca, 'Yscale', 'log', 'fontsize', 20)
xlabel('f*=fB/V')
ylabel('|A_i|^2')
legend show
title('Admittance functions Lift Upstream')
ylim([0 10])
% saveas(gcf,sprintf('10_00_%d_000_UpstreamLift.jpg',file))
% saveas(gcf,sprintf('10_00_%d_000_UpstreamLift.fig',file))

figure(); hold on;
plot(fredU, AD_up, 'displayname', 'A_D')
plot(fredU, sears,'displayname', 'Sears', 'linewidth', 2)
plot(fredU,(abs(ADw_up)).^2, 'displayname', 'A_{Dw}')
plot(fredU, (abs(ADu_up)).^2, 'displayname', 'A_{Du}')
set(gca, 'Yscale', 'log', 'fontsize', 20)
xlabel('f*=fB/V')
ylabel('|A_i|^2')
legend show
title('Admittance functions Drag Upstream')
ylim([0 10])
% saveas(gcf,sprintf('10_00_%d_000_UpstreamDrag.jpg',file))
% saveas(gcf,sprintf('10_00_%d_000_UpstreamDrag.fig',file))

figure(); hold on;
plot(fredU, AM_up, 'displayname', 'A_M')
plot(fredU, sears,'displayname', 'Sears', 'linewidth', 2)
plot(fredU,(abs(AMw_up)).^2, 'displayname', 'A_{Mw}')
plot(fredU, (abs(AMu_up)).^2, 'displayname', 'A_{Mu}')
set(gca,'Yscale', 'log', 'fontsize', 20)
```

```matlab
xlabel('f*=fB/V')
ylabel('|A_i|^2')
legend show
title('Admittance functions Moment Upstream')
ylim([0 10])
% saveas(gcf,sprintf('10_00_%d_000_UpstreamMoment.jpg',file))
% saveas(gcf,sprintf('10_00_%d_000_UpstreamMoment.fig',file))

figure()
plot(f, SL_upstream);
title('Force lift upstream spectra')


figure(); hold on;
plot(f, AL_up, 'displayname', 'A_L')
plot(f, sears,'displayname', 'Sears', 'linewidth', 2)
plot(f,(abs(ALw_up)).^2, 'displayname', 'A_{Lw}')
plot(f, (abs(ALu_up)).^2, 'displayname', 'A_{Lu}')
set(gca, 'Yscale', 'log', 'fontsize', 20)
xlabel('f*=fB/V')
ylabel('|A_i|^2')
legend show
title('Admittance functions Lift Upstream')
ylim([0 10])
% saveas(gcf,sprintf('10_00_%d_000_UpstreamLift.jpg',file))
% saveas(gcf,sprintf('10_00_%d_000_UpstreamLift.fig',file))

figure(); hold on;
plot(f, AD_up, 'displayname', 'A_D')
plot(f, sears,'displayname', 'Sears', 'linewidth', 2)
plot(f,(abs(ADw_up)).^2, 'displayname', 'A_{Dw}')
plot(f, (abs(ADu_up)).^2, 'displayname', 'A_{Du}')
set(gca, 'Yscale', 'log', 'fontsize', 20)
xlabel('f*=fB/V')
ylabel('|A_i|^2')
legend show
title('Admittance functions Drag Upstream')
ylim([0 10])
% saveas(gcf,sprintf('10_00_%d_000_UpstreamDrag.jpg',file))
% saveas(gcf,sprintf('10_00_%d_000_UpstreamDrag.fig',file))

figure(); hold on;
plot(f, AM_up, 'displayname', 'A_M')
plot(f, sears,'displayname', 'Sears', 'linewidth', 2)
plot(f,(abs(AMw_up)).^2, 'displayname', 'A_{Mw}')
plot(f, (abs(AMu_up)).^2, 'displayname', 'A_{Mu}')
set(gca,'Yscale', 'log', 'fontsize', 20)
xlabel('f*=fB/V')
ylabel('|A_i|^2')
legend show
title('Admittance functions Moment Upstream')
ylim([0 10])
% saveas(gcf,sprintf('10_00_%d_000_UpstreamMoment.jpg',file))
% saveas(gcf,sprintf('10_00_%d_000_UpstreamMoment.fig',file))


%% --------------------Downstream box----------------------
```

```matlab
CdD=0.4857; ClD=-0.06335; CmD=0.0482;
dCdD=-0.8596; dClD=1.46; dCmD=-1.086;

aDD=2*CdD;
aLD=2*ClD;
aMD=2*CmD;

%bf
bDD=(dCdD-ClD);
bLD=(dClD+CdD);
bMD=dCmD;

fredD=f*B/V;
Sears=1./(1+2*pi^2*fredD);

%-----------AL--------------------------------------------------------
-
AL_down = SL_downstream./((0.5*rho*B*V).^2*(aLD.^2*Su + bLD.^2*Sw));
ALw_down = (Su.*SLw_down-Suw.*SLu_down)./((0.5*rho*B*V).^1*(bLD*(Su.*Sw-
Swu.*Suw)));
ALu_down = (Sw.*SLu_down-Suw.*SLw_down)./((0.5*rho*B*V).^1*(aLD*(Su.*Sw-
Swu.*Suw)));
%------------ AD------------------------------------------------------
-
AD_down = SD_downstream./((0.5*rho*B*V)^2*(aDD.^2*Su +bDD.^2*Sw));
ADw_down = (Su.*SDw_down-Suw.*SDu_down)./((0.5*rho*B*V).^1*(bDD*(Su.*Sw-
Swu.*Suw)));
ADu_down = (Sw.*SDu_down-Suw.*SDw_down)./((0.5*rho*B*V).^1*(aDD*(Su.*Sw-
Swu.*Suw)));
%-----------AM--------------------------------------------------------
AM_down = SM_downstream./((0.5*rho*B*B*V).^2*(aMD.^2*Su +bMD.^2*Sw));
AMw_down = (Su.*SMw_down-Suw.*SMu_down)./((0.5*rho*B*B*V).^1*(bMD*(Su.*Sw-
Swu.*Suw)));
AMu_down = (Sw.*SMu_down-Suw.*SMw_down)./((0.5*rho*B*B*V).^1*(aMD*(Su.*Sw-
Swu.*Suw)));


figure(); hold on;
plot(fredD, AL_down, 'displayname', 'A_L')
plot(fredD, sears,'displayname', 'Sears', 'linewidth', 2)
plot(fredD,(abs(ALw_down)).^2, 'displayname', 'A_{Lw}')
plot(fredD, (abs(ALu_down)).^2, 'displayname', 'A_{Lu}')
set(gca, 'Yscale', 'log', 'fontsize', 20)
xlabel('f*=fB/V')
ylabel('|A_i|^2')
legend show
title('Admittance functions Lift Downstream')
ylim([0 10])
% saveas(gcf,sprintf('10_00_%d_000_DownstreamLift.jpg',file))
% saveas(gcf,sprintf('10_00_%d_000_DownstreamLift.fig',file))

figure(); hold on;
plot(fredD, AD_down, 'displayname', 'A_D')
plot(fredD, sears,'displayname', 'Sears', 'linewidth', 2)
plot(fredD,(abs(ADw_down)).^2, 'displayname', 'A_{Dw}')
plot(fredD, (abs(ADu_down)).^2, 'displayname', 'A_{Du}')
```

```matlab
set(gca, 'Yscale', 'log', 'fontsize', 20)
xlabel('f*=fB/V')
ylabel('|A_i|^2')
legend show
title('Admittance functions Drag Downstream')
ylim([0 10])
% saveas(gcf,sprintf('10_00_%d_000_DownstreamDrag.jpg',file))
% saveas(gcf,sprintf('10_00_%d_000_DownstreamDrag.fig',file))

figure(); hold on;
plot(fred, AM_up, 'displayname', 'A_M')
plot(fred, sears,'displayname', 'Sears', 'linewidth', 2)
plot(fred,(abs(AMw_up)).^2, 'displayname', 'A_{Mw}')
plot(fred, (abs(AMu_up)).^2, 'displayname', 'A_{Mu}')
set(gca,'Yscale', 'log', 'fontsize', 20)
xlabel('f*=fB/V')
ylabel('|A_i|^2')
legend show
ylim([0 10])
title('Admittance functions Moment Downstream')
% saveas(gcf,sprintf('10_00_%d_000_DownstreamMoment.jpg',file))
% saveas(gcf,sprintf('10_00_%d_000_DownstreamMoment.fig',file))
```